الجمهورية الجزائرية الديمقراطية الشعبية

People's Democratic Republic of Algeria

وزارة التعليم العالي والبحث العلمي

Ministry of Higher Education and Scientific Research

University of Mila

جامعة ميلة

Faculty of Mathematics and Computer Sciences
Order N°: …………………
Registration number: M240/2023

Department: Mathematics
Field : Mathematics
Specialty: Applied Mathematics

Dissertation

Submitted in fulfillment of the requirements
for the degree of Doctorate LMD

Contributions to the Qualitative Analysis and Stabilization of Fractional Chaotic Systems

Authored by: Rayene Abir Meskine

Publicly defended on: 23/07/2026

Scientific Committee :

Allel Mehazzem	MCA	University of Mila	Chairman
Smail Kaouache	MCA	University of Mila	Supervisor
Mohamed Dalah	Pr	UFMC1	Examiner
Lotfi Meddour	MCA	UFMC1	Examiner
Widad Laouira	MCA	University of Mila	Examiner
Rabah Bououden	MCA	University of Mila	Examiner

University year: 2025/2026

DEDICATION

It is with the deepest honour and affection that I dedicate this modest work to:

My beloved and noble parents. No words could ever suffice to express the deep regard, profound respect, unending love and gratitude I have for you. Thank you for the unwavering support, the boundless care, and the countless sacrifices you have offered me since my earliest days. May your blessings will always lead me, and may I never falter in being the source of pride and joy you deserve.

To my beloved brothers, my cherished sister-in-law, and my precious niece, for the love that unites us, for your encouragement, empathy, and unwavering presence in my life.

To my dear aunts and uncle.

To my dear cousins, for the shared laughter, the countless memories, lifelong relationships, and friendship that time cannot weaken.

To my dear friends, my journey's sweetest companions, with whom I have experienced growth, joy, and trust over the years.

To my beloved grandparents, whose memory lives forever within my heart, even though they are no longer here. Their love continues to guide me tenderly, like a light that never fades.

Finally, to all those who love me and all those whom I deeply love; this work is as much yours as it is mine. It belongs to every hand that has lifted me up and every heart that has believed in me.

ACKNOWLEDGEMENTS

I would like to express my sincere gratitude to Allah for granting me the will, perseverance, and patience necessary to complete this work.

I am deeply grateful to my dissertation supervisor, Dr. Kaouache Smail, for kindly accepting to guide this project. I sincerely thank him for his continuous support, valuable advice, insightful feedback, and constructive criticism, all of which have greatly contributed to the development of this work.

I would also like to extend my heartfelt thanks to the members of the examination committee—Prof. Dalah, Dr. Mehazzem, Dr. Meddour, Dr Laouira and Dr. Bououden—for agreeing to review this dissertation. I am truly appreciative of their time, expertise, and thoughtful consideration.

I would like to take this opportunity to acknowledge my gratitude to all the teachers for their collaboration, availability, and kindness throughout my academic journey.

My deepest thanks to my family, whose unwavering and constant support has been invaluable. I can never be grateful enough for the sacrifices they have made and for their tireless efforts to ensure my growth and fulfilment in all my endeavours.

lastly, I would like to thank every person who, in one way or another, has contributed to the completion of this work.

ملخص

تقدم هذه الأطروحة البحثية دراسة نوعية وتحليلية شاملة للأنظمة الديناميكية غير الخطية من خلال إطار عمل حساب التفاضل والتكامل الكسري ونظرية التحكم الحديثة. تبدأ الدراسة باستكشاف منهجي للخصائص الأساسية للأنظمة الديناميكية، بما في ذلك الاستقرار وسلوك التفرع والتطور النوعي. بالاعتماد على حساب التفاضل والتكامل الكسري، تم تطوير إطار عمل تحليلي موحد لوصف الأنظمة ذات التأثيرات الذاكرة والديناميكيات غير المحلية، مما يوفر توصيفًا أكثر دقة من النماذج التقليدية. في هذه الأطروحة يتم تقديم العديد من الأنظمة الفوضوية الجديدة في أشكال تقليدية وكسرية، ويتم فحص خصائصها الديناميكية بدقة من خلال تحليل الاستقرار وحساب أسس ليابونوف ودراسات التفرع والمحاكاة العددية عالية الدقة. توضح النتائج كيف تؤثر ديناميكيات الترتيب الكسري على التعقيد والأبعاد والحساسية، مما ينتج عنه سلوكيات غير موجودة في نظيراتها.

بناءً على هذا الأساس، تقدم الأبحاث تصميم استراتيجيات تحكم تكيفية ونشطة لتحقيق استقرار النظام والتزامن الكامل لنظام رباعي الأبعاد تم تطويره حديثًا. تم توسيع نطاق التحليل النوعي ليشمل تطبيقًا عمليًا في إنشاء مفاتيح قائمة على الأنتروبيا للمحفظة الالكترونية وبالتالي ربط التحليل النظري بالتنفيذ العملي للتشفير.

مواصلةً لهذا العمل ، تمت صياغة وتنفيذ استراتيجية تحكم ديناميكية بالسطح باستخدام طريقة «الرجوع إلى الوراء» لنظام وانغ-تشن، مما يوفر منهجية منهجية لتثبيت الأنظمة غير الخطية مع تقليل العبء الحسابي. وتُطبق حالات النظام على تشفير الصور عبر صندوق **S-box** مبني من التسلسلات الفوضوية للنظام، مما يُظهر قوة تشفير عالية، وحساسية قوية للمفتاح، ومقاومة قوية ضد الهجمات الإحصائية والتفاضلية.

أخيرًا، يتم إنشاء إطار عمل للتزامن قائم على التحكم في الوضع المنزلق لنظام جديد فائق الفوضى ذو رتبة اشتقاق كسرية، مما يضمن التزامن الكامل مع دقة ومتانة محسّنتين. تؤكد المحاكاة العددية الشاملة صحة التنبؤات النظرية، وتثبت فعالية استراتيجيات التحكم المقترحة وقابليتها للتطبيق في أنظمة الاتصالات الآمنة.

الكلمات المفتاحية: الأنظمة الفوضوية، المشتقة الكسرية، دالة ليابونوف، أسس ليابونوف

Abstract

This doctoral research presents a comprehensive qualitative and analytical investigation of nonlinear dynamic systems through the framework of fractional calculus and modern control theory. The study starts with a methodical exploration of the fundamental properties of dynamic systems, including stability, bifurcation behaviour, and qualitative evolution. Leveraging fractional calculus, a unified analytical framework is developed to describe systems with memory effects and non-local dynamics, providing a more precise characterization than conventional integer-order models. Several novel chaotic and hyperchaotic systems are introduced in both integer and fractional forms, and their dynamical properties are rigorously examined through stability analysis, Lyapunov spectrum computation, bifurcation studies, and high-precision numerical simulations.

Building on this foundation, the research advances the design of adaptive and active control strategies to achieve system stabilization and complete synchronization of the newly developed four-dimensional system using RBFNN scheme. The qualitative analysis is further extended to a practical application in entropy-based key generation for Blockchains, thereby linking theoretical analysis with practical cryptographic implementation.

Building further on this work, a backstepping dynamic surface control strategy is formulated and implemented for the Wang–Chen system, providing a systematic methodology for stabilizing nonlinear systems with reduced computational overhead. The system's states are applied to image encryption via an S-box constructed from the system's chaotic sequences, demonstrating high encryption strength, strong key sensitivity, and robust resistance against statistical and differential attacks.

Finally, a sliding mode control-based synchronization framework is established for a new fractional-order hyperchaotic system, ensuring complete synchronization with enhanced precision and robustness. Extensive numerical simulations validate the theoretical predictions, confirming the efficacy of the proposed control strategies and their applicability to secure communication systems.

Keywords: Chaotic systems, Fractional derivative, Lyapunov function, Lyapunov exponents.

Résumé

Cette thèse doctorale présente une étude qualitative et analytique des systèmes dynamiques non linéaires à travers le calcul fractionnaire et la théorie du contrôle. L'étude porte sur les propriétés fondamentales des systèmes dynamiques, incluant stabilité, bifurcations et évolution qualitative. En s'appuyant sur le calcul fractionnaire, un cadre analytique unifié est développé pour caractériser les systèmes à mémoire et dynamique non locale, offrant une description plus précise que les modèles classiques. Plusieurs systèmes chaotiques et hyperchaotiques originaux, entiers et fractionnaires, sont analysés dans cette thèse rigoureusement par stabilité, spectre de Lyapunov, bifurcations et simulations numériques.

Sur ces fondements, la thèse propose des stratégies de contrôle adaptatif et actif pour stabiliser les systèmes et synchroniser le système quadrimensionnel nouvellement développé. L'analyse qualitative est également appliquée à la génération de clés basée sur l'entropie pour les blockchains établissant ainsi un lien entre les résultats théoriques et leur application dans des systèmes cryptographiques réels..

Dans la continuité de ce travail, un contrôle par surface dynamique avec rétroaction (backstepping dynamic surface control) est mis en œuvre pour le système Wang–Chen, stabilisant les systèmes non linéaires tout en réduisant la complexité de calcul. Les états du système sont utilisées pour le chiffrement d'images via une S-box construite à partir des séquences chaotiques, assurant robustesse, sensibilité aux clés et résistance aux attaques statistiques et différentielles.

Enfin, un cadre de synchronisation par contrôle en mode glissant est développé pour un nouveau système hyperchaotique fractionnaire, garantissant synchronisation complète avec précision et robustesse. Des simulations étendues valident l'efficacité des stratégies de contrôle et leur applicabilité aux systèmes de communication sécurisés.

Mots-clés: Systèmes chaotiques, Dérivées fractionnaires, Fonction de Lyapunov, Exposants de Lyapunov.

Contents

List of Figures

List of Abbreviations

Symbol	Meaning
${}^{RL}\mathcal{D}^{\alpha}$	The Riemann–Liouville fractional operator of order α
${}^{GL}\mathcal{D}^{\alpha}$	The Grünwald–Letnikov fractional operator of order α
${}^{C}\mathcal{D}^{\alpha}$,$\mathcal{D}^{\alpha}$	Caputo fractional operator of order α
$AC([a,b])$	The space of absolutely continuous functions on $[a,b]$
$L^{\alpha}[a,b]$	Lebesgue space of α-integrable functions on $[a,b]$
$C_{+}^{k}([a,b])$	k-times continuously differentiable functions vanishing at $t=a$
$L_{\text{loc}}^{\alpha}([a,b])$	Space of locally α-integrable functions on $[a,b]$
RBF	Radial Basis Function
RL	Riemann-Liouville
FDEs	Fractional Differential Equations
GLM	Grünwald–Letnikov Method
ADM	Adomian Decomposition Method
ABM	Adams–Bashforth–Moulton
CSPRNG	cryptographically secure pseudorandom number generator
RBFNN	Radial Basis Function neural network
SNR	signal-to-noise ratio
FDECS	Fractional differential equations in the Caputo sense

General Introduction

Summary

This general introduction provides a critical review of existing literature, highlighting key aspects addressed by the present study. It then outlines the novel contributions of the research and concludes with a roadmap of the thesis structure.

Contents

Literature review

The study of dynamical systems represents a cognitive complex and interdisciplinary domain within the mathematical sciences, with application to pure mathematics, theoretical physics and engineering, biological modelling and economic theory. Dynamical systems theory unifies the framework to describe the evolution of quantities governed by deterministic rules over times. It constitutes the mathematical formalism of the evolution of a state within geometric or topological space, typically expressed as systems of ordinary of partial differential equations, or as iterated maps under the common concepts of phase space, trajectories and invariant sets [1]. The formal foundation of this field may be traced to the late nineteenth century, with the pioneering contributions of Henry Poincaré, who investigated the three-body problem revealing that even systems governed by elementary deterministic rules could produce trajectories of extraordinary complexity [2]. Subsequent to this seminal insight, dynamical systems theory has evolves into pivotal component of non linear science, providing indispensable analytical and computational tools for the comprehension of various phenomenas.

Among the most transformative developments within this field was the emergence of chaos theory. *Chaos* often means variations over time without regularity and out of control, was formally introduced into the mathematical lexicon by Li and Yorke in 1975 in their landmark paper "Period Three Implies Chaos" [3], demonstrating that even simple one-dimensional maps could generate infinitely complex behaviour. However, the first concrete realisation of chaos in a continuous-time system is linked to the pivotal work of E. Lorenz [4] that revealed that even a system of merely three ordinary differential equations could exhibit aperiodic trajectories highly sensitive to initial conditions and randomness. Other canonical exemplars include the Rössler system [5], the Chua circuit [6], and the Hénon map [7] each illustrating distinct mechanistic pathways to chaos, such as period-doubling cascades, intermittency, or homoclinic bifurcations.

Extending beyond classical chaos, the notion of hyperchaos was introduced to characterise systems possessing more than one positive Lyapunov exponent—thereby indicating exponential divergence along multiple independent directions in phase space, and consequently, a significantly higher degree of dynamical complexity. Hyperchaos was first introduced by Otto Rössler in 1979, who extended his original three-dimensional chaotic attractor into a four-dimensional system capable of exhibiting two simultaneously expanding directions [8]. Hyperchaotic models have proliferated in the subsequent decades as the hyperchaotic Lü system [9], the hyperchaotic Chen system [10], and modified version of the Lorenz-Stenflo equations [11]. The significance of hyperchaotic systems resides not merely in their theoretical richness, but also in their practical utility: they offer enhanced cryptographic security in communication protocols [12, 13], improved entropy for pseudo-random number generation [14], and more nuanced representations of high-dimensional nonlinear phenomena in biological [15], financial [16], and engineering contexts [17, 18].

Concurrent with these advancements, the study of non-integer order integration and differentiation has developed into a thriving mathematical field with significant applications. Although its conceptual origins derives from a correspondence between Leibniz and L'Hôpital in the seventeenth century, rigorous formulations were advanced by Liouville, Riemann and others in the nineteenth century [19, 20]. In recent decades fractional calculus has been incorporated into the investigations of dynamical systems through the substitution of integer–order derivatives with fractional operators. This approach introduces memory effects and additional degrees of freedom, often altering stability and bifurcation structures. Fractional versions of well-known chaotic systems such as the fractional-order Lorenz system [16], the fractional-order Chua system [21], the fractional-order Chen system [22] and the fractional-order Lü system [23] exhibiting chaotic and hyperchaotic behaviours when the effective total order of the equations exceeds certain thresholds. Fractional dynamics therefore provide both a richer theoretical landscape and more accurate representations of physical systems whose dynamics exhibit memory or spatial heterogeneity [22, 24].

A further strand of research addresses the control and synchronisation of dynamical systems. Control seeks either to steer a system towards a desired behaviour or to suppress unwanted oscillations[25]. Early landmark contributions include the method of Ott, Grebogi and Yorke (OGY) [26], which stabilises unstable periodic orbits embedded within chaotic attractors, as well as continuous strategies including adaptive control [27, 28, 29],active control [30], backstepping control [31, 32, 33, 34], sliding-mode control [35, 36], fuzzy control [37, 38], and event-triggered control [39, 40]. Whilst, Synchronisation, first demonstrated for chaotic oscillators by Pecora and Carroll [41], refers to the phenomenon in which two or more systems evolve so that, after an initial transient, the state of the response system is determined uniquely by the state of the drive system, despite each system's intrinsic sensitivity to initial conditions. Numerous forms of synchronisation such as complete [42, 43], anti-synchronisation [44, 45], phase synchronisation [46], projective synchronisation [47, 48], generalised synchronisation [49], and Q-S synchronisation [50] have since been identified. The intersection of hyperchaos, fractional dynamics and advanced control thus constitutes a rich field of contemporary research. Fractional hyperchaotic systems combine high-dimensional unpredictability with long-memory effects, offering opportunities for enhanced secure communication and information processing, but also presenting significant challenges for analysis and control. Innovative stabilisation and synchronisation techniques are being developed to these systems to benefit their complexity while ensuring robust performance.

Contributions

Research objectives

The primary aim of this work is to advance to the theoretical and applied study of chaotic dynamical systems. The thesis starts by establishing the fundamental background required for rigorous qualitative study. It includes an examination of key concepts in dynamical systems theory, together with a structured treatment of non-integer calculus and its extension to dynamical systems and their behavioural study.

The thesis proceeds to the development of new nonlinear dynamics in both integer and fractional order. These systems are designed to display complex and flexible hyperchaotic dynamics, their qualitative properties are investigated through analytical tools and detailed numerical studies.

A further objective of the study applies control and synchronisation techniques to different chaotic and hyperchaotic systems under the study. Several control strategies are examined and the thesis demonstrates their effectiveness in regulating the systems' behaviours. Additionally, complete synchronisation is achieved for the novel hyperchaotic systems proposed, with numerical simulations demonstrating its feasibility.

Finally, the dissertation seeks to illustrate the practical relevance of theoretical contributions. The models and methods developed in this work are applied to real world problems in information security, including cryptographic key generation for blockchain wallets, image encryption, and secure communication schemes. These applications proves how chaotic and hyperchaotic dynamics can enhance unpredictability and robustness.

Overall, the research aims to deepen our understanding of chaotic and hyperchaotic dynamical systems in both integer and fractional order settings, while establishing their significance as tools for modern engineering and security related application.

Journal papers

Smail Kaouache, Rayene Abir Meskine, Orhan Ozgur Aybar, Nasr-eddine Hamri. **Advanced control of the Wang-Chen chaotic system via backstepping dynamic surface method**.Dynamics of Continuous, Discrete and Impulsive Systems Series B: Applications and Algorithms, 2025, 32(5), 311-327.

This paper provides a comprehensive qualitative study of the Wang Chen chaotic system. A backstepping dynamic surface control strategy is subsequently applied to stabilise and regulate the system, and extensive numerical simulations are conducted to demonstrate both the feasibility and robustness of the proposed strategy.

Rayene Abir Meskine, Smail Kaouache. **Exploring hyperchaotic synchronization of a fractional-order system without equilibrium points: A sliding mode control approach**. Iranian Journal of Numerical Analysis and Optimization, 2025,15(2).

This paper introduces a novel four dimensional fractional order hyperchaotic system and provides a rigorous qualitative and numerical analysis. Complete synchronisations is subsequently achieved via a sliding mode control strategy and a secure communication scheme is implemented to demonstrate the system's practical applicability.

Thesis structure

The rest of the dissertation is divided into six major chapters, each devoted to a key aspect of the of qualitative analysis of dynamical systems and their control and synchronisation schemes.

The second chapter lays the theoretical foundations. It presents the fundamental concepts of dynamical systems, encompassing their qualitative behaviour, intrinsic properties and stability analysis. It also surveys chaotic dynamics, and main types of synchronisation, which gives the study a conceptual framework.

The third chapter addresses the mathematical underpinnings of fractional calculus. It conducts a thorough review of essential functions, and discusses fractional integration together with the different definitions of fractional derivation. It also explores geometric and physical interpretation of the different fractional operators under consideration. Lastly, it outlines several techniques for solving fractional differential equations, and discusses the criteria governing stability in systems of fractional-order.

The fourth chapter introduces a new hyperchaotic systems of order four with exponential nonlinearity. An in-depth descriptive study of the system is presented. Adaptive control strategies have been developed to stabilise the system, and the feasibility of complete synchronisation is demonstrated through detailed numerical computations. Furthermore, an entropy-based key generation algorithm is implemented to simulate block-chain and digital key wallets, thereby illustrating the practical applicability of the proposed model to real-world problems.

Chapter 5 investigates the stabilisation of the Wang–Chen chaotic system using a backstepping dynamic-surface control methodology. It presents the system model, outlines the control design and reports simulation results that confirm the enhanced stabilisation performance achieved by the proposed approach. In addition, the system is applied to an image encryption scheme, demonstrating the potential of chaotic systems in the fields of encryption and cryptography.

Chapter 6 addresses the synchronisation of equilibrium-free non-integer order hyperchaotic system via a sliding mode approach. The system's dynamics, the evolution of the control laws, and the related synchronisation analysis are all examined, and these developments are backed up by extensive numerical simulations. To substantiate the applicability of the novel system to real-world engineering and information security problems, a secure communication scheme is put into place.

Finally, the last chapter concludes the work by distilling the core results established throughout the thesis and assessing their overall contribution. The chapter also delineates avenues for future investigation that naturally emerge from the present study.

Chapter 1

Theoretical foundations of nonlinear dynamics

Summary

This chapter addresses the fundamental concepts of nonlinear dynamics, exploring dynamic systems, attractors, bifurcation phenomena, and chaos theory. It further examines mechanisms of synchronisation, providing the theoretical foundation for the subsequent analytical and control developments in the thesis.

Contents

1.1 Introduction

Understanding how natural and artificial processes evolve over time depend on the theory of dynamical systems. They provide a unified theoretical construct for analysing temporal evolution, whether it is used to depict the behaviour of electrical circuits, the motion of celestial bodies, or the spread of epidemics. The chapter offers a qualitative exposition of the fundamental concepts, behaviours, and properties of these systems.

The discussion starts with substantial concepts about dynamical systems, focusing on their representation in phase space, the importance of equilibrium points and stability analysis. It then considers the qualitative behaviour of nonlinear dynamics and the mechanisms by which stability is preserved or lost. The analysis advances to the notion of attractors, which delineate the asymptotic regimes towards which trajectories converge, encompassing both regular and strange attractors, the latter marking the emergence of chaotic dynamics.

The following sections discuss bifurcation theory, which elucidates how small variations can precipitate qualitative changes in system behaviour, and chaos theory, which formalises the paradoxical coexistence of determinism and unpredictability. The chapter ends with an investigation of synchronisation phenomena, which demonstrate how even chaotic systems may evolve in coordinated way.

The chapter systematically constructs a robust qualitative framework that contextualises classical theory within a contemporary setting, establishing a foundation for future analytical and numerical explorations of complex dynamical systems.

1.2 Dynamic systems

1.2.1 Concepts of dynamic systems

A dynamic system is portrayed in the literature as a framework evolving over time. The study of the evolution of a system therefore requires the knowledge of its initial state, and its law of evolution. A dynamic system is a model describing the evolution over time of a set of interacting objects. It is defined by a triplet $(X;T;f)$ consisting of the state space X, the time domain T, and an application of transition state $f : X \times T \to T$, which is used to determine the state of the system at any time from a vector of initial conditions. We distinguish two types of dynamical systems. Dynamic systems derived from iterative equations are categorised as discrete time systems. Whereas, those governed by differential are designated as continuous-time systems.

1. **Discrete time dynamic systems:** In discrete-time framework, the evolution of dynamical system can be expressed as

$$x_{i+1} = f(x_i) \tag{1.1}$$

where $x_i \in \mathbb{R}^n$ denotes the state vector at the step n, and f a mapping that governs the system's evolution over time.
A canonical example is the Henon discrete system, defined by

$$\begin{cases} u_{n+1} = 1 - \alpha u_n^2 + v_n \\ v_{n+1} = \beta u_n \end{cases} \tag{1.2}$$

where α and β denote real parameters.

2. **Continuous dynamical systems:** In continuous time, the state dynamics are described by

$$\frac{dx}{dt} = f(x,t) \tag{1.3}$$

where $x(t) \in \mathbb{R}^n$ denotes the state vector at time t, and f describes the state's evolution.
Consider the Van der Pol Oscillator defined by:

$$\begin{cases} \frac{dx_1}{dt} = x_2 \\ \frac{dx_2}{dt} = \mu(1-x_1^2)x_2 - x_1 \end{cases} \tag{1.4}$$

where μ controls the strength of the damping. The rest of our study will focus on continuous dynamical systems.

Autonomous and non autonomous systems: A dynamic system is deemed autonomous if the vector field f does not depend explicitly on the time t. Conversely, if the term t appears explicitly in the equation, the system is classified as non autonomous. Non autonomous systems are characterised by a greater degree of complexity in their numerical handling. However, it is possible to transform such systems into autonomous ones by introducing appropriate variable changes, thereby increasing the dimension of the system by one. This transformation serves to simplify numerical solving by eliminating explicit dependencies.

Classification of conservative and dissipative systems: Dynamic systems are said to be conservative if the presence of a quantity, remains constant during motion. Moreover, a dissipative system is defined as one which disperses energy.

We define a deterministic system as non-dissipative if and only if the evolution of the system corresponding to each initial condition x_0 results in one and only one final state $x(t)$, to fulfil the requirement, there must exist a one-to-one mapping of the phase space defined as [1]

$$\begin{gathered} \varphi : I \times \mathbb{R} \to I \\ (x,t) \mapsto \varphi_t(x) = \varphi(x,t) \end{gathered} \tag{1.5}$$

where φ is called flow of dynamic system. In conservative systems, the flow generated by the vector fields preserves volumes in phase space.
Alternatively, if the flow contracts or expands over time, the system is said to be dissipative. This expansion is quantified by the divergence of the Vector field.

Theorem 1.1 (**Divergence Theorem** [51])**.** *Consider ϕ_t be the flow of (1.3) , let V be the volume of the phase space at $t = 0$, where $V(t) = \phi_t(V)$. The image of V by ϕ_t, we obtain*

- $\frac{dV}{dt}_{t=0} = \int div f dx_1..dx_n$ *with* $div f = \sum_{i=1}^{n} \frac{\partial f}{\partial x_i}$
- *The system (1.3) is conservative if* $\frac{dV}{dt} = 0$
- *The system (1.3) is dissipative if* $\frac{dV}{dt} < 0$

1.2.2 Qualitative behaviour of dynamic systems

This part examines how the behaviour of dynamic systems can be understood through the geometric and qualitative analysis of their evolution over time. We will explore how the system's state traces out trajectories in state space or phase space, and how these trajectories form orbits that reveal patterns in the system's dynamics. The notion of flows will also be introduced to describe the continuous motion of states and to comprehend the system's structure and its evolution over time.

Phase space and State space: The phase space constitutes a multidimensional framework that facilitates the geometric interpretation of the temporal behaviour of a dynamic system. The state space denotes a set of coordinates or variables required to characterise the system fully.

Flow of a dynamic system: The flow of the system (1.3) is the set with a parameter of applications $\phi_{t(t\in\mathbb{R})}$ of ω given as

$$\phi_t(a) = x(t, a),\ \forall a \in \omega \tag{1.6}$$

where, $x(t, a)$ is the one and only solution of the Cauchy problem

$$\begin{cases} \frac{dx}{dt} = f(x, t) \\ x(0) = a \end{cases} \tag{1.7}$$

The flow ϕ_t fulfils the properties as follows

1. ϕ_t is differentiable on ω.
2. $\phi_t(x_0) = x_0$.
3. $\phi_{t+s}(x_0) = \phi_t(\phi_s(x_0))$.

Trajectories and orbits: Let be a dynamic system and x a state in the phase space. The trajectory of a point x of M is the application defined on G with values in M by

$$\begin{aligned} \phi : G \to M \\ t \mapsto \phi_t(x) \end{aligned} \tag{1.8}$$

Therefore, a trajectory represents a solution of the system (1.3). More precisely, the solution to (1.3) is a differentiable function noted $x(t)$ defined from an interval $I \in \mathbb{R}$ into G.The image of a solution $x(t)$ is called an orbit and denoted as

$$\gamma_x = a \in \omega; \exists t \in I : x(t) = a \tag{1.9}$$

Geometrically, the orbit defines a continuous curve in the phase space is, everywhere tangent to the vector field F.

1.2.3 Properties of dynamical systems

The characteristics of nonlinear dynamical systems, are intrinsically related to the evolution of the system's equilibrium points. Alterations in the number or stability of these equilibria may exert drastic effect on the system's behaviour. Moreover, such modifications follow a restricted number of scenarios, allowing for a classification of the corresponding behavioural changes.

Equilibrium point and limit points: Equilibrium points constitute a fundamental concept to understand and analyse a system's local behaviour. These points also called fixed, critical points play a crucial role in dynamical systems.

Definition 1.2. The equilibrium point of the system (1.3) is a state x^* in the phase space satisfying the equation $f(x^*) = 0$.

Definition 1.3. A point $a \in I$ is a $\omega-$limit point of the trajectory $x(x_0, t)$ if there exists a sequence $t_n \to +\infty$ such that

$$\lim_{n \to +\infty} \phi_{t_n} = a \tag{1.10}$$

Definition 1.4. A point $a \in I$ is a $\alpha-$limit point of the trajectory $x(x_0, t)$ if there exists a sequence $t_n \to -\infty$ such that

$$\lim_{n \to +\infty} \phi_{t_n} = a \tag{1.11}$$

Phase portrait: A phase portrait provides a graphical depiction of the set of trajectories describing the evolution of a dynamical system within its phase space. It often include arrows to indicate the directions of motion, and it illustrates the local and global behaviour of the solutions, in particularly near equilibrium points x^*. The phase portrait provides a qualitative graphical representation of the system's behaviour over time. it enables the visualisation of the solution's evolution over time, and reveal key features such as

- Stability and equilibria.
- Existence and nature of periodic orbits.
- Limit cycles.
- invariant sets or attractors.

Example 1.5. Consider the modified Chua system presented in [52] defined by

$$\begin{cases} \dot{x} = \alpha\Big(y + mx - x|x|\Big) \\ \dot{y} = x - cy + z \\ \dot{z} = -\beta y \end{cases} \tag{1.12}$$

where x, y, and z denote the state variables of the three-dimensional system, and α, β, m, and c are the system parameters.

For the parameters values as follows

$$\alpha = 42, \quad \beta = 100, \quad m = 0.2 \quad and \quad c = 1.6 \tag{1.13}$$

and the initial states are

$$x_0 = [0.01, 0, 0.01] \tag{1.14}$$

Figure 1.1 shows the phase-space trajectories of system (1.12) in the x-y and x-z planes.

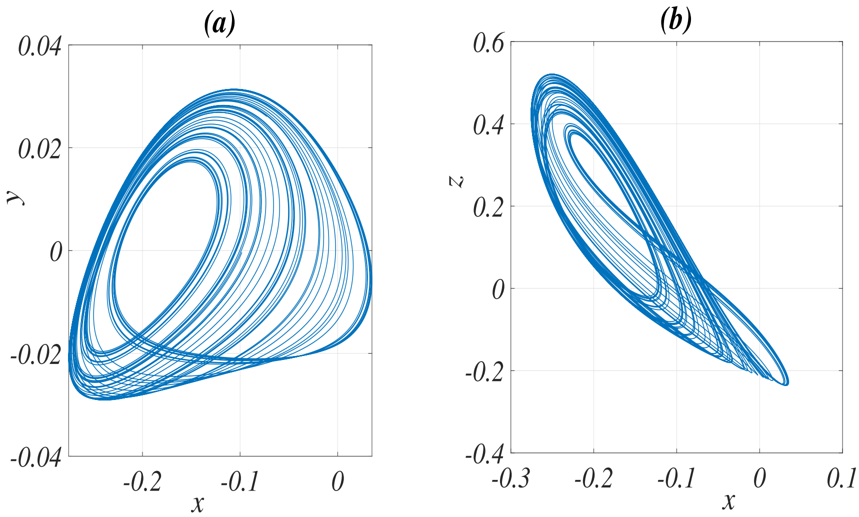

Figure 1.1: Projection of the phase portrait of the modified Chua system (1.12): (a) in the $x-y$ plane, and (b) in the $x-z$ plane.

Limit cycles: A closed trajectory C in the phase space defines a limit cycle, it represents an isolated periodic orbit of a dynamical system. The autonomous system (1.3) may admit a limit cycle if there exists an interval $[t_0, t_0 + T]$ and a point $x_0 \in C$, such that

$$\phi_t \in C, \; \forall t \in [t_0, t_0 + T] \tag{1.15}$$

with

$$\phi(t_0 + T) = x_0 \tag{1.16}$$

for some $T > 0$. $\phi(t)$ denote a periodic trajectory with period T, while C represents the associated closed trajectory.

Classification of limit Cycles: Let C be a limit cycle of the system (1.3). Then

- **Stable Limit Cycle:** All trajectories initiated sufficiently close to C asymptotically approach C as $t \to \infty$.
- **Unstable Limit Cycle:** All nearby trajectories diverge from C as $t \mapsto \infty$.
- **Semi-stable Limit Cycle:** Some trajectories that initiate near C approach it as $t \to \infty$, whereas others diverge from it.

1.2.4 Stability analysis of dynamic systems

The notion of stability refers to behaviour that persists over time, allowing us to formalise the concept of whether the trajectory becomes the solution at a point close to an equilibrium point. This is an important consideration because, in practice, initial conditions are uncertain and it is desirable for two neighbouring initial conditions to lead to neighbouring trajectories at all times, including infinitely long times. A natural approach to studying this behaviour would be to solve the differential equation and analyse the solutions. In general, however, differential equations are not solvable in closed form.

Stability in Lyapunov sense: The concept of stability in dynamic systems is characterised by the behaviour of its trajectories around its equilibrium points. The stability of an equilibrium point determines whether or not solutions nearby the equilibrium point remain nearby, get closer, or get further away. The dynamics of a nonlinear system class is expressed by the equation

$$\begin{cases} \dot{x} = f(x(t), t) \\ x(t_0) = 0 \end{cases} \tag{1.17}$$

Definition 1.6 (**Stability**)**.** The solution x^* is a stable point of the system (1.17), if there exists a positive real $\delta(\varepsilon)$ such that

$$\forall \varepsilon > 0 \, \exists \, \delta(\varepsilon) > 0 : \|x_0 - x^*\| < \delta \Rightarrow \|x(t) - x^*\| < \varepsilon \tag{1.18}$$

Definition 1.7 (**Attractiveness**)**.** The equilibrium x^* is said to be an attractive point of the system (1.17), whenever a positive scalar ρ exists such that

$$\|x_0 - x^*\| < \rho \Rightarrow \lim_{t \to +\infty} \|x(t)\| = x^* \tag{1.19}$$

Attractiveness indicates that the trajectory resulting from the initial state will converge to the equilibrium over time, if the state is initialised in a certain neighbourhood of the equilibrium state.

Definition 1.8 (**Asymptotic stability**)**.** The solution x^* constitutes an asymptotically stable equilibrium of the system (1.17), if it is stable and attractive i.e;

$$\|x_0 - x^*\| < \delta \Rightarrow \lim_{t \to +\infty} \|x(t, x_0) - x(t, x^*)\| = 0 \tag{1.20}$$

Remark 1.9.

1. Asymptotic stability requires that the trajectories converge to x^* as $t \to +\infty$. In contrast, stability only implies that the trajectories remain in a neighbourhood of x^* without necessarily approaching it.

2. The difference between a stable and an asymptotically stable equilibrium remains in the response of the system to small perturbations of the initial state. For a stable equilibria, such perturbations may lead to small but persistent oscillations. In contrast, around an asymptotically stable equilibrium, the oscillations diminish over time and the system reverts to equilibrium.

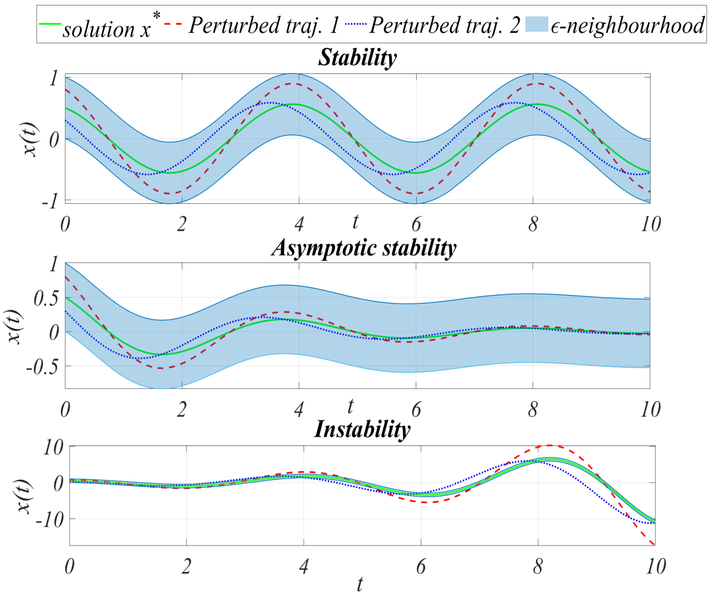

Figure 1.2: Stability concepts.

Lyapunov's direct method: The Lyapunov's direct method is fundamental to analyse the stability of nonlinear systems (1.17), without needing their analytical solutions. It is based construction of a scalar function, known as a Lyapunov function, whose properties reflect the stability of the system. The stability according Lyapunov's direct Method is defined as follows:

Theorem 1.10 (Lyapunov's stability theorem[51]**).** *Suppose that $x^* \in D$ is an equilibria of the nonlinear system (1.17), where D an open subset in $\mathbb{R}^\ltimes$. If there exists a continuous function V satisfying*

- $\forall x \in \mathbb{R}^\ltimes V(x) > 0$
- $V(x^*) = 0$
  Then

  1. *x^* is stable if $\dot{V}(x) \leq 0$, $\forall x \in D$.*
  2. *x^* is asymptotically stable if $\dot{V}(x) < 0$, $\forall x \in D|\{x^*\}$.*
  3. *x^* is unstable if $\dot{V}(x) > 0$, $\forall x \in D|x^*$.*

The term $V\dot{(x)} = dV(x)f(x)$, where $dV = (\frac{\partial V}{\partial x_1}, ..., \frac{\partial V}{\partial x_n})$.

Lyapunov's indirect method for dynamical systems: The Lyapunov's indirect method is based on the Jacobian linearisation of the system (1.17) around its equilibrium x^*. Concretely, we analyse the eigenvalues of the Jacobian matrix J evaluated at the equilibrium x^*, given by (1.21). Then , depending on their values, conclusions can be drawn regarding the stability of the equilibrium points. The Jacobian takes the form

$$J_{x^*} = \begin{bmatrix} \frac{\partial f_1}{\partial x_1} & \frac{\partial f_1}{\partial x_2} & \cdots & \frac{\partial f_1}{\partial x_n} \\ \frac{\partial f_2}{\partial x_1} & \frac{\partial f_2}{\partial x_2} & \cdots & \frac{\partial f_2}{\partial x_n} \\ \vdots & \vdots & \ddots & \vdots \\ \frac{\partial f_n}{\partial x_1} & \frac{\partial f_n}{\partial x_2} & \cdots & \frac{\partial f_n}{\partial x_n} \end{bmatrix} \tag{1.21}$$

According to the linearisation method, the equilibria x^* of the system (1.17) verify

- The equilibria x^* is asymptotically stable if all the eigenvalues of the Jacobian matrix J posses strictly negative real parts.
- The instability of x^* arises if the Jacobian J has an eigenvalue whose real part is positive.

Remark 1.11. Lyapunov's linearisation method is not effective when one of the eigenvalues of the Jacobian matrix J has a zero real part while all the others have negative real parts. In this cases, it is not possible to determine the stability of x^* based solely on this method.

Definition 1.12. Hyperbolic equilibrium point. An equilibrium point x^* of the system (1.17) is said to be hyperbolic if non of the eigenvalues of the Jacobian matrix J have zero real part i.e. $Re(\lambda) \neq 0$.

Theorem 1.13. *A hyperbolic equilibria is either asymptotically stable or unstable.*

Theorem 1.14 (**Hartmann-Grobman theorem** [53])**.** *Let x^* be a hyperbolic equilibrium point of the system (1.17). Let $\phi_t^L : y \to e^{tDf(x^*)y}$ denotes the flow of the linearised system Df at x^*. Thus, there exists a homeomorphism h such that*

$$\begin{gathered} \phi_t^L : V_{x^*} \to V_0 \\ \phi_t^L\Big(h(x)\Big) = h\Big(\phi_t(x)\Big) \end{gathered} \tag{1.22}$$

where V_{x^*} and V_0 are the neighbourhoods of x^* and 0 in $\mathbb{R}^\ltimes$, respectively.

Theorem (1.14) is a fundamental result in the local qualitative theory of differential systems. It states that, in a neighbourhood of a hyperbolic equilibrium pointx^*, the nonlinear system

$$\dot{x} = f(x) \tag{1.23}$$

has the same qualitative structure as its linearisation

$$\dot{x} = Df(x^*)(x) \tag{1.24}$$

1.3 Attractors

According to the theory of dynamical systems, an attractor is a key concept that describes the asymptotic evolution of system trajectories evolving under given flow. It represents the outcome of the system's evolution over-time, regardless of its initial conditions,provided those conditions fall within the attractor's domain of influence.

Definition 1.15 (**Invariant subset**)**.** Let X be a set and $f : X \mapsto X$ a function. A subset $A \subseteq X$ is said to be invariant under f if

$$f(A) \subseteq A \tag{1.25}$$

Additionally, if $f(A) = A$, A is strictly invariant.

Definition 1.16 (**Topological definition of an attractor**)**.** Let X be the phase space of a dynamical system, ϕ_t denotes its flow. A non-empty subset $A \subset X$ that is both compact and invariant is called an attractor if the following properties are satisfied

1. **Invariance:** $\phi_t(A) = A$, $\forall t \geq 0$, the flow maps the set onto itself.

2. **Asymptotic stability:** For every neighbourhood U of A, there exists a smaller neighbourhood $V \subset A$ such that all trajectories starting in V remain in U, and converge asymptotically toward A.

3. **Attractivity:** The intersection of the forward images of V equal to A i.e. $\cup_{t>0} \phi_t(V) = A$.

4. **Existence of a dense orbit:** There exists at least one trajectory within A that is dense in A.

Definition 1.17 (**Guckenheimer and Holmes**[54])**.** According to Guckenheimer and Holmes, A an attractor satisfying:

1. A is closed and invariant under the flow.

2. A is indecomposable.

3. The union of A and its basin of attraction is a positive Lebesgue measure, i.e. the attractor captures a significant portion of the phase space in term of volume.

1.3.1 Regular attractors

Regular attractors appear in deterministic, non-chaotic systems. They exhibit smooth, predictable dynamics and can be classified into three principal types

- **Fixed-point attractors:**These are the simplest attractors. They consist of a single point x^* such that $\phi_t(x^*) = x^*$, $\forall t$. Therefore, any trajectory starting sufficiently close to x^* will converge to it as $t \to \infty$.

- **Limit cycles:** These are defined as closed, isolated periodic orbits that attract nearby trajectories. A limit cycle is defined as a solution to a system that exhibits repetitive behaviour after a fixed interval.

- **Tori:** The phenomenon of these attractors emerges from the superposition of two or more incommensurate frequencies. The resulting motion is confined to an invariant toroidal surface T^n, which the trajectory densely fills without ever repeating.

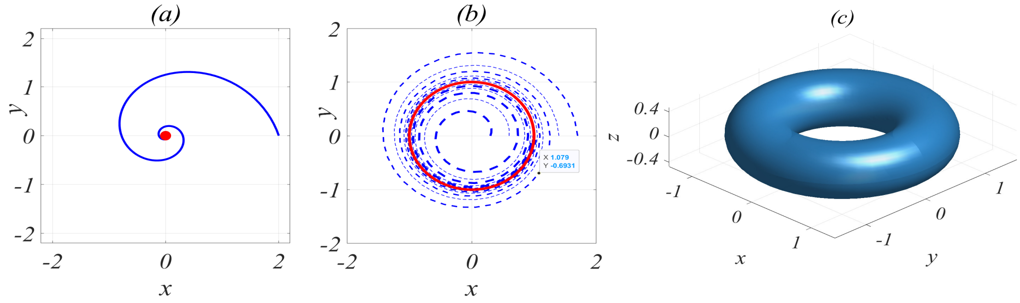

Figure 1.3: Regular attractors: (a) fixed point, (b) limit cycle, and (c) torus.

1.3.2 Strange attractors

Strange attractors arise in chaotic dynamical systems and exhibit complex, irregular behaviour. They possess the following defining properties

- **Invariance:** The set is invariant under the dynamics of the system.
- **Fractal Geometry:** Strange attractors have non-integer (fractal) Hausdroff dimension d satisfying $2 < d < n$, where n is the dimension of the phase space.
- **Sensitivity to initial conditions:** Nearby trajectories diverge exponentially fast, a hallmark of chaotic behaviour.
- **Indecomposability:** They cannot be decomposed into smaller invariant subsets.
- **Zero-volume set:** A strange attractor lies on a set of null Lebesgue measure in the phase space.

Example 1.18. Figure 1.4 illustrates the strange attractor of the modified Chua system (1.12), obtained for the set of parameters specified in (1.13) and the initial conditions given in (1.14).

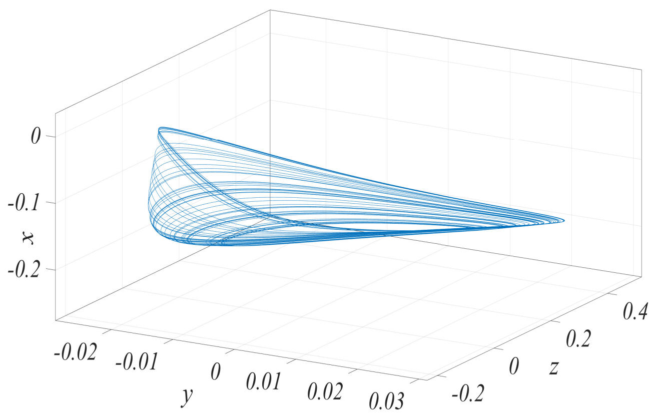

Figure 1.4: The strange attractor of the modified Chua system (1.12)

Remark 1.19. The qualitative behaviour of a dynamical system is fundamentally governed by the structure of its attractors and the geometry of their basins of attraction. Boundaries of these basins can be smooth or exhibit fractal characteristics, depending on the nature of the system. Changes in the structure of these basins—known as *metamorphoses*—are indicative of bifurcations or transitions between different dynamical regimes.

Coexisting attractors: A nonlinear dynamical system may have multiple attractors for the same set of parameters, a phenomenon referred to as multi-stability. The respective attractors are said to be coexisting attractors.

Definition 1.20. Let ϕ_t denote the flow associated with a dynamical system. A collection of compact, invariant sets $\{A_1, A_2, ..., A_n\} \subset \mathbb{R}^n$, each defining an attractor, are said to be coexisting attractors if

1. There exists $W(A_i) \subset \mathbb{R}^n, \forall i = 1, ..., n$, representing the basin of attraction of A_i, satisfying
$$\lim_{t\to\infty} d(\phi_t(x), A_i) = 0 \tag{1.26}$$

2. The basins of attraction $W(A_i)$ are mutually disjoint, i.e
$$W(A_i) \cap W(A_j) = \phi, \forall\, i \neq j \tag{1.27}$$

3. Each basin $W(A_i)$ has a positive Lebesgue measure:
$$\mu(W(A_i)) > 0 \tag{1.28}$$

4. The union $\cup_{i=1}^{n} W(A_i)$ forms a partition of a positively invariant region $\Omega \subset \mathbb{R}^n$.

The presence of coexisting attractors introduces sensitive dependence on initial conditions near basin boundaries, which may be smooth, fractal, or riddled. The system's long-term dynamics are then non-unique for a given parameter set and depend intricately on initial states.
Figure 1.5 illustrates two coexisting attractors of the modified Chua system (1.12), for the same parameters set (1.13), associated with two distinct sets of initial conditions.

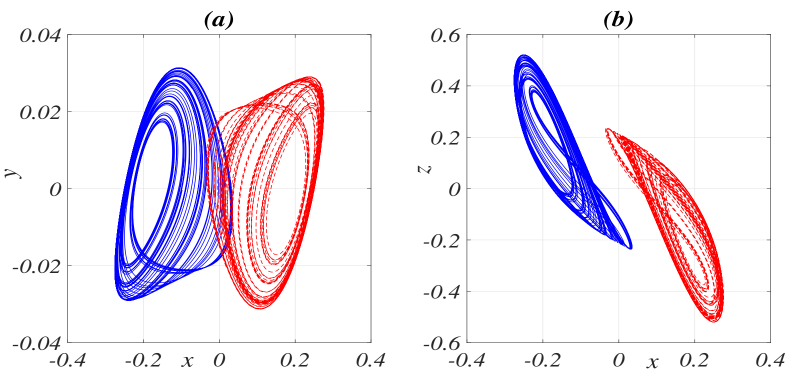

Figure 1.5: Coexisting attractors in the modified Chua system (1.12);
(a): $x_{01} = (-0.01, 0, -0.01)$; (b): $x_{02} = (0.01, 0, 0.01)$.

Hidden attractors: Within the paradigm of dynamical systems, an attractor defines the long-term asymptotic behaviour of trajectories in the phase space. They are conventionally classified according to their relationship between their basins of attraction and their equilibria.

Definition 1.21. An attractor $A \subset \mathbb{R}^n$ is defined as Hidden attractor if

1. A is invariant.
2. There does not exist any open neighbourhood V of any equilibria x^* such that

$$V \cap W(A) = \phi \tag{1.29}$$

Consequently, standard computational procedures based on linearisation around the equilibrium point can not detect hidden attractors. They often emerge in systems that are equilibrium-free or in systems with one stable equilibria. They are often, discovered by relying on specialised analytical methods such as continuation techniques, global search algorithms, or basin scanning.

Figure 1.6 illustrates the two coexisting attractors previously discussed in the preceding subsection, alongside the hidden attractor of the system (1.12). The figure highlights the distinct dynamical behaviours that emerges under different conditions, where the hidden attractor is obtained for the initial conditions $Ic_H = (0.3900, -0.2065, 1.5600)$[52]. The figure emphasises the system's sensitivity to initial states and coexistence of multiple attractors within the same parameter set (1.13).

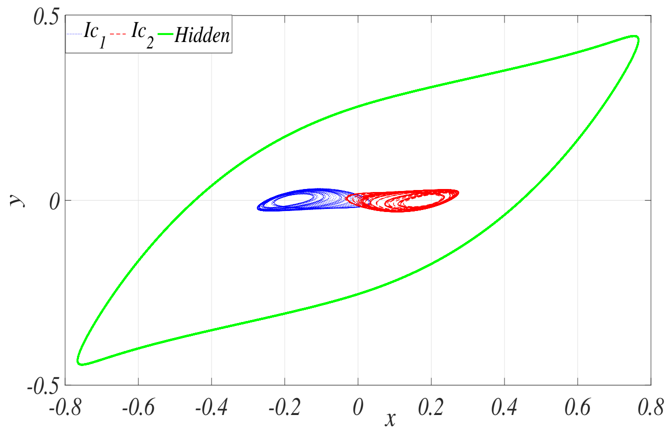

Figure 1.6: Hidden attractor in the modified Chua system (1.12).

1.3.3 Basin of attraction

The basin of attraction of an attractor A, denoted $W(A)$, is the set of all initial conditions in the phase space whose trajectories converge asymptotically toward A, is

$$W(A) = \{x \in X | \lim_{t \to \infty} d(\phi_t(x), A) = 0\} \tag{1.30}$$

The basin of attraction serves a pivotal role in the study of global behaviour of a system, as it delineates the region in the phase space governed by the attractor.
Figure.1.7 illustrates the basin of attraction of the modified Chua system (1.12) with the set parameter (1.13), for $z_0 = -1$.

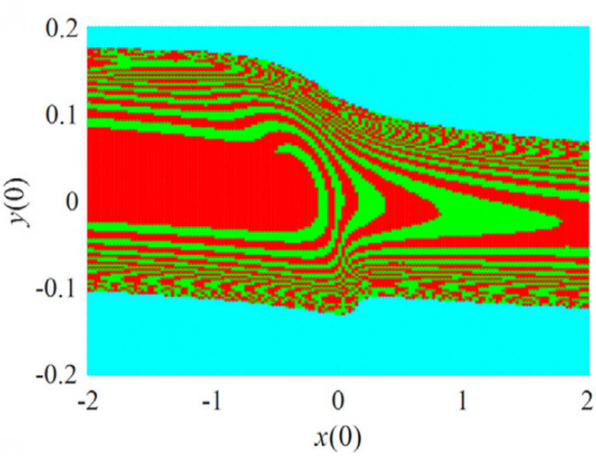

Figure 1.7: Basin of attraction of the modified Chua's system (1.12).

1.3.4 Poincaré map

The Poincaré map is an effective mathematical tool employed in the qualitative analysis of continuous-time dynamic systems. It proposes a method to reduce dimensionality of a system and covert continuous time flow into discrete-time map, facilitating detection of periodic orbits, bifurcations, and chaotic behaviour.
Let us consider the dynamical system (1.17), and let ϕ_t denotes its flow. Analysing such systems in higher dimensions is difficult especially while analysing trajectories. We introduce the Poincaré section denoted Σ, a smooth $n-1$ dimensional surface, such that

$$\forall x \in \Sigma, \; f(x) \notin A_x\Sigma \tag{1.31}$$

The Poincaré map $P : U \subset \Sigma \mapsto \Sigma$ defined on a neighbourhood $U \subset \Sigma$ as follows

$$P(x) = \phi_{A(x)}(x) \tag{1.32}$$

where $A(x) > 0$ denotes the first return defined as

$$A(x) = inf\{t > 0 | \phi_t(x) \in \Sigma \tag{1.33}$$

This formula define a discrete dynamical system on Σ, where the section $\{x_k\}$ of successive intersections of trajectories with the section is characterised by the recurrence formula stated below

$$x_{k+1} = P(x_k), \quad k \in \mathbb{N} \tag{1.34}$$

We may note the following key properties

- A continuous system of dimension n is reduced to a discrete system of dimension $n-1$, preserving topological and qualitative properties.
- A point $x_0 \in \Sigma$ is a fixed point of P if and only if $\phi_t(x_0)$ is a periodic orbit, i.e

$$P(x_0) = x_0 \Leftrightarrow \phi_t(x_0) = x_0, \quad for\ A > 0 \tag{1.35}$$

- The stability of a periodic orbit can be analysed through the eigenvalues of $DP(x_0)$. If all the eigenvalues lies within the unit circle C, the orbit is locally asymptotically stable. Conversely, the orbit is said to be unstable.

- The Poincaré map help analyse recurrent or chaotic behaviour through its geometrical structure. The presence of strange attractors, quasi-periodic trajectories, or bifurcations is revealed through the distribution of the iterations of x_k on the Poincaré section.

The Poincaré section acts as a snapshot of the flow, where we observe how trajectories pierce a given hyperplane. This is illustrated geometrically by intersecting a trajectory $\phi_t(x_0)$ with a fixed hyper surface Σ, typically chosen to be transverse to the flow and ideally intersected repeatedly by trajectories. The map retains the essential dynamical features of the full flow but is easier to study due to its reduced dimension and discrete nature.

Figures.1.8 and 1.9 depict the two- and three- dimensional Poincaré maps of the modified Chua system (1.12). The dense irregular scattering of points reveals the intricate geometry of the attractor demonstrating chaotic behaviour and sensitive dependencies of the system.

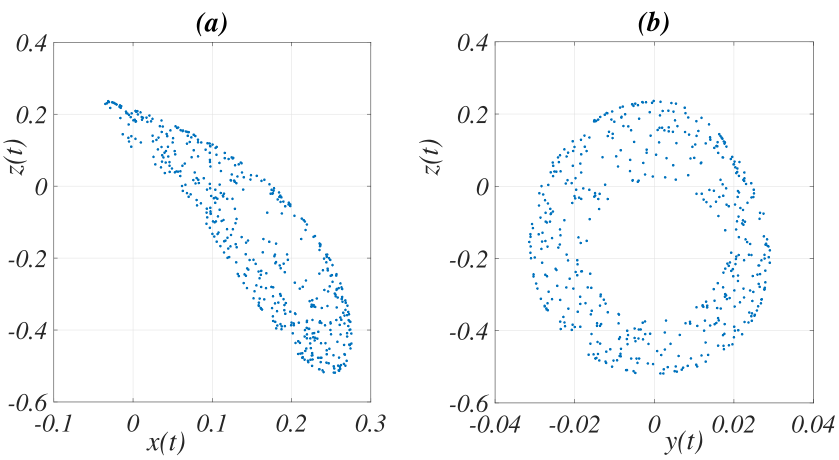

Figure 1.8: Two-dimensional Poincaré map of the modified Chua system.
(a) In the x–z plane, (b) in the y–z plane.

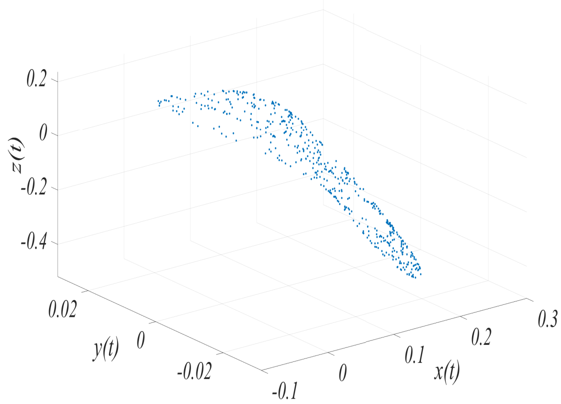

Figure 1.9: The 3D Poincaré map of the modified Chua system.

1.4 Bifurcation theory

In the rigorous analysis of nonlinear dynamic systems arising from biological, physical, or engineering models, the uncertainty inherent in parameter estimation represents a fundamental challenge. Such uncertainties have the capacity to exert a substantial influence on the predicted behaviour, thereby compromising the descriptive and the predictive reliability of the model. within such paradigm, the study of the system's structural robustness is imperative. Bifurcation analysis as a theoretical and methodological tool of primary significance, enables the identification of critical parameter values - referred to as bifurcation points - at which the system exhibits a qualitative change in its asymptotic behaviour. These transitions may entail the loss of stability of an equilibrium point, the emergence or disappearance of periodic solutions, or the onset of complex dynamical regimes, including chaotic behaviour.

The precise location of these critical thresholds serves as an indicator of the model's sensitivity to parametric perturbations. In the event that the uncertainty interval associated with one or more parameters contains no bifurcation values, the model is regarded as being structurally stable within this zone. Conversely, the presence of one or more bifurcation values within the uncertainty interval is indicative of a potential loss of robustness and thus warrants a more in depth investigation.

From a theoretical standpoint, a bifurcation corresponds to a qualitative transition in the phase portrait induced by a continuous variation of a parameter. in the context of a dynamical system depending on parameter r and admitting an equilibria x^*, is said to undergo a bifurcation at $r = r_c$ at this critical value, at this critical value r_c the linearised system around x^* has at least one eigenvalue with zero real part. This condition indicates the emergence of non-hyperbolic equilibria - a necessary, albeit insufficient condition, for the occurrence of local bifurcation. Such transitions are of pivotal significance in the qualitative analysis of dynamical systems. The identification and classification of these phenomena are of paramount importance for comprehending the range of dynamical behaviours that a model may exhibit, as well as for anticipating structural changes induced by parameter variations.

Definition 1.22. A system is structurally stable if its phase portrait remains unaltered when its parameters are perturbed.
A bifurcation corresponds to the loss of structural stability, i.e. the value of the parameter r_c for which the system is not structurally stable.

1.4.1 Local bifurcation

Local bifurcation refers to qualitative changes in the behaviour of a dynamical system that occur in a neighbourhood of an equilibrium point x^*, typically of a smooth changes of one or more parameters.

The co-dimension of a bifurcation refers to the minimum number of parameters that must be varied for the bifurcation to occur. In this context, we focus on co-dimension-one bifurcations, which are the most commonly encountered and correspond to generic behaviours in dynamic systems. There are four primary types of co-dimension-one bifurcations.

Saddle-Node bifurcation: The Saddle-Node bifurcation is the simplest type of bifurcations occurring when a real parameter r crosses a critical value. At this point, a stable fixed point (node) and an unstable one (saddle) emerge simultaneously, representing the creation of two equilibria from a previously non-existent one. This bifurcation characterises the coalescence and subsequent disappearance of fixed points as r varies. This phenomenon occurs when a real eigenvalue of the linearised system, in the neighbourhood of a fixed point, intersects with the imaginary axis. This intersection signals a qualitative change in the system's dynamics near $r = r_c$. The canonical form is given by

$$\dot{x} = r + x^2 \tag{1.36}$$

where r is the bifurcation parameter. For $r < 0$, the system possesses two equilibria at $x^* =$ ś$\sqrt{-r}$, at $r = 0$, these coalesce into a single non-hyperbolic fixed point, and for $r > 0$, no real equilibria exist.

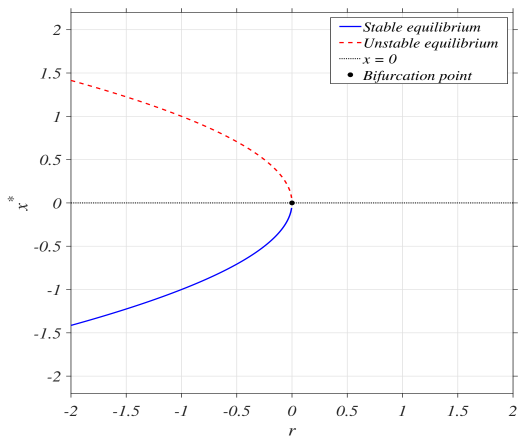

Figure 1.10: Saddle-Node Bifurcation Diagram.

Pitchfork bifurcation: The Pitchfork bifurcation arises in symmetric dynamical systems that are invariant under the transformation $x \to -x$, which is characterised by a transition of a fixed point as the parameter r crosses a critical value r_c. At this point, a single equilibrium point may either destabilise to give rise to two new stable equilibria (supercritical case), or an unstable equilibrium point may give rise to two unstable branches with a central stable point (sub-critical case). This bifurcation reflects the emergence of symmetry breaking solutions and occurs when a real eigenvalue of the linearised system crosses the imaginary axis in the neighbourhood of $r = r_c$. The Pitchfork bifurcation represents a fundamental mechanism of qualitative change in symmetric nonlinear systems. The supercritical pitchfork, described by

$$\dot{x} = rx - x^3 \tag{1.37}$$

exhibits a stable origin for $r < 0$, which becomes unstable at $r = 0$, giving rise to two new stable equilibria at $x^* =$ ś$\sqrt{r}$ when $r > 0$. In contrast, the subcritical pitchfork

$$\dot{x} = rx + x^3 \tag{1.38}$$

has an unstable pair of equilibria at $x^* =$ ś$\sqrt{-r}$, for $r < 0$, and the origin loses stability at $r = 0$ without stable alternatives often leading to abrupt jumps or hysteresis.

Transcritical bifurcation: A transcritical bifurcation is defined as the exchange of

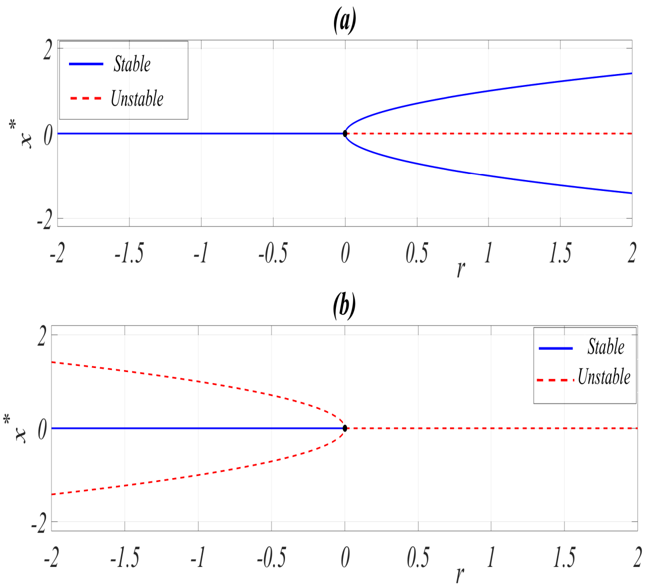

Figure 1.11: Pitchfork bifurcation diagram: (a) supercritical and (b) subcritical.

stability between two fixed points as the parameter r crosses a critical value r_c. In contrast to the Saddle-Node bifurcation, the equilibria persist for all nearby values. Yet their stability properties are exchanged: one stable point becomes unstable, while the other unstable point becomes stable. This type of bifurcation manifests when a real eigenvalue of the linearised system passes through zero, denoting a transition in local dynamics. The system frequently manifests a straightforward interaction between equilibria, which can be captured by a normal form involving quadratic nonlinearity. Transcritical bifurcation commonly arises in a variety of systems, including population dynamics and those exhibiting conservation or competing effects. The normal form is given by

$$\dot{x} = rx - x^2 \tag{1.39}$$

The equation (1.39) admits two fixed points $x^* = 0$ and $x^* = r$, For $r < 0$, the origin is stable while $x^* = r$ is unstable, for $r > 0$, their stabilities are reversed. The bifurcation occurs at $r = 0$, where the equilibria coincide.

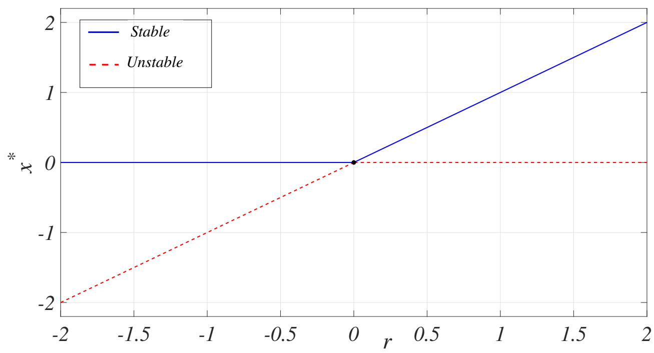

Figure 1.12: Transcritical Bifurcation Diagram.

Hopf bifurcation: A Hopf bifurcation arises when a pair of conjugate eigenvalues of the Jacobian matrix intersect the imaginary axis as r exceeds a critical value r_c. This bifurcation leads towards oscillatory behaviour emerging in a form of limit cycle. A stable equilibrium point loses stability at $r = r_c$, and a stable or unstable periodic orbit emerges contingent on whether the bifurcation is supercritical or subcritical. The system transitions from steady-state to periodic dynamics, marking a fundamental change in its qualitative behaviour. Hopf bifurcations represent a pivotal component in the domain of nonlinear oscillations, within both natural and engineered systems. The normal form in polar coordinates is

$$\begin{cases} \dot{x} = \mu x - \omega y - x(x^2 + y^2) \\ \dot{y} = \omega x + \mu y - y(x^2 + y^2) \end{cases} \tag{1.40}$$

where μ is the bifurcation parameter and $\omega > 0$ is the oscillation frequency. The sign of the first Lyapunov coefficient,$l_1(\mu)$, , determines the stability of the bifurcating periodic orbit: for $l_1(\mu) < 0$, the origin is a stable focus, at $l_1(\mu) = 0$, it loses stability, and for $l_1(\mu) > 0$, a stable limit cycle of radius $\sqrt{\mu}$ emerges.

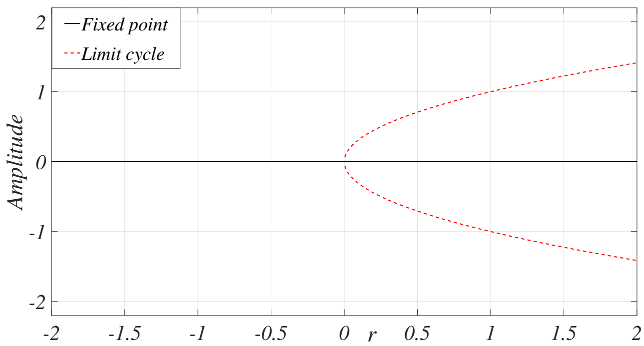

Figure 1.13: Hopf Bifurcation Diagram.

1.5 Chaos theory

Chaos a term historically associated with disorder along with confusion, has evolved to describe a structured concept within dynamical systems' theory. The etymology of the word 'chaos ' traces back to Greek mythology, where it denoted a primordial void or state of formlessness. The word has long conveyed a notion of unpredictability and absence of order. For centuries, the scientific realm, particularly classical mechanics, was founded on the principles of determinism, predictability, and reversibility, contrasting sharply with the intuitive understanding of chaos.

However, in the late 19^{th} century, that Henri Poincaré, through his pioneering study of the three-body problem in celestial mechanics, first uncovered what would later be recognized as chaotic behaviour. He revealed that deterministic systems could exhibit sensitive dependence on initial conditions, thereby rendering long-term predictions effectively impossible, even when the governing equations are perfectly known. This laid to the foundation and development of modern chaos theory.

In contemporary mathematics, chaos does not bear the same connotations as the colloquial sense of randomness or disorder. Instead, it alludes to deterministic behaviour that manifests as irregular and unpredictable owing to the system's extreme dependence on initial states. In other words, minor uncertainties in the initial state of the system increases exponentially over time making predictions impractical.

1.5.1 Definition of chaos

Despite the absence of a formal definition of chaos and the lack of a universally accepted mathematical definitions, rigorous frameworks have been proposed. One of the most widely adopted definitions are that proposed by Li.Yorke and Devany.

Li-Yorke's definition of chaos: The first mathematical definition of chaos were introduced by Li and Yorke. It was established on " the presence of three periods involves chaos".

Theorem 1.23 (**Li-Yorke Theorem** [3])**.** *Consider $I \subset \mathbb{R}$, $f : I \mapsto I$ a continuous map. Suppose there exists a point $a \in I$, such that $b = f(a)$, $c = f^2(a)$, and $d = f^3(a)$ satisfying*

$$d \leq a < b < c \quad (\text{or } d \geq a > b > c) \tag{1.41}$$

then

1. *There exists a k-periodic point i.e for every $k = 1, 2, ...,\quad f^k(x^*) = x^*$.*
2. *It exists an uncountable set $S \subset I$, containing no periodic points, satisfying*
   - *i) for every $x_1, x_2 \in S$ with $x_1 \neq x_2$*

     $$\lim_{n\to\infty} sup|f^n(x_1) - f^n(x_2)| > 0 \tag{1.42}$$

     $$\lim_{n\to\infty} inf|f^n(x_1) - f^n(x_2)| = 0 \tag{1.43}$$

   - *ii) For each $x \in S$ and periodic point $x_{per} \in I$, with $x \neq x_{per}$*

     $$\lim_{n\to\infty} sup|f^n(x) - f^n(x_{per})| = 0 \tag{1.44}$$

Devaney's chaos: Let S denote a set in a topological space, f^m is the m^{th} iteration of a map $f : S \to S$.

Definition 1.24. A point $\bar{x} \in S$ is referred to as a periodic $m-$point of period m if it satisfies $\bar{x} = f^m(\bar{x})$ while ensuring $\bar{x} \neq f^k(\bar{x})$ for any integer k such that $1 \leq k < m$.

Definition 1.25 (**Devany's definition** [55])**.** A map $f : S \to S$ is considered chaotic if

- f exhibits sensitive dependence on initial conditions i.e $\forall x \in S,\ \forall N(x) \ni x,\ \exists y \in N(x),\ \exists m \geq 0,\quad d(f^m(x), f^m(y)) > \delta$.
- The map f is topologically transitive, in the sense for any pair of non-empty subsets $U, V \subset S$, there exists an integer $m > 0 :\ f^m(U) \cap V = \phi$.
- The periodic points of f are dense in S i.e. $\forall x \in S,\ \forall \varepsilon > 0, \exists p \in \mathbb{N} : d(x, p) < \varepsilon$.

1.5.2 Properties of chaotic systems

Chaotic systems constitute a class of deterministic dynamical systems that display highly complex and unpredictable behaviour, notwithstanding their evolution being entirely governed by deterministic laws. While their trajectories are dictated by initial conditions and governing equations, they exhibit extreme sensitivity to those conditions, rendering reliable long-term prediction effectively impossible. The seminal work of Edward Lorenz in 1963, through his atmospheric convection model, first demonstrated how infinitesimal variations in initial states could produce drastically divergent outcomes, a phenomenon later termed the butterfly effect. Such systems are typically at least three-dimensional and are governed by nonlinear equations, which generate intricate and irregular dynamics. To gain a deeper understanding of their behaviour, the discussion that follows delineates the principal properties of chaotic systems.

Determinism: Chaotic systems are inherently deterministic Their evolution is completely governed by initial equation and governing equations, with no involvement of stochastic or random components. However, owing to the inherent dependence on initial conditions and the impossibility of measuring these conditions with infinite accuracy, chaotic systems exhibit behaviours that appears to be random. Consequently, determinism in chaotic systems coexists paradoxically with unpredictability.

Dissipativity: Chaotic systems are typically dissipative, which implies that the trajectories are ultimately confined to a subset of zero measure know as strange attractor. This attractor governs the long-term behaviour of the system, and its geometry often exhibits fractal structures. Dissipativity assures that, despite the initial divergence of the trajectories, the global dynamics of the system remain bounded and are attracted to a lower-dimensional subset of phase space.

Sensitivity to initial conditions: A hallmark of chaos is extreme dependence to initial states. Formally, a dynamical system $f(x(t), t)$ demonstrates sensitivity if, for any point $x \in D$, where D is a domain, and for any small perturbations $\delta > 0$:

$$\exists y \in D : ||x - y|| < \delta \Rightarrow ||f(x(t), t) - f(y(t), t)|| > \varepsilon, \quad where\, \varepsilon > 0,\ t > 0 \tag{1.45}$$

This implies that even minor differences in initial stated can lead to exponentially divergent trajectories, rendering long-term prediction impossible.
Figure 1.14 illustrates the sensitivity to initial conditions of the modified Chua system (1.12), comparing the trajectories corresponding to the initial states $x_{01} = [0.01,\ 0,\ 0.01]$ and $x_{02} = [-0.01,\ 0,\ -0.01]$. A slight difference in the initial conditions results in markedly different oscillatory behaviours, thereby demonstrating the system's chaotic nature.

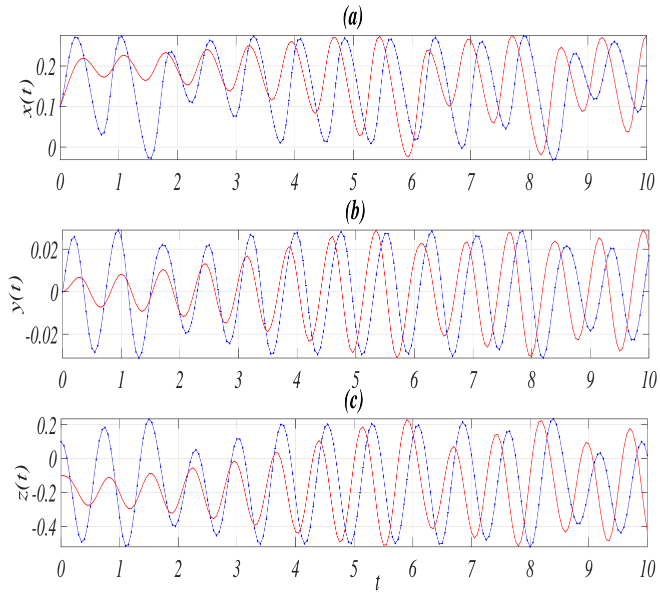

Figure 1.14: Sensitivity to initial conditions in the modified Chua system: (a) $x(t)$, (b) $y(t)$, and (c) $z(t)$.

1.5.3 Transition to chaos scenarios

The transition from stable to chaotic dynamics often results from the variations of one or more parameters. as these parameters changes, the system may undergo a serie of bifurcations that progressively alter the qualitative nature of its attractors. Although there is no general analytical criterion that predicts chaos, three universal scenarios dominate the literature.

1. ***Intermittency:*** Intermittency describes a transition to chaos characterised by an irregular alternation between quasi-periodic behaviour and bursts of chaotic dynamics. These chaotic bursts, often called turbulent bursts occur sporadically in time and dominate frequently as the bifurcation parameter increases, until the system's regime eventually become chaotic. From a mathematical perspective, intermittency is often associated with saddle-Node or sub-critical bifurcations, and is categorised into different types depending on the local dynamics near the bifurcation point.

2. ***Period-doubling:*** The period doubling route is associated with loss of stability through a cascade of Pitchfork bifurcations. the route is characterised by a sequence of bifurcations in which the period of an initially limit cycle doubles repeatedly, as the bifurcation parameter increases. The dynamic evolves from a fixed point to a periodic orbits, then to orbits with doubled periods.

3. ***Quasi periodic road:*** The quasi-periodic transition to chaos entails the destruction of an invariant torus through the interaction of two or more incommensurate frequencies. It occurs when a periodic system is perturbed by another oscillatory component with incommensurate frequency, the resulting dynamics manifest as a motion in a torus in the phase space. As a third incommensurate frequency is added, the invariant torus break down due to nonlinear resonances, leading the onset of chaos.

1.5.4 Hyperchaotic systems

Hyperchaos, first introduced by Rossler in 1979, refers to a dynamical regime that extends the concept of classical chaos by exhibiting an increased sensitivity to initial conditions, higher level of instability, and complexity in the evolution of trajectories. Hyperchaotic systems display a divergence of nearby trajectories in multiple independent directions within phase space. This multidimensional instability gives rise to a richer and more intricate dynamical behaviour.
For a system to exhibit hyperchaotic behaviour, the following structural conditions must be satisfied

1. It is imperative that the system under considerations possesses a phase space within a minimum dimension of four, thereby facilitating instability in different directions.

2. It must have at least two positive Lyapunov exponents, indicating divergence along two or more independent orientations.

Example 1.26. Consider the hyperchaotic Chua systems defined in [56] as

$$\begin{cases} \dot{x} = \alpha\Big(y - f(x)\Big) \\ \dot{y} = x - y + z + w \\ \dot{z} = -\beta y + w \\ \dot{w} = -\gamma x + \rho y + \omega w \end{cases} \tag{1.46}$$

where x, y, z, and w denote the state variables of the system, α, β, γ, ρ, and ω are system parameters, and f is a nonlinear function given by:

$$f(x) = px + qx^3 \tag{1.47}$$

with $p, q \in \mathbb{R}$.

Figure 1.15 illustrates the hyperchaotic Chua system (1.46), where panels (a), (b), and (c) display the phase portraits in two-dimensional planes, and panel (d) depicts the attractor in the three-dimensional space.

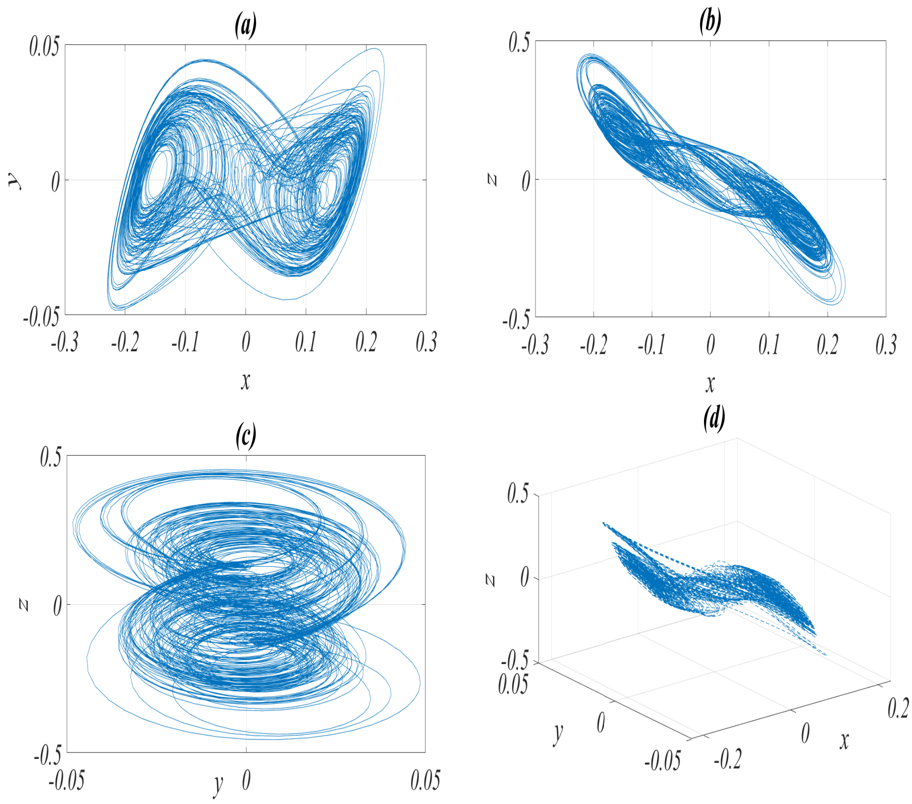

Figure 1.15: Phase portraits of the hyperchaotic Chua system (1.46): (a) projection on the (x, y) plane, (b) projection on the (x, z) plane, (c) projection on the (y, z) plane, and (d) the attractor in the three-dimensional (x, y, z) space.

1.6 Chaos detection

The identification of chaos in nonlinear dynamical systems is an important task in the qualitative study of complex dynamics. It is evident that among the most effective and widely used methods are Lyapunov exponents, fractal dimensions, and Bifurcation diagrams. This tools provide complementary perspectives thereby quantifying sensitivity to initial states, and the geometrical complexity of the attractor in the phase space.

1.6.1 Lyapunov exponents

The Lyapunov exponents measures the average exponential rate at which nearby trajectories in the phase space converge or diverge. For a $n-$dimensional system, An infinitesimal $n-$sphere of initial states evolves under the system dynamics into an ellipsoid. The principal axes of this ellipsoid exhibit exponential growth or shrinkage, and the Lyapunov exponents λ_i provide the quantitative measure of this behaviour in each direction.
Formally, the Lyapunov exponent λ is defined by

$$\lambda = \lim_{t \to +\infty} \frac{1}{t - t_0} log_2(\frac{d(t)}{d_0}) \tag{1.48}$$

where, d_0 define the initial infinitesimal separation between two nearby trajectories, $d(t)$ is the separation at time t, and t_0 is the initial time.

This leads to the fundamental divergence law

$$d(t) = d_0\, 2^{\lambda(t-t_0)} \tag{1.49}$$

A Positive Lyapunov exponent is a hallmark of chaotic behaviour, indicating extreme sensitivity to initial conditions. For an $n-$dimensional system, there exists a spectrum for n Lyapunov exponents, denoted $\lambda_1 > \lambda_2 > ... > \lambda_n$. The following classification of attractors is obtained based on the number of positive exponents

1. If $\lambda_i < 0$ for all i, the system exhibits an asymptotically stable fixed point.
2. If $\lambda_1 = 0$ and $\lambda_i < 0$ for all $i \geq 2$, the system admits a stable limit cycle.
3. If at least one Lyapunov exponent satisfies $\lambda_i > 0$, the system displays chaotic dynamics.
4. If at least two Lyapunov exponents satisfy $\lambda_i > 0$ and the system dimension satisfies $n \geq 4$, the dynamics are hyperchaotic.

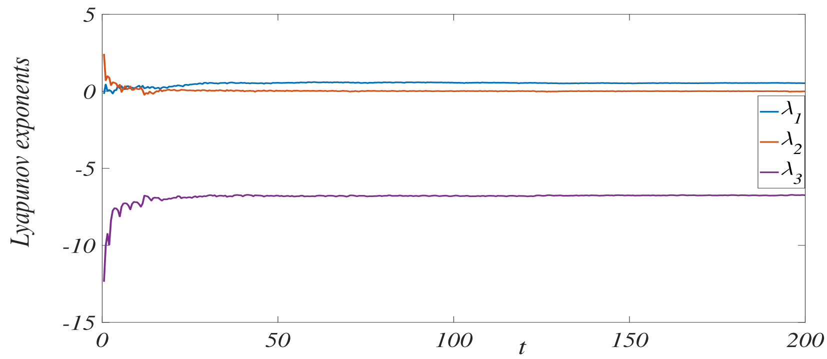

Figure 1.16: Lyapunov spectrum of the modified Chua system.

1.6.2 Fractal dimension

Chaotic attractor often exhibit complex geometric structue and self-similarity quantified by fractal dimensions. A Fractal dimension is a quantitative measure the capture the inherent geometrical complexity of an attractor, often taking non-integer values that reflect how structure of an attractor scales across different spatial resolutions. Several notions of fractal dimension have been introduced in the literature, we briefly outline the primary types

1. **Hausdroff Dimension d_H:** is the most general and rigorous definition. It is established via coverings of the set by subsets of arbitrarily small diameters satisfying

$$d_H(M) = inf\{d \in \mathbb{R}\ : \mathbb{H}^d(M) = 0\} \tag{1.50}$$

2. **Box-Counting Dimension d_C:** Also know as the Kolmogrov dimension, it requires to cover the attractor by hypercubes, given by

$$d_C = \lim_{\varepsilon \to 0} \frac{logN(\varepsilon)}{log(\frac{1}{\varepsilon})} \tag{1.51}$$

where $N(\varepsilon)$ is the number of hypercubes of side ε.

3. **Correlation Dimension d_c:** measures the probability that two random points on the attractor are within a distance ε, defined as

$$d_c = \lim_{\varepsilon \to 0} \frac{log(\frac{1}{N^2} \sum_{i \neq j} H(\varepsilon - ||x_i - x_j||)}{log(\varepsilon)} \tag{1.52}$$

where, H is the Heaviside function.

4. **Kaplan-Yorke Dimension D_{KY}:** Proposed in 1979, it combines the information from the Lyapunov exponents into a single measure of attractor complexity. Let the Lyapunov exponents $\lambda_1 > \lambda_2 > ... > \lambda_n$ satisfying

$$\sum_{i=1}^{j} \lambda_i \geq 0, \; and \; \sum_{i=1}^{j+1} \lambda_i < 0 \tag{1.53}$$

Hence, the Kaplan-Yorke dimension is given by:

$$D_{KY} = j + \frac{\sum_{i=1}^{j} \lambda_i}{|\lambda_{j+1}|} \tag{1.54}$$

1.6.3 Bifurcation diagram

A bifurcation diagram is a pivotal tool in the qualitative analysis of dynamical systems, providing a graphical representation of the changes in the long-term behaviour of a system as a control parameter varies. The equilibrium points or periodic orbits are illustrated as a function of parameters. This process capture the emergence, disappearance, or qualitative transitions of these states. The primary purpose of bifurcation diagram is to identify critical parameters known as bifurcation points, at which a qualitative change in the system's structure occurs. This tool is indispensable in both theoretical investigations and numerical simulations as it facilitates the prediction of the global behaviour of nonlinear systems. Figure 1.17 illustrates the bifurcation diagram of the modified Chua system (1.12) for the parameter range $\alpha \in [30, 65]$.

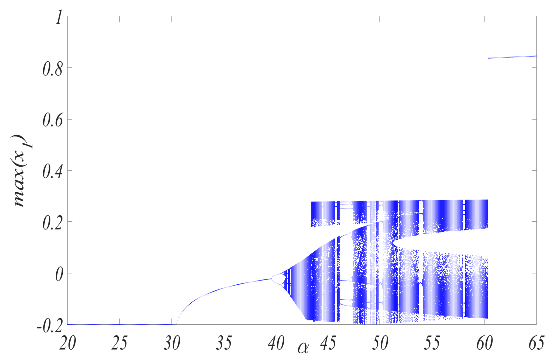

Figure 1.17: Bifurcation diagram of the modified Chua system.

1.7 Synchronisation

The idea of synchronisation, originating from the Greek "syn" meaning "together" and "chronos" signifying "time", refers to the phenomenon whereby two or more systems align a certain aspect of their motion to operate in unison. Within the realm of dynamical systems, namely chaotic systems, synchronisation refers to a regime in which the state variables of coupled systems evolve in a coordinated and correlated manner.

The contemporary examination of synchronisation in chaotic systems began with the pioneering research of Pecora and Carroll (1990), who demonstrated that two chaotic systems can synchronise their trajectories under certain coupling configurations, despite the fact that chaotic systems are inherently sensitive to initial conditions.

Introduced by Rulkov, Sushchik, Tsimring, and Abarbanel in 1995, and formalised by Kocarev and Parlitz in 1996. Generalised synchronisation provides a more general and abstract definition of synchronisation that does not rely solely on trajectorie's matching. Instead, it is based on the existence of a functional relationship between the system's states. Consider two coupled systems

$$\begin{cases} \dot{x}(t) = f(x, y, t) \\ \dot{y}(t) = g(x, y, t) \end{cases} \tag{1.55}$$

where f and g govern the evolution of the coupled states.

Definition 1.27 (**Kocarev and Parlitz** [57]). Let ϕ_t denotes the flow of the global systems with initial state $w_0 = (x_0, y_0)$. We assume the existence of an observation function $g_x : \mathbb{R}^n \times \mathbb{R} \mapsto \mathbb{R}^d$ and $g_y : \mathbb{R}^m \times \mathbb{R} \mapsto \mathbb{R}^d$, mapping the system trajectories to a shared feature space. The system are said to be synchronised if there exist an independent mapping $h : \mathbb{R}^d \times \mathbb{R}^d \mapsto \mathbb{R}^d$ satisfying

$$\begin{aligned} h(g_x(x(t)), g_y(y(t))) = 0 \quad & for\ all\ t \\ \|h(g_x, g_y)\| \to 0 \quad & \text{as } t \to \infty \end{aligned} \tag{1.56}$$

This abstract framework accommodates all known types of synchronisation by suitable choice of the observation functions g_x, g_y, and the comparison map h.

1.7.1 Types of synchronisation

Depending on the nature of the relationship between the coupled systems, several types of synchronisation have been defined in the literature. These include

1. **Complete Synchronisation (CS):** Let us Consider two dynamical systems: a drive system and a response system, defined as follows

$$\begin{cases} \dot{x}(t) = f(x(t), t) \\ \dot{y}(t) = f(x(t), t) + u(x, t) \end{cases} \tag{1.57}$$

where, $x(t), y(t) \in \mathbb{R}^n$ are the state vectors of the first and second systems, respectively, and $f : \mathbb{R}^n \times \mathbb{R}^m \times \mathbb{R} \to \mathbb{R}^n$ is a nonlinear vector functions describing the dynamics and coupling.

Definition 1.28 (**Pecora and Caroll**[41]). The drive and response systems are said to achieve complete synchronisation if the synchronisation error $e(t) = y(t) - x(t)$ satisfies

$$\lim_{t\to\infty} ||e(t)|| = 0 \tag{1.58}$$

equivalently, the trajectory of two systems converge and become identical. CS is entirely based on the comparison of the time history of the two system's states.

2. **Projective Synchronisation (PS):** It is a type of synchronisation where the response system is proportional to the drive system, and the synchronisation error defined as $e(t) = y(t) - \alpha x(t)$ satisfies equation (2.27).

3. **Phase Synchronisation:** was first observed in oscillatory systems, by Rosenblum, Pikovsky, and Kurths in 1996. Phase synchronisation occurs whene the phases of two systems align while their amplitude remain uncorrelated, i.e

$$|n\phi_x(t) - m\phi_y(t)| < C, \quad \forall t \in \mathbb{R}, \quad m, n \in \mathbb{N} \tag{1.59}$$

   where m, n are natural integers, and C denotes a positive constant.

4. **Lag Synchronisation:** Let $x(t), y(t) \in \mathbb{R}^n$ be the state vectors of two dynamical systems. Lag synchronisation is achieved if the response system follow the drive system within a time delay $\tau > 0$ satisfying

$$\lim_{t\to\infty} ||x(t-\tau) - y(t)|| = 0 \tag{1.60}$$

1.8 Conclusion

This chapter provides a qualitative analysis of dynamic systems; highlighting their role in understanding the temporal evolution of natural and engineered processes. Rather than focusing on technical derivations, the discussion emphasises the theoretical foundations that underpin stability, complexity, and long-term behaviour. It provides a framework within which diverse phenomena may be interpreted. A recurring theme has been the interplay between predictability and unpredictability. While dynamical systems are governed by deterministic rules. Their outcomes may range from stable equilibria to highly irregular dynamics. This duality highlights the significance of qualitative analysis as a means of grasping both the order and the apparent disorder that such systems display.

Finally, it constructs a rigorous yet comprehensible perspective that contextualises classical concepts with modern contexts. It also prepares the ground for the more detailed analytical and numerical investigations that follow; ensuring that subsequent discussions are firmly rooted in a coherent understanding of dynamic systems.

Chapter 2

Analytical framework of fractional dynamics

Summary

Building on the previous chapter. This chapter develops a comprehensive analytical framework for fractional-order dynamics. it covers the mathematical foundations of fractional calculus including, differentiation, integration, and fractional differential equations, alongside geometric and physical interpretations. The chapter concludes with applications to fractional-order dynamical systems, providing a rigorous basis for subsequent control and synchronisation studies.

Contents

2.1 Introduction

Fractional calculus extends the concept of differentiation and integration to an arbitrary non-integer orders, has emerged as a fundamental framework in contemporary mathematics and applied science. Unlike classical calculus, which is restricted to instantaneous change and finite accumulation, fractional operators capture long-term memory and hereditary phenomena. Those features endow fractional calculus with the capacity to describe processes that integer-order formulations cannot access. This chapter has two main goals. The theoretical and computational keys are introduced first, and secondly, the necessary tools for the analysis of dynamical systems of fractional-order.

The chapter starts with the mathematical preliminaries, including the Gamma, Beta,and Mittag–Leffler functions, in addition to the Laplace transform, which together constitute the analytic basics of fractional calculus. Then, it examines the principal formulations of fractional integration and differentiation, with particular emphasis on the Riemann–Liouville, Grünwald–Letnikov, and Caputo definitions. In both theory and practice, each of these definitions holds a significant position. Their structural properties confirm the consistency of the fractional framework and its ability to extend classical analysis.

The ensuing discussion delves into the geometric and physical interpretations of fractional operators, emphasising their pertinence in modelling phenomena such as memory, dissipation, and temporal distortion. The chapter subsequently offers an in-depth analysis of fractional differential equations, for both linear and nonlinear contexts. It also investigate the principal numerical strategies that have been identified as effective methodologies for addressing these equations. The study is concluded with examination of dynamical systems of fractional-order, with particular attention to equilibria, stability, and the expansion of Lyapunov theory.

2.2 Mathematical basis of fractional calculus

In this section, we will present some special functions that are extensively employed in the field of fractional calculus and play a fundamental role in the formulation of related problems, These include:

1. The Gamma and Beta functions,
2. The Mittag-Leffler function,
3. The Laplace transform.

2.2.1 The Gamma and Beta functions

Euler's Gamma is one of the most important functions in fractional calculus, denoted $\Gamma(z)$. It serves as a natural extension of the factorial function to the complex plane while excluding its poles. Specificcaly, for any complex number z with $\Re(z) > 0$, The gamma function is defined by the following improper integral

$$\Gamma(z) = \int_0^\infty t^{z-1} e^{-t}\, dt, \quad \Re(z) > 0 \tag{2.1}$$

This integral is absolutely convergent in the right half of the complex plane. An essential property of the Gamma function is its recurrence relation

$$\Gamma(z+1) = z\Gamma(z) \tag{2.2}$$

which can be derived using integration by parts. This recurrence relation highlights the Gamma function's role in generalizing the factorial, as it satisfies

$$\Gamma(n+1) = n!, \quad \forall n \in \mathbb{N} \tag{2.3}$$

Hence, the Gamma function is a cornerstone in many analytical techniques, including those in fractional calculus, where it underpins the definitions of fractional integrals and derivatives.

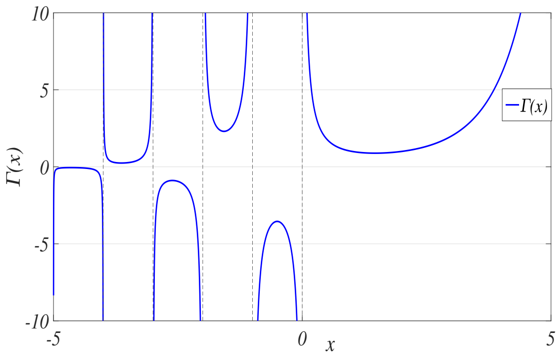

Figure 2.1: The Gamma function.

The Beta function known as Euler's integral of first kind, is another important special function. For complex arguments x, y with positive real parts is defined by

$$B(x,y) = \int_0^1 t^{x-1}(1-t)^{y-1}\,dt = \frac{\Gamma(x)\Gamma(y)}{\Gamma(x+y)}, \quad \Re(x), \Re(y) > 0 \tag{2.4}$$

Both functions are extensively used in analysis and fractional calculus due to their fundamental properties and interrelations.

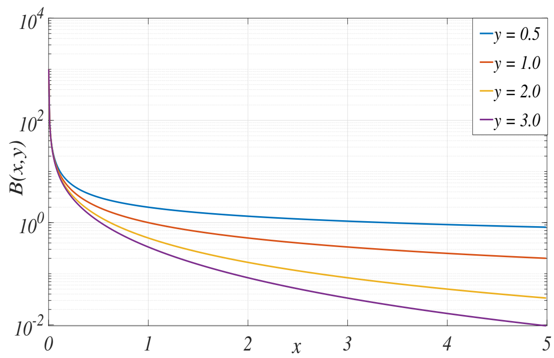

Figure 2.2: The Beta function.

2.2.2 The Mittag-Leffler function

The Mittag-Leffler function is a crucial function that generalises the exponential function in the FDEs' theory. For $\alpha > 0$ and $z \in \mathbb{C}$, the one-parameter ML function is defined by the power series [58]

$$E_\alpha(z) = \sum_{k=0}^{\infty} \frac{z^k}{\Gamma(\alpha k + 1)} \tag{2.5}$$

When $\alpha = 1$, it reduces to the classical exponential function

$$E_1(z) = e^z \tag{2.6}$$

The two-parameter ML function, introduced by Agarwal [59], is defined for $\alpha > 0$ and $\beta > 0$ by

$$E_{\alpha,\beta}(z) = \sum_{k=0}^{\infty} \frac{z^k}{\Gamma(\alpha k + \beta)} \tag{2.7}$$

This generalised function is crucial in fractional calculus, especially in expressing solutions to FDEs.

Characteristics of the ML function: The ML function has the following properties

1. For $|z| < 1$, the ML function satisfies the integral relation

$$\int_0^{+\infty} e^{-t} t^{\beta-1} E_{\alpha,\beta}(z t^\alpha)\, dt = \frac{1}{z-1} \tag{2.8}$$

2. The integral of the ML function with regard to z is given by

$$\int_0^z \lambda t^\alpha t^{\beta-1} E_{\alpha,\beta}(\lambda t^\alpha)\, dt = z^\beta E_{\alpha,\beta+1}(\lambda z^\alpha), \quad \lambda \in \mathbb{R}, \quad \beta > 0 \tag{2.9}$$

3. The n-th derivative of the two-parameter ML function is expressed as

$$\frac{d^n}{dz^n} E_{\alpha,\beta}(z) = \sum_{k=0}^{\infty} \frac{(k+n)!}{k!} \frac{z^k}{\Gamma(\alpha k + \alpha n + \beta)} \tag{2.10}$$

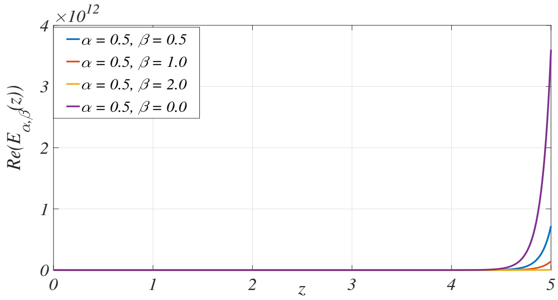

Figure 2.3: Graph of the Mittag-Leffler function for selected parameters.

2.2.3 The Laplace transform

The Laplace transform is a fundamental integral transform extensively used for solving differential equations, including those of fractional order. Let $f : [0, \infty) \to \mathbb{R}$ be a function of exponential order ω, i.e., suppose that the constants $M, T > 0$ exist such that

$$|f(t)| \leq Me^{\omega t}, \quad \forall t > T \tag{2.11}$$

The Laplace transform of f is defined by

$$\mathcal{L}[f](s) = F(s) = \int_0^\infty e^{-st} f(t)\, dt, \quad \Re(s) > \omega \tag{2.12}$$

Key operational properties include the transform of the n-th derivative of f

$$\mathcal{L}[f^{(n)}](s) = s^n F(s) - \sum_{k=0}^{n-1} s^{n-k-1} f^{(k)}(0) \tag{2.13}$$

and the transform of the convolution of two functions f and g

$$\mathcal{L}[f * g](s) = F(s)G(s) \tag{2.14}$$

where the convolution is expressed as

$$(f * g)(t) = \int_0^t f(t-\tau) g(\tau)\, d\tau \tag{2.15}$$

The Laplace transform thus provides a powerful tool for converting fractional differential equations into algebraic equations in the complex domain, greatly facilitating their analysis and solution.

2.3 Fractional integration

As is conventional in the majority of introductory works on fractional calculus. We adopt the Riemannian framework to define a first notion of fractional integration, namely, Riemann-Liouville fractional integral. Subsequent sections will introduce alternative formulations. It will be evident that all definitions considered herein are left-sided, meaning they depend on the past values of the function. Symmetric right-seeded counterparts do exist; however, they are seldom used in practise due to their anti-causal nature, as they require knowledge of the function's future values.

2.3.1 Riemann-Liouville integral

Functions defined over $[a, b]$***:*** Let $f : [a, b] \mapsto \mathbb{R}^n$. The first step, we denote ${}_aI_t^1$ the primitive of f that is reduced to zero 0 at a

$$\forall t \in [a, b],\ {}_aI_t^1\, f(t) = \int_a^t f(u)du \tag{2.16}$$

The iteration of ${}_aI_t^1$ yield the second primitive of f which annuls at a and whose derivative cancels at a. According to Fubini theorem [60, 61]

$$\begin{aligned} {}_aI_t^1 \circ_a I_t^1 &=_a I_t^2 \\ &= \int_a^t (\int_a^\tau d\tau) f(u)du \\ &= \int_a^t (t-u) f(u)du \end{aligned} \tag{2.17}$$

For $n \in \mathbb{N}^*$, let ${}_aI_t^{(n)}$ denote the iteration of order n of ${}_aI_t^1$, using a straightforward recurrence we obtain

$$ {}_aI_t^{(n)} f(t) = \frac{1}{(n-1)!} \int_a^t (t-u)^{n-1} f(u) du \tag{2.18} $$

represents the n^{th} left-hand integral of f where, equation (2.18), satisfies

$$ \forall 0 \leq k \leq n-1,\ {}_aI_t^{(k)}(a) = 0,\ and\ {}_aI_t^{(n)} = f \tag{2.19} $$

Definition 2.1. The left-handed fractional integral of Riemann-Liouville for $q > 0$ is described by

$$ \forall t \in [a,b],\ {}_aI_t^q f(t) = \frac{1}{\Gamma(q)} \int_a^t (t-u)^{q-1} f(u) du \tag{2.20} $$

Functions defined on $\mathbb{R}^+ and\, \mathbb{R}$**:** It is only natural to extend the definition (2.1) to the axes $\mathbb{R}^+$ and $\mathbb{R}$. Let's denote these operators I_{0+}^α and I_+^α respectively, defined by

$$ \begin{aligned} \forall t > 0,\ I_{0+}^q f(t) &= \frac{1}{\Gamma(q)} \int_0^t (t-u)^{q-1} f(u) du \\ \forall t > 0,\ I_{+}^q f(t) &= \frac{1}{\Gamma(q)} \int_{-\infty}^t (t-u)^{q-1} f(u) du \end{aligned} \tag{2.21} $$

If $0 < \alpha < 1$, if $f \in L^1(\mathbb{R})$, then I_+^α is defined almost everywhere.

The right-handed fractional integral: Going back to the initial equation (2.16) for a function f, we can see

$$ {}_bI_t^1 f(t) = \int_b^t f(u) du = -\int_t^b f(u) du \tag{2.22} $$

The integral (2.22) is also a primitive of f, who annuls at b and involving values on the right of f.
By the same way, we can define the right-hand integral of order n of f as in

$$ \forall t \in [a,b],\ {}_bI_t^1 f(t) = \frac{(-1)^n}{(n-1)!} \int_t^b (u-t)^{n-1} f(u) du \tag{2.23} $$

satisfying the same conditions as in equation (2.19).

Definition 2.2. The right-handed fractional integral of Riemann-Liouville of order q, is described by

$$ \forall t \in [a,b],\ {}_bI_t^q f(t) = \frac{(-1)^n}{\Gamma(q)} \int_t^b (u-t)^{q-1} f(u) du \tag{2.24} $$

The extension on $[a, +\infty[$ and $\mathbb{R}$ is denoted I_-^q, defined as

$$ \forall t \in \mathbb{R},\ {}_bI_-^q f(t) = \frac{(-1)^n}{\Gamma(q)} \int_t^{+\infty} (u-t)^{q-1} f(u) du \tag{2.25} $$

2.4 Fractional derivation

Many different definitions of fractional derivative exists in the literature. In this section we will present the most used definitions: Riemann-Liouville, Grunwald-Letnikov, and Caputo.

2.4.1 Fractional derivative in the Riemann-Liouville sense

The Riemann-Liouville approach of fractional derivative of order q is based on a relationship between the Riemann fractional integral and integer order derivative

$$^{RL}\mathcal{D}_t^q = \mathcal{D}^n I^{n-q} f \tag{2.26}$$

where $q > 0$, and $n = \lceil q \rceil$.

Functions defined over $[a, b]$***:***

Definition 2.3. For $q > 0$ and $n = \lceil q \rceil$. The left-handed RL fractional derivative of a function f defined on $[a, b]$ of order q is given as

$$\begin{aligned} {}_a^{RL}\mathcal{D}_t^q f(t) &= (\frac{d}{dt})^n \circ_a I_t^{n-q} f(t) \\ &= \frac{1}{\Gamma(n-q)} \frac{d^n}{dt^n} \int_a^t (t-u)^{n-1-q} f(u) du \end{aligned} \tag{2.27}$$

Definition 2.4. For $q > 0$ and $n = \lceil \alpha \rceil$. The right-handed RL fractional derivative of a function f defined on $[a, b]$ is defined as

$$\begin{aligned} {}_t^{RL}\mathcal{D}_b^q f(t) &= (-\frac{d}{dt})^n \circ_t I_b^{n-q} f(t) \\ &= \frac{(-1)^n}{\Gamma(n-q)} \frac{d^n}{dt^n} \int_t^b (t-u)^{n-1-q} f(u) du \end{aligned} \tag{2.28}$$

Function defined over $\mathbb{R}$***:*** If $f : \mathbb{R} \mapsto \mathbb{R}^{\ltimes}$, the previous definitions (2.3) and (2.4) are generalised directly and referred Liouville derivatives.

Definition 2.5. For $q > 0$ and $n = \lceil q \rceil$. The left-handed Liouville fractional derivative of a function f defined on $\mathbb{R}$ of order q is defined as

$$^{RL}\mathcal{D}_+^q f(t) = \frac{1}{\Gamma(n-q)} \frac{d^n}{dt^n} \int_{-\infty}^t (t-u)^{n-1-q} f(u) du \tag{2.29}$$

Definition 2.6. For $q > 0$ and $n = \lceil q \rceil$. The right-handed Liouville fractional derivative of order q of a function f defined on $\mathbb{R}$ is given as

$$^{RL}\mathcal{D}_-^q f(t) = \frac{(-1)^n}{\Gamma(n-q)} \frac{d^n}{dt^n} \int_t^b (t-u)^{n-1-q} f(u) du \tag{2.30}$$

2.4.2 Fractional derivative in the Grünwald-Letnikov sense

The Grünwald- Letnikov approach is based on a fractional finite difference scheme, where the key distinction from the integer order case lies in extending the factorial function via Gamma function. The GL fractional derivative is a function of f obtained based on

$$f'(t) = \lim_{h\to 0} \frac{1}{h}(f(t) - f(t-h)) = \lim_{h\to 0} e_h f \tag{2.31}$$

where, $e_h = \frac{1}{h}(I_d - \tau_h)$ designates the retrograde Euler operator.
Extending equation (2.31) to $n - th$ order, we obtain

$$f^{(n)}(t) = \lim_{h\to 0} e_h^n f(t), \quad = \lim_{h\to 0} \frac{1}{h^n} \sum_{k=0}^{n} (-1)^k \binom{n}{k} f(t-kh) \tag{2.32}$$

where $\binom{n}{k}$ denotes binomial coefficients
using the Gamma function for a positive real $q \in \mathbb{R}^+ \setminus \mathbb{N}$ and $k \in \mathbb{N}$, we get

$$\binom{q}{k} = \frac{\Gamma(q+1)}{\Gamma(k+1)\Gamma(q-k+1)} \tag{2.33}$$

Definition 2.7. Let $q > 0$. The left-handed fractional operator in Grünwald-Letnikov sense is given by

$$\forall t \in \mathbb{R},\ {}^{GL}\mathcal{D}_{+}^{q} f(x) = \lim_{h\to 0^+} \frac{1}{h^q} \sum_{k=0}^{\infty} (-1)^k \binom{q}{k} f(t-kh) \tag{2.34}$$

Definition 2.8. Let $q > 0$. The right-handed fractional operator in Grünwald-Letnikov sense is given by

$$\forall t \in \mathbb{R},\ {}^{GL}\mathcal{D}_{-}^{q} f(x) = \lim_{h\to 0^+} \frac{1}{h^q} \sum_{k=0}^{\infty} (-1)^k \binom{q}{k} f(t+kh) \tag{2.35}$$

2.4.3 Fractional derivative in the Caputo sense

Within the RL framework, the concept of fractional derivatives requires initial conditions in term of fractional-order derivatives. This issue poses a significant challenge in the context of physical modelling, as the initial conditions in such cases frequently lack a straightforward physical interpretation. Furthermore, a fundamental deficiency inherent in the definition of RL is the non-null fractional derivative of a constant, a property opposites classical expectations. To address these issues, the Italian mathematician M. Caputo introduced an alternative definition in 1967 [62]. The approach offers more physical interpretations by virtue of the fact that it enables the using of classical initial conditions in solving FDEs. The primary concept underlying Caputo's modification pertains to the reversal of the order of operations in the RL definition. In contrast to the conventional RL derivative, which is derived by following the standard order of operations, Caputo's approach involves the reordering of the operations to yield the desired result.

Definition 2.9. Let $q > 0$ and $n = \lceil q \rceil$. The Caputo's fractional derivative denoted as ${}_a^C\mathcal{D}_t^q$ is defined by

$${}_a^C\mathcal{D}_t^q f(t) = I_a^{n-q}\mathcal{D}^n f \quad = \frac{1}{\Gamma(n-q)} \int_a^t (t-u)^{n-1-q} f^{(n)}(u)du \tag{2.36}$$

Whenever $f^{(n)} \in L_1[a, b]$.

2.4.4 Fractional operator properties

Among major interests of fractional calculus lies in its capacity to extend several properties of differentiation and integration from the integer case. Especially, the fractional derivative of a fractional integral of the same order yields the identity operator, under suitable regularity conditions, the application of fractional derivatives successively can generate higher order derivatives, the concept of integration by parts remains valid in the fractional context, and notably, fractional operators interact with inherently with integral transforms. This latter property is of particular significance and underpins many of the application areas outlined in the preceding section.

Linearity: Both the fractional differentiation and integration operators exhibit linearity, that is

$$\mathcal{D}^q(\gamma f(t) + \eta g(t)) = \gamma \mathcal{D}^q f(t) + \eta D^q g(t) \tag{2.37}$$

are considered for any derivation approach in this thesis.

Combinations between operators: The composition property of classical derivatives, are given by

$$\frac{d^n}{dt^n}\frac{d^m}{dt^m} = \frac{d^{n+m}}{dt^{n+m}} \tag{2.38}$$

It is limited to the fractional case for functions whose successive derivatives are null at the boundary (unless $m + n < 1$).

- Let $q > 0$, $p > 0$ and $f \in L^1([a, b])$. Then

$$_aI_t^q\, _aI_t^p f = {}_aI_t^{q+p} f \tag{2.39}$$

- Let $q > 0$ and $f \in L_1([a, b])$. Then

$$^{RL}_{\ a}\mathcal{D}_t^q\, _aI_t^q f(t) = f \tag{2.40}$$

- Let $q > 0$, $n = E(q) + 1$, and $f \in AC^n([a, b])$. Then

$$_aI_t^q\, ^{\mathcal{C}}_a\mathcal{D}_t^q f(t) = f(t) - \sum_{k=0}^{n-1} \frac{(t-a)^k}{k!} f^{(k)}(a) \tag{2.41}$$

- For $0 < q < 1$, $f \in AC([a, b])$. Then

$$_aI_t^q\, ^{RL}_{\ a}\mathcal{D}_t^q f = {}^{RL}_{\ a}\mathcal{D}_t^q\, _aI_t^q f = f \tag{2.42}$$

- For $0 < q < p$, $f \in L^1([a, b])$. Then

$$^{RL}_{\ a}\mathcal{D}_t^q\, _aI_t^p f =_a I_t^{p-q} f \tag{2.43}$$

- Concerning the compositions between derivatives. If $m \in \mathbb{N}$, $q > 0$, and $n = E(q) + 1$. Then

$$\begin{aligned}\frac{d^m}{dt^m}\, ^{RL}_{\ a}\mathcal{D}_t^q &= \frac{d^{m+n}}{dt^{m+n}}\, _aI_t^{n-q} \\ &=^{RL}_{\ a} \mathcal{D}_t^{m+q}\end{aligned} \tag{2.44}$$

  Likewise,

$$\frac{d^m}{dt^m}\, ^{\mathcal{C}}_a\mathcal{D}_t^q =^{\mathcal{C}}_a \mathcal{D}_t^{m+q} \tag{2.45}$$

- Let $q > 0$, $p > 0$, If $f \in C^p([a,b])$. Then
$$ {}_a^{RL}\mathcal{D}_t^q \, {}_a^{RL}\mathcal{D}_t^p f = {}_a^{\mathrm{RL}}\mathcal{D}_t^{q+p} f \tag{2.46}$$
The results remains valid with the Caputo operator
$$ {}_a^{\mathcal{C}}\mathcal{D}_t^q \, {}_a^{\mathcal{C}}\mathcal{D}_t^p f = {}_a^{\mathrm{C}}\mathcal{D}_t^{q+p} f \tag{2.47}$$
- Let $0 < q < 1$, $k \in \mathbb{N}^*$, and $f \in C_+^k([a,b])$. Then
$$ ({}_a^{\mathcal{C}}\mathcal{D}_t^q)^k f = {}_a^{\mathcal{C}}\mathcal{D}_t^{qk} f \tag{2.48}$$

All proofs are in [63]

Integration by parts: Integrating by parts is one of the classical properties that can be extended to fractional operators, although such an extension is valid only under certain restrictions.Here, we present a simplified version with explicit assumptions as in [64].

Corollary 2.10. *Let $q > 0$ and $n \in \mathbb{N}$ such that $n-1 < q \leq n$. Assume $f \in AC^n([a,b])$ and $g \in C_0^n([a,b])$. Then the following identity holds*
$$ \int_a^b f(t)\, {}_a^{RL}\mathcal{D}_t^q g(t)\, dt = \int_a^b {}_t^{RL}\mathcal{D}_b^q f(t)\, g(t)\, dt \tag{2.49}$$
$$ \int_a^b f(t)\, {}_t^{\mathrm{RL}}\mathcal{D}_b^q g(t)\, dt = \int_a^b {}_a^{\mathrm{RL}}\mathcal{D}_t^q f(t)\, g(t)\, dt \tag{2.50}$$

Leibniz Rule: In classical cases, for an integer n, we have
$$ \frac{d^n}{dt^n}(f(t)\cdot g(t)) = \sum_{k=0}^{n} \binom{n}{k} f^{(k)}(t) g^{(n-k)}(t) \tag{2.51}$$
generalising the formula we have
$$ \mathcal{D}^q(f(t)\cdot g(t)) = \sum_{k=0}^{n} \binom{q}{k} f^{(k)}(t)\mathcal{D}^{q-k} g(t) - R_n^q(t) \tag{2.52}$$
where, $n \geq q+1$ and
$$ R_n^q(t) = \frac{1}{n!\,\Gamma(-q)} \int_a^t (t-u)^{-q-1}\, g(u)\, du \int_u^t f^{(n+1)}(\xi)\,(u-\xi)^n\, d\xi, \qquad \text{with } \lim_{n\to\infty} R_n^q(t) = 0 \tag{2.53}$$
If f and g, along with their derivatives are continuous on the interval $[a,t]$, the formula becomes
$$ \mathcal{D}^q(f(t)\cdot g(t)) = \sum_{k=0}^{\infty} \binom{q}{k} f^{(k)}(t) D^{q-k} g(t) \tag{2.54}$$
Here, $\mathcal{D}^q$ holds for the RL and GL derivatives only due to their mathematical equivalence under suitable regularity conditions.
In the case of the Caputo operator, the rule is slightly different, because we subtract the initial conditions, as a result [65]
$$ {}_{t_0}\mathcal{C}\mathcal{D}(f(t)\cdot g(t)) = \sum_{k=0}^{\infty} \binom{q}{k} f^{(k)}(t) D^{q-k} g(t) - \frac{(t-t_0^{-q}}{\Gamma(1-q)} f(t_0) g(t_0), \quad t \in [t_0, T] \tag{2.55}$$

Laplace transform: We define sub-exponential growth for a function $f : \mathbb{R}^+ \to \mathbb{R}^N$ by the existence of constants $A > 0$, $s_0 \in \mathbb{R}$, and $t_0 > 0$ such that

$$\forall t > t_0, \quad |f(t)| \leq Ae^{s_0 t} \tag{2.56}$$

If $f \in L^1_{\text{loc}}(\mathbb{R}^+)$ and satisfies the sub-exponential growth condition, its Laplace transform is defined for all $s > s_0$ by

$$\mathcal{L}[f](s) = \int_0^\infty e^{-st} f(t)\, dt \tag{2.57}$$

Furthermore, for any integer $n \in \mathbb{N}$, if $f \in C^n(\mathbb{R}^+)$ is of sub-exponential growth, then the Laplace transform of its n-th derivative is given by

$$\forall s > s_0, \quad \mathcal{L}[f^{(n)}](s) = s^n \mathcal{L}[f](s) - \sum_{k=0}^{n-1} s^{n-k-1} f^{(k)}(0) \tag{2.58}$$

This expression extends naturally to the fractional-order setting via fractional integral and differential operators with support bounded below by zero.

Lemma 2.11. *Let $q > 0$, and let $f \in L^1_{\text{loc}}(\mathbb{R}^+)$ be a function of sub-exponential growth. Then*

$$\forall s > s_0, \quad \mathcal{L}\left[{}_0I_t^q f\right](s) = s^{-q} \mathcal{L}[f](s) \tag{2.59}$$

Lemma 2.12. *Let $q > 0$ and define $n = \lfloor q \rfloor + 1$. Suppose $f \in C^n_+(\mathbb{R}^+)$ is of sub-exponential growth. Then*

$$\forall s > s_0, \quad \mathcal{L}\left[{}^{RL}\mathcal{D}_t^q f\right](s) = s^q \mathcal{L}[f](s) \tag{2.60}$$

It is worth noting that the RL derivative requires that all initial conditions of lower-order derivatives to be null.

Theorem 2.13. *Let $q > 0$, $f \in L^1([a, b])$, the Laplace transform of the RL operator of a given function f is defined by*

$$\mathcal{L}({}_0^{RL}\mathcal{D}_t^q f)(p) = p^q (\mathcal{L}f)(p) - \sum_{k=0}^{n-1} p^k \left[{}_0^{RL}\mathcal{D}_t^{q-k-1} f(x)\right]_{x=0} \tag{2.61}$$

where $n - 1 < q < n$.

Let $f \in C^n$, equation (2.34) can be rewritten in the form

$${}^{GL}\mathcal{D}^q f(x) = \sum_{k=0}^{n-1} \frac{f^{(k)}(x-a)^{-q+k}}{\Gamma(-q+k+1)} + \frac{1}{\Gamma(-q+n)} \int_a^x (x-t)^{-q+n-1} f^{(n)}(u) du \tag{2.62}$$

Theorem 2.14. *Let $0 < q < 1$, the Laplace transform of the GL fractional operator of a given function f is given by*

$$\mathcal{L}({}_0^{GL}\mathcal{D}_t^q f)(p) = p^q (\mathcal{L}f)(p) \quad p \in [n-1, n] \tag{2.63}$$

Theorem 2.15. *Let $f \in C^n[0,t]$, $q > 0$ the Laplace transform of the Caputo fractional operator of a given function f is given by*

$$\mathcal{L}({}_0^{\mathcal{C}}\mathcal{D}_t^q f)(p) = p^q(\mathcal{L}f(p) - \sum_{k=0}^{n-1} p^{q-k-1} f^{(k)}(0) \tag{2.64}$$

Proof. Applying lemma (2.11) to $f^{(n)}$, and using equation. 2.58 we obtain

$$\begin{aligned}
\mathcal{L}\left\{{}_0^{\mathcal{C}}\mathcal{D}_t^q f\right\}(s) &= \mathcal{L}\left\{{}_0T_t^{n-q}(f^{(n)})\right\}(s) \\
&= s^{-q}\mathcal{L}\left\{f^{(n)}\right\}(s) \\
&= s^{q-n}\left[s^n\mathcal{L}\{f\}(s) - \sum_{k=0}^{n-1} s^{n-1-k} f^{(k)}(0)\right] \\
&= s^q\mathcal{L}\{f\}(s) - \sum_{k=0}^{n-1} s^{q-k-1} f^{(k)}(0)
\end{aligned} \tag{2.65}$$

□

2.5 Geometric and physical interpretations of fractional operators

Classical calculus is founded on intuitive geometric and physical interpretations. Specifically, the derivative of a function at a point a quantifies the instantaneous rate of change and, geometrically represents the slope of the tangent line, whereas the integral corresponds to the accumulated quantity and geometrically represents the area under the curve . These foundations have enabled the precise modelling of natural phenomena for centuries. In contrast, fractional calculus can be traced to a correspondence between l'Hôpital and Leibniz in 1695 regarding the interpretation of a derivative of order $\frac{1}{2}$ which lacked clear and rigorous geometric or physical interpretations. For more than three centuries the foundation of non-integer order operators remained obscure, with most advancement arising from analytical generalisations rather than intuitive comprehension.

The mathematical deficit was officially acknowledged at the First International Conference on Fractional Calculus in New Haven in 1974, and echoed in subsequent gatherings. Although, the effectiveness of fractional derivatives and integrals in modelling complicated systems, their significance beyond mere manipulations remained elusive. Whereas some researchers attempted to link fractional calculus with fractal geometry offering suggestive metaphors but lacking rigorous mathematical consistency [66]. A pivotal moment emerged in the early 2000s with Igor Podlubny's pioneering work, which reinterpreted fractional integration via domain deformation and Stieltjes integration [20]. This section presents a cohesive overview of these developments, categorising them into geometric foundations, physical analogies, and implications for fractional differentiation.

2.5.1 Geometric framework for memory effects in fractional integration

In 2001-2002 Podlubny made a significant breakthrough in the geometric comprehension of fractional integration [67]. He introduced a spatial reinterpretation of the left-sided RL fractional integral. We investigate a function $f(t)$ with $q > 0$, the operator is stated as

$$ {}_aI_t^q f(t) = \frac{1}{\Gamma(q)} \int_a^t (t-u)^{q-1} f(u)\, du \tag{2.66} $$

The equation (2.66) generalises the n-fold iteration to non-integer orders; its geometric significance remained opaque until Podlubny reformulated it as a Stieltjes-type integral

$$ {}_aI_t^q f(t) = \int_a^t f(u)\, dg_t(u) \tag{2.67} $$

and the auxiliary function $g_t(\tau)$ is given by

$$ g_t(u) = \frac{1}{\Gamma(q+1)} (t-u)^q \tag{2.68} $$

Geometrically, $g_t(u)$ might be regarded as a deformation of the time axis. For a given t, a surface could be generated through graphing $f(u)$ along the vertical axis, while the horizontal direction is distorted according to $g_t(u)$. This develops a three-dimensional structure, and the projection of its area onto various coordinate planes offers insight into the fractional integral:

- The projection onto the (u, f)-plane corresponds to the classical integral,
- The projection onto the (g, f)-plane results in the fractional integral ${}_aI_t^q f(t)$.

When $q = 1$, $g_t(u)$ becomes linear, resulting in the convergence of both projections, and thereby reinstating the traditional geometric interpretation of integration. For $q \neq 1$, the situation alters considerably: the power-law distortion of the time axis induces a hierarchical prioritisation of historical values, therefore embedding memory into geometric framework of integration. This structure demonstrate the fractional integration may be regarded as integration over a 'stretched' or 'compressed' domain, hence generalising the notion of area under a curve to non-integer dimensions of accumulations. In this context, fractional integration emerges as a geometric calculus of non-uniform accumulation within dimensionally intermediate domains.

2.5.2 Temporal distortion via the Stieltjes integral

To anchor this geometric layout in physical intuition, Podlubny presented a compelling analogy involving a vehicle fitted with a defective clock. Let τ denote the time recorded by the driver, and suppose the true physical time T is related to τ via a non linear transformation $T = g(\tau)$. If the vehicle's speed is measured as $v(\tau)$ with respect to the faulty clock, then the distance computed on board is

$$ S_A(t) = \int_0^t v(\tau)\, d\tau \tag{2.69} $$

which is a standard Riemann integral reflecting accumulation over perceived time.

Conversely, an external observer possessing accurate temporal information calculates the actual distance via the Stieltjes integral

$$ S_O(t) = \int_0^t v(\tau)\, dg(\tau) \tag{2.70} $$

where $g(\tau)$ represents the nonlinear correlation between recorded and actual time. If $g(\tau)$ is singular or exhibits power-law behaviour, the resulting integral encompass non-local temporal dependencies of systems with memory or internal hierarchy.

This analogy connects directly to the framework of the RL integral. When $g(\tau)$ is selected as in equation (2.68), the measured distance $S_O(t)$ becomes equivalent to a fractional integral of the velocity. Therefore, fractional integration naturally emerges as the suitable framework for characterising physical processes that evolve on non-uniform or dynamically distorted time scales. Such scenarios occur in various contexts, including viscoelasticc materials with extended relaxation times, anomalous diffusion in heterogeneous media, and biological systems with history-dependent dynamics.

2.5.3 Fractional differentiation and its physical significance

By expanding the aforementioned framework, the RL fractional derivative is a natural inverse operation to fractional integration and can be interpreted within the same physical context of time distortion. For $0 < q < 1$, the left-sided RL derivative is given by

$$ {}_a\mathcal{D}_t^q f(t) = \frac{1}{\Gamma(1-q)} \frac{d}{dt} \int_a^t (t-u)^{-q} f(u)\, du \tag{2.71} $$

Furthermore, the fractional derivative is non-local: the value of ${}_a\mathcal{D}_t^q f(t)$ is reliant upon the complete history of $f(u)$ over $[a, t]$, modulated by a power-law kernel. This inherent memory property essentially differentiate fractional derivatives from their classical counterparts, which rely solely on local behaviour.

Let us assume that the observed distance $S_O(t)$ is known for time-distorted analogy. The actual instantaneous velocity can be retrieved from the observer's perspective via fractional differentiation

$$ v(t) = {}_0\mathcal{D}_t^q S_O(t) \tag{2.72} $$

In contrast, the observed velocity $V_O(t)$, which incorporate temporal deformation, is related to the measured velocity $v(t)$ by the following equation

$$ V_O(t) = {}_0\mathcal{D}_t^{1-q} v(t) \tag{2.73} $$

These equations indicate that fractional derivatives function as transformation operators between dynamics observed across varying temporal scales, facilitating the reconstruction fundamental physical quantities in systems where time is effectively stretched or compressed due to internal complexity or environmental heterogeneity.

Thus, fractional operators acquire concrete physical meaning as descriptors of non-local, history-dependent, and scale-invariant processes. The combined geometric and physical viewpoints supply a coherent interpretative basis that links abstract theory with real-world applications.

2.6 Fractional differential equations

Fractional differential equations generalise classical ODEs by allowing derivatives of non-integer order. They provide a more accurate description of systems with memory and hereditary properties phenomena that integer-order models often fail to capture. Consequently, FDEs have become essential tools in various scientific and engineering disciplines, including viscoelasticity, anomalous diffusion, control theory, and biological modelling [67, 68, 69, 70].

In this section, we focus on FDEs defined in the *Caputo sense*, which are particularly suitable for physical applications where initial conditions are given in terms of integer-order derivatives [62, 69].
In the subsequent sections, the Caputo operator of order α denoted as $\mathcal{D}^\alpha$ will be employed.

2.6.1 Fractional differential equations in the Caputo sense

Let us consider the initial value problem defined as

$$\begin{cases} \mathcal{D}^\alpha y(t) = f(t, y(t)) \\ \left.\dfrac{d^j y(t)}{dt^j}\right|_{t=0} = b_j, \quad j = 0, 1, \ldots, n-1 \end{cases} \tag{2.74}$$

where $n - 1 < \alpha \leq n$, $n \in \mathbb{N}^*$.

Existence and uniqueness of the solution

Theorem 2.16. *[20]. Let $\alpha > 0$, $n = \lfloor \alpha \rfloor + 1$, and let $b_0, \ldots, b_{n-1} \in \mathbb{R}$. Given constants $K > 0$ and $h^* > 0$, define the domain*

$$G = [0, h^*] \times [b_0 - K, b_0 + K] \tag{2.75}$$

Suppose $f : G \to \mathbb{R}$ is continuous, and let $M = \sup_{(t,z)\in G} |f(t, z)|$. Then there exists $h > 0$ and a function $y \in C[0, h]$ that solves the Caputo initial value problem of equation ((2.74)). For $\alpha \in (0, 1)$, one may choose

$$h = \min\left\{h^*, \left(\frac{K\Gamma(\alpha + 1)}{M}\right)^{1/\alpha}\right\} \tag{2.76}$$

Moreover, if f satisfies the Lipschitz condition with respect to the second variable, i.e

$$|f(t, y_1) - f(t, y_2)| \leq L|y_1 - y_2|, \quad \forall (t, y_1), (t, y_2) \in G \tag{2.77}$$

for some $L > 0$, then the solution $y \in C[0, h]$ is unique.

The proof relies on the equivalence between the Caputo problem and a Volterra integral equation.

Lemma 2.17. *Under the assumptions of Theorem 2.16, a function $y \in C[0, h]$ is a solution of (2.74) if and only if it satisfies the Volterra integral equation*

$$y(t) = \sum_{k=0}^{n-1} \frac{b_k}{k!} t^k + \frac{1}{\Gamma(\alpha)} \int_0^t (t - \tau)^{\alpha-1} f(\tau, y(\tau)) d\tau \tag{2.78}$$

Lemma 2.18. *Assuming the conditions of Theorem 2.16, the Volterra equation (2.78) possesses a unique solution $y \in C[0, h]$.*

Proof. The proof is divided into two cases.

Case $\alpha > 1$: The kernel $(t-\tau)^{\alpha-1}$ is continuous for $t > \tau$, and the forcing term is continuous. Standard results on Volterra integral equations guarantee existence. Uniqueness follows from the Lipschitz condition (2.77) and successive approximation methods.

Case $\alpha \in (0,1)$: Equation (2.78) reduces to

$$y(t) = b_0 + \frac{1}{\Gamma(\alpha)} \int_0^t (t-\tau)^{\alpha-1} f(\tau, y(\tau)) d\tau \tag{2.79}$$

Define the closed set

$$U = \{y \in C[0,h] : \|y - b_0\|_\infty \le K\} \tag{2.80}$$

where U is bounded, and convex in the Banach space $C[0,h]$ equipped with the Chebyshev norm $\|y\|_\infty = \max_{t\in[0,h]} |y(t)|$. Define the operator $A : U \to C[0,h]$ by

$$(Ay)(t) = b_0 + \frac{1}{\Gamma(\alpha)} \int_0^t (t-\tau)^{\alpha-1} f(\tau, y(\tau)) d\tau \tag{2.81}$$

We show that A maps U into itself. For any $y \in U$ and $t \in [0,h]$

$$\begin{aligned} |(Ay)(t) - b_0| &\le \frac{1}{\Gamma(\alpha)} \int_0^t (t-\tau)^{\alpha-1} |f(\tau, y(\tau))| d\tau \\ &\le \frac{M}{\Gamma(\alpha)} \cdot \frac{t^\alpha}{\alpha} = \frac{Mt^\alpha}{\Gamma(\alpha+1)} \le \frac{Mh^\alpha}{\Gamma(\alpha+1)} \le K \end{aligned} \tag{2.82}$$

Under a specific choice of h, we obtain the inclusion $A(U) \subseteq U$.

Next, we show that $A(U)$ is equicontinuous. For $0 \le t_1 < t_2 \le h$, we may write

$$\begin{aligned} |(Ay)(t_1) - (Ay)(t_2)| \le \frac{1}{\Gamma(\alpha)} \Bigg| &\int_0^{t_1} \left[(t_1-\tau)^{\alpha-1} - (t_2-\tau)^{\alpha-1}\right] f(\tau, y(\tau)) d\tau \\ &+ \int_{t_1}^{t_2} (t_2-\tau)^{\alpha-1} f(\tau, y(\tau)) d\tau \Bigg| \\ \le{}& \frac{M}{\Gamma(\alpha)} \left(\int_0^{t_1} \left[(t_1-\tau)^{\alpha-1} - (t_2-\tau)^{\alpha-1}\right] d\tau + \int_{t_1}^{t_2} (t_2-\tau)^{\alpha-1} d\tau \right) \\ ={}& \frac{M}{\Gamma(\alpha+1)} \left(2(t_2-t_1)^\alpha + t_1^\alpha - t_2^\alpha\right) \end{aligned} \tag{2.83}$$

which tends to zero uniformly as $|t_2 - t_1| \to 0$. Hence, $A(U)$ is equicontinuous and bounded. By the Arzelà–Ascoli theorem [71], $A(U)$ is relatively compact. Since A is continuous, Schauder's fixed-point theorem implies that A has a fixed point in U, i.e., a solution to equation (2.79).

To prove uniqueness under equation (2.77), consider the iterated operator A^j. One can show by induction that for all $j \in \mathbb{N}$

$$\|A^j y - A^j \tilde{y}\|_{L^\infty[0,t]} \le \frac{(Lt^\alpha)^j}{\Gamma(j\alpha+1)} \|y - \tilde{y}\|_{L^\infty[0,t]} \tag{2.84}$$

Taking the supreme over $[0, h]$, we obtain

$$\|A^j y - A^j \tilde{y}\|_\infty \leq \frac{(Lh^\alpha)^j}{\Gamma(j\alpha + 1)} \|y - \tilde{y}\|_\infty \tag{2.85}$$

As $\sum_{j=1}^{\infty} \frac{(Lh^\alpha)^j}{\Gamma(j\alpha+1)} < \infty$, Weissinger's fixed-point theorem [72] ensures that A has a unique fixed point. Therefore, the solution to equation (2.74) is unique. □

2.6.2 Linear Fractional Differential Equations

For linear FDEs, solutions can often be expressed explicitly using the ML function.

Theorem 2.19. *Let $\alpha > 0$, $n = \lfloor \alpha \rfloor + 1$, and $\lambda \in \mathbb{R}$. The solution to the initial value problem*

$$\mathcal{D}^\alpha y(t) = \lambda y(t), \quad y(0) = 1, \quad y^{(k)}(0) = 0, \quad k = 1, \ldots, n-1 \tag{2.86}$$

is given by

$$y(t) = E_\alpha(\lambda t^\alpha), \quad t \geq 0 \tag{2.87}$$

Proof. From Theorem 2.16, there exists a unique solution. It remains to verify that $y(t) = E_\alpha(\lambda t^\alpha)$ satisfies (2.86).

The ML function is defined as

$$E_\alpha(z) = \sum_{j=0}^{\infty} \frac{z^j}{\Gamma(1 + j\alpha)} \tag{2.88}$$

Thus

$$y(t) = \sum_{j=0}^{\infty} \frac{(\lambda t^\alpha)^j}{\Gamma(1 + j\alpha)} \tag{2.89}$$

At $t = 0$, $y(0) = 1$. For $k = 1, \ldots, n-1$, since $k < \alpha j$ for all $j \geq 1$, the k-th derivative of each term (except the constant) vanishes at $t = 0$. Hence, $y^{(k)}(0) = 0$ for $k = 1, \ldots, n-1$.

Now we compute the Caputo derivative

$$\begin{aligned}
\mathcal{D}^\alpha y(t) &= \mathcal{D}^\alpha \left[\sum_{j=0}^{\infty} \frac{\lambda^j t^{\alpha j}}{\Gamma(1 + j\alpha)} \right] \\
&= \sum_{j=0}^{\infty} \frac{\lambda^j}{\Gamma(1 + j\alpha)} \mathcal{D}^\alpha (t^{\alpha j}) \\
&= \sum_{j=1}^{\infty} \frac{\lambda^j}{\Gamma(1 + j\alpha)} \cdot \frac{\Gamma(1 + j\alpha)}{\Gamma(1 + j\alpha - \alpha)} t^{\alpha j - \alpha} \\
&= \sum_{j=1}^{\infty} \frac{\lambda^j t^{\alpha(j-1)}}{\Gamma(1 + \alpha(j-1))} \\
&= \lambda \sum_{m=0}^{\infty} \frac{(\lambda t^\alpha)^m}{\Gamma(1 + m\alpha)} = \lambda y(t)
\end{aligned} \tag{2.90}$$

Interchange of derivative and summation is justified by uniform convergence on compact subsets of $[0, \infty)$. Hence, $y(t)$ satisfies equation (2.86). □

2.7 Dynamical systems of fractional-order

Dynamical systems of fractional-order extend classical integer-order models by incorporating non-local operators that account for memory and hereditary effects in physical processes. FDEs characterise these systems, which are widely used to model intricate phenomena in engineering, physics, biology, and control theory, when traditional models fall short in capturing long-term dependencies and anomalous dynamics. This section delineates the essential framework for the analysis of fractional-order systems using the Caputo operator, emphasising equilibrium points, stability of both linear and nonlinear systems, and the extension of Lyapunov's direct approach.

2.7.1 Equilibrium points

Consider a dynamical system of fractional-order governed by the FDESC

$$\mathcal{D}^\alpha x(t) = f(t, x(t)) \tag{2.91}$$

where $0 < \alpha < 1$, $x \in \mathbb{R}^n$, and $f : \mathbb{R} \times \mathbb{R}^n \to \mathbb{R}^n$ denotes a continuous function.

An equilibria $x^* \in \mathbb{R}^n$ of system (2.91) is defined as a constant solution for which the fractional derivative vanishes, that is

$$\mathcal{D}^\alpha x(t) = 0 \tag{2.92}$$

Substituting the conditions yields

$$f(x^*) = 0 \tag{2.93}$$

The equilibrium points of the system correspond to the roots of the algebraic equation $f(x) = 0$.

2.7.2 Stability analysis of fractional-order dynamics

Stability analysis plays a central role in understanding the long-term behaviour of dynamical systems. For fractional-order systems, the presence of memory effects introduces new challenges and richer dynamics compared to their integer-order counterparts. A number of foundational results have been established for both linear and nonlinear systems [73]. We begin with the stability of linear systems, where a complete characterization is possible, and then extend these ideas to nonlinear systems via linearisation and Lyapunov methods.

Stability of fractional-order linear systems: The asymptotic stability of linear fractional-order systems was decisively characterized by Matignon [73], who provided a necessary and sufficient condition based on the argument of the eigenvalues of the system matrix. This result has become a cornerstone in the theory of fractional dynamical systems and applies to systems of order $0 < \alpha \leq 1$. Subsequent works have extended and refined these criteria for various classes of systems.

We analyse the autonomous linear system

$$\begin{cases} \mathcal{D}^\alpha x(t) = Ax(t) \\ x(t_0) = x_0 \end{cases} \tag{2.94}$$

where $A \in \mathbb{R}^{n\times n}$. The stability of this system is determined entirely by the spectral properties of A.

Theorem 2.20. *The system (2.94) is asymptotically stable if and only if*

$$|arg(spec(A))| > \frac{\alpha\pi}{2} \tag{2.95}$$

where $spec(A)$ denotes the set of eigenvalues of A, and $arg(\lambda)$ is the principal argument of $\lambda \in \mathbb{C}$.

This condition requires all eigenvalues to lie outside the so-called *stability sector* in the complex plane, which widens as α increases. When $\alpha = 1$, it reduces to the classical requirement that all eigenvalues have negative real parts.

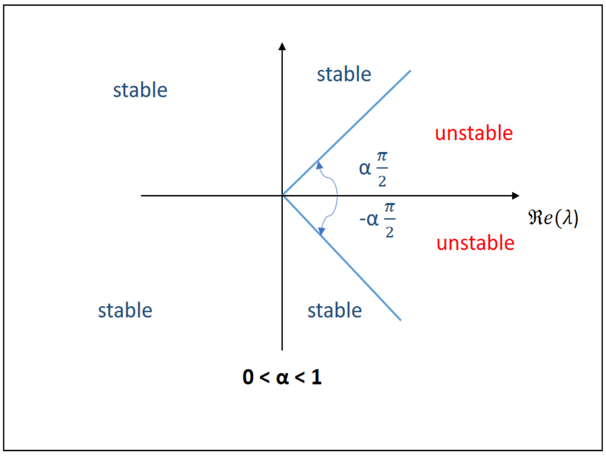

Figure 2.4: The region of stability for systems of fractional-order.

Remark 2.21.

Fractional-order systems may also be defined for orders $\alpha \in (1, 2)$, which arise in models of super-diffusion and viscoelastic materials..

The stability theory for such systems involves modified conditions and is beyond the scope of this work.

Stability of nonlinear systems of fractional-order: we now consider the nonlinear autonomous system

$$^{C}\mathcal{D}^{\alpha}x(t) = f(x(t)) \tag{2.96}$$

where $f : \mathbb{R}^n \to \mathbb{R}^n$ is nonlinear and continuous, and $0 < \alpha < 1$.

To analyse local stability near an equilibrium point, we introduce the following concepts.

Definition 2.22 (**Hyperbolic Equilibrium Point**)**.** Let E be an equilibrium point of system (2.96). If all eigenvalues λ of the Jacobian matrix $Df(E)$ satisfy $\lambda \neq 0$ and $|\arg(\lambda)| \neq \frac{\alpha\pi}{2}$, then E is referred to as hyperbolic equilibrium.

Definition 2.23 (**Topological Equivalence**)**.** Let f and g be continuous vector fields on open sets $U, V \subseteq \mathbb{R}^n$, generating flows $\phi_{t,f}$ and $\phi_{t,g}$, respectively. If there exists a homeomorphism $h : U \to V$ such that

$$h \circ \phi_{t,f} = \phi_{t,g} \circ h \tag{2.97}$$

in a neighbourhood of $y_0 \in U$, then f and g are *locally topologically equivalent.* If this holds globally, they are globally equivalent.

The following result establishes a fractional-order analogy of the Hartman–Grobman theorem, allowing linearisation-based stability analysis.

Theorem 2.24. *If the origin O is a hyperbolic equilibrium point of system (2.96), then the nonlinear vector field $f(x)$ is locally topologically equivalent to its linearization $Df(O)\,x$ in a neighbourhood of O.*

Combining Theorems 2.20 and 2.24, we conclude that local asymptotic stability of an equilibrium E of system (2.96) holds if the Jacobian matrix $Df(E)$ satisfy

$$|\arg(\lambda)| > \frac{\alpha\pi}{2} \tag{2.98}$$

2.7.3 Fractional-order extension of Lyapunov's direct method

Lyapunov's direct method provides a powerful framework for stability analysis without explicitly solving the system dynamics. In the context of fractional-order systems, this method can be extended by appropriately defining fractional derivatives of Lyapunov functions. Unlike integer-order systems, the resulting stability is often characterized in terms of Mittag-Leffler decay rather than exponential convergence.

Theorem 2.25. *Consider $x = 0$ as an equilibrium of the system given by equation (2.91), and let $D \subseteq \mathbb{R}^n$ be a domain containing the origin. Suppose there exists a continuously differentiable function $V(t, x(t)) : [0, \infty) \times D \to \mathbb{R}$, locally Lipschitz in x, such that*

$$\alpha_1 \|x\|^a \le V(t, x(t)) \le \alpha_2 \|x\|^{ab} \tag{2.99}$$

$$^{C}\mathcal{D}^{\beta} V(t, x(t)) \le -\alpha_3 \|x\|^{ab} \tag{2.100}$$

for all $t \ge 0$, $x \in D$, where $\beta \in (0, 1)$, and $\alpha_1, \alpha_2, \alpha_3, a, b > 0$ are constants. Then, the equilibrium $x = 0$ is asymptotically stable. If these conditions hold for all $x \in \mathbb{R}^n$, then the origin is globally asymptotically stable.

Theorem 2.26. *Let $x = 0$ be an equilibrium point of system (2.96), with $\alpha \in (0, 1)$, and suppose $f(x, t)$ satisfies a Lipschitz condition with constant L. If there exists a Lyapunov function $V(t, x)$ satisfying*

$$\alpha_1 \|x\| \le V(t, x) \le \alpha_2 \|x\| \tag{2.101}$$

$$\dot{V}(t, x) \le -\alpha_3 \|x\| \tag{2.102}$$

where $\alpha_1, \alpha_2, \alpha_3 > 0$ and $\dot{V} = \frac{dV}{dt}$, then the state trajectory satisfies

$$\|x(t)\| \le \frac{V(0, x(0))}{\alpha_1} E_{1-\alpha}\left(-\frac{\alpha_3}{\alpha_2} t^{1-\alpha}\right) \tag{2.103}$$

with $E_{1-\alpha}(\cdot)$ being the ML function. Consequently, the equilibrium $x = 0$ is asymptotically stable.

Remark 2.27. For proofs and further details, see [74].

2.8 Numerical methods for Caputo FDEs

Analytical solutions to fractional differential equations (FDEs) are available only in limited cases. Consequently, numerical methods play a pivotal role in the simulation and analysis of fractional-order systems. In this section, we present three widely used numerical techniques for solving Caputo-type FDEs: the Grünwald–Letnikov method, the Adomian Decomposition Method (ADM), and the Adams–Bashforth–Moulton predictor–corrector scheme. Each method offers distinct advantages in terms of implementation, accuracy, and applicability, and is suitable for different classes of problems.

2.8.1 Grünwald–Letnikov method

The GLM provides a direct discretization of the fractional derivative. For the Caputo derivative $\mathcal{D}^\alpha y(t)$ with $0 < \alpha < 1$, the approximation at time $t = t_k = kh$ is given by

$$ {}^{C}\mathcal{D}^\alpha y(t_k) \approx \frac{1}{h^\alpha} \sum_{j=0}^{k} (-1)^j \binom{\alpha}{j} y(t_k - jh) \tag{2.104} $$

the binomial coefficients are

$$ \binom{\alpha}{j} = \frac{\Gamma(\alpha+1)}{\Gamma(j+1)\Gamma(\alpha-j+1)} $$

This approach is straightforward to implement and efficient for brief time periods. Nevertheless, it has cumulative truncation errors and exhibit inadequate stability during long integration intervals, particularly for highly nonlinear systems. Furthermore, the approach necessitates storing all previous states, resulting in high computational expense and memory consumption.

2.8.2 Adomian Decomposition Method

The ADM expresses the solution as an infinite series

$$ y(t) = \sum_{n=0}^{\infty} y_n(t) \tag{2.105} $$

and decomposes the nonlinear term $f(t, y(t))$ into a series of *Adomian polynomials*

$$ f(t, y) = \sum_{n=0}^{\infty} A_n(y_0, \ldots, y_n) \tag{2.106} $$

The components $y_n(t)$ are determined recursively. Given initial conditions, we set $y_0(t)$ as the solution to the homogeneous problem or the initial data, and subsequent terms are computed via

$$ y_{n+1}(t) = \mathcal{I}^\alpha A_n(t), \quad n \geq 0 \tag{2.107} $$

where $\mathcal{I}^\alpha$ denotes the Riemann–Liouville fractional integral of order α. The method yields a rapid convergent series for many nonlinear problems and avoids linearisation or discretization. However, computing Adomian polynomials can be cumbersome for complex nonlinearities, and convergence is not guaranteed for all systems.

2.8.3 Adams–Bashforth–Moulton Method

The ABM method is a predictor–corrector scheme widely used for its accuracy and stability in solving nonlinear FDEs. It combines an explicit predictor step with an implicit corrector to improve precision.

Predictor step:

$$y_{k+1}^{p} = \sum_{j=0}^{n-1} \frac{t_{k+1}^{j}}{j!} y_0^{(j)} + \frac{1}{\Gamma(\alpha)} \sum_{j=0}^{k} b_{j,k+1} f(t_j, y_j) \tag{2.108}$$

where $b_{j,k+1} = \frac{h^\alpha}{\alpha}\left((k+1-j)^\alpha - (k-j)^\alpha\right)$, and y_{k+1}^p is the predicted value.

Corrector step:

$$y_{k+1} = \sum_{j=0}^{n-1} \frac{t_{k+1}^{j}}{j!} y_0^{(j)} + \frac{1}{\Gamma(\alpha)} \left(\sum_{j=0}^{k} a_{j,k+1} f(t_j, y_j) + a_{k+1,k+1} f(t_{k+1}, y_{k+1}^p) \right) \tag{2.109}$$

where the coefficients $a_{j,k+1}$ depend on the quadrature weights of the fractional integral.

This method is highly accurate for smooth solutions and exhibits good convergence properties (typically $O(h^{\min(2,\alpha+1)})$). It is particularly effective for nonlinear systems and is one of the most reliable methods for numerical simulation of Caputo FDEs. However, it requires iterative correction and storage of all past function values, increasing computational complexity. Owing to these advantages, this is the method adopted throughout this thesis for the numerical simulation of the fractional-order systems under study.

2.9 Conclusion

This chapter has consolidated the fundamental concepts and methods of fractional calculus, demonstrating its power as an analytical framework that extends well beyond classical calculus. In this context the main principles have emerged, and the main formulations of fractional integration and differentiation were presented, contributing to the coherence of the theory.

The interpretations of fractional operators emphasised their ability to model physical processes exhibiting memory and hereditary effects, while the study of fractional differential equations and their numerical resolution illustrated the practical methodsfor building such models. The final analysis of fractional-order dynamic systems revealed the impact of fractional operators on stability theory, equilibrium analysis, and system behaviour.

In conclusion, the chapter has developed from foundational mathematics to interpretive and computational perspectives, displaying fractional calculus as both theoretically robust and practically vital. It laid the groundwork for the systematic study of fractional-order systems used in the following chapters.

Chapter 3

Analysis of a four-dimensional hyperchaotic system exhibiting exponential nonlinearity

Summary

This chapter introduces a novel four dimensional hyperchaotic system with exponential nonlinearity and develops an adaptive control strategy for its stabilisation. It further presents an adaptive RBFNN- based complete synchronisation scheme and demonstrate the system's application in entropy-based key generation for secure digital wallets, highlighting its practical cryptographic framework.

Contents

3.1 Introduction

This chapter presents a novel four-dimensional hyperchaotic system generated from the modified three-dimensional Lü system [75], incorporating a nonlinear term of exponential type. The dynamical behaviour of the suggested system is thoroughly investigated, focusing on equilibrium points, Lyapunov exponents spectrum, and phase-space trajectories to confirm the hyperchaotic behaviour.

An adaptive control approach is subsequently established to stabilise the system despite parametric uncertainty, leveraging Lyapunov-based design to ensure asymptotic convergence. A dedicated active control scheme is then formulated to achieve complete synchronisation between two identical instances of the system. Theoretical derivations are supported by computational results, that verify the efficacy and robustness of the proposed control methodologies.

To demonstrate the practical relevance of our proposed model, an entropy based key generation scheme is implemented to produce pseudo-random cryptographic keys. This work provides a rigorous foundation for the design, control, and secure application of higher-dimensional chaotic systems with complex nonlinearities.

3.2 A novel hyperchaotic system with exponential nonlinearity

The Lü system, introduced in [75], is a well-known three-dimensional chaotic dynamical system expressed by the following ODEs

$$\begin{cases} \dot{x}_1 = a(x_2 - x_1) \\ \dot{x}_2 = -x_1x_3 + bx_2 \\ \dot{x}_3 = x_1x_2 - cx_3 \end{cases} \tag{3.1}$$

where x_1, x_2, and x_3 are state variables, and a, b, c are positive real parameters. When parameter values are set to $a = 36$, $b = 3$, and $c = 20$, the system exhibits a canonical chaotic attractor, as demonstrated in [75].

It is established that for an autonomous system to exhibit hyperchaotic behaviour, two fundamental conditions must be satisfied:

1. The system must be at least four-dimensional (i.e., described by at least four first-order differential equations).

2. The system must possess at least two positive Lyapunov exponents, with the sum of all Lyapunov exponents being negative, ensuring dissipativity.

Motivated by these criteria, we propose a novel four-dimensional hyperchaotic system derived from a modification of the Lü system [75]. The new system incorporates an exponential nonlinearity and an additional state variable to enable hyperchaos. The proposed system is described by

$$\begin{cases} \dot{x}_1 = a(x_2 - x_1) + x_4 \\ \dot{x}_2 = -x_1x_3 + bx_2 \\ \dot{x}_3 = -1 + \exp(x_1x_2) - cx_3 \\ \dot{x}_4 = dx_1 \end{cases} \tag{3.2}$$

where x_1, x_2, x_3, x_4 are the state variables, and a, b, c, d are positive real parameters. This incorporation of the exponential term $\exp(x_1 x_2)$ results in a significant nonlinearity enhancing the system's complexity and enabling the emergence of hyperchaotic behaviour.

Hyperchaotic behaviour is observed in system (3.2) for a range of parameter values. Specifically, numerical analysis confirms hyperchaos when

$$(a, b, d) = (25, 20, 8) \quad \text{and} \quad c \in [0.5, 2.5] \tag{3.3}$$

Numerical integration is performed using the fourth-order Runge-Kutta method is employed with a sufficiently small integration step size. The initial states are set as

$$x_1(0) = x_2(0) = x_3(0) = x_4(0) = 0.001 \tag{3.4}$$

where the parameter's set is specified as

$$(a, b, c, d) = (25, 20, 1.78, 8) \tag{3.5}$$

Under these conditions, the system appears to exhibit a hyperchaotic attractor, as illustrated in Figure 3.1, which presents the projections of the phase portrait of system (3.2) in the $x_1 - x_2$ and $x_1 - x_3$ planes. Figure 3.2 depicts the three-dimensional projection of the attractor, further suggesting the presence of hyperchaotic dynamics.

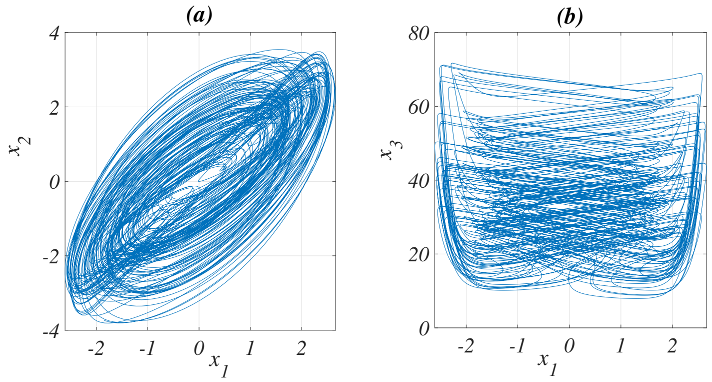

Figure 3.1: Projections of the phase portrait of system:
(a) (3.2) in the $x_1 - x_2$ plane and (b) in the $x_1 - x_3$ plane.

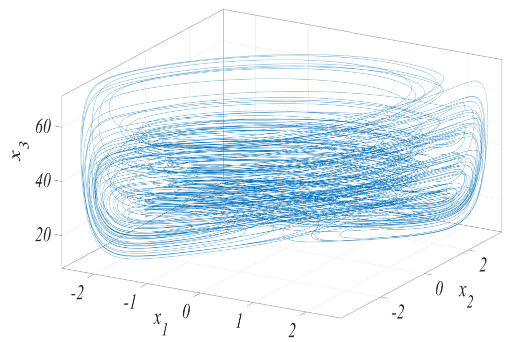

Figure 3.2: Three-dimensional projection of the attractor of system (3.2).

Additionally, Figure 3.3 displays both the two- and three-dimensional projections of the system's (3.2) Poincaré map. It depicts discrete trajectory intersections with a selected hypersurface. The irregular and dispersed point distribution in both projections suggests the presence of multiple positive Lyapunov exponents, indicating sensitive dependence on initial conditions and complex phase-space evolution characteristic of hyperchaotic behaviour. However, further studies and analyses will confirm this assumption. The proposed system demonstrates the following dynamical properties

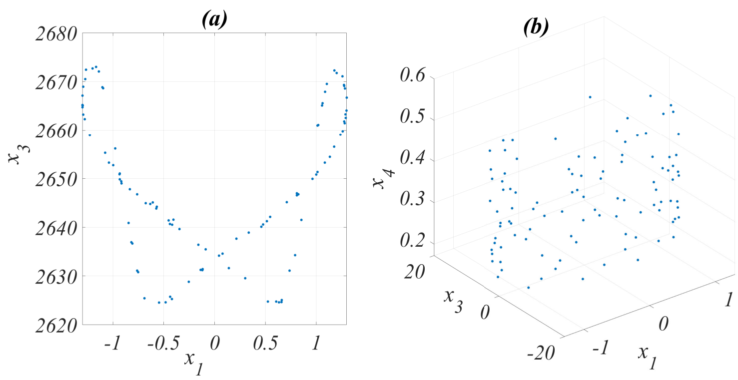

Figure 3.3: (a) Two-dimensional projection and (b) three-dimensional projection of the Poincaré map of system (3.2).

Symmetry: The dynamical system (3.2) admits a discrete reflection symmetry described by the transformation

$$(x_1, x_2, x_3, x_4) \mapsto (-x_1, -x_2, x_3, -x_4) \tag{3.6}$$

To establish this, consider the vector field

$$f = (\dot{x}_1, \dot{x}_2, \dot{x}_3, \dot{x}_4)^\top \tag{3.7}$$

Applying the transformation (3.6), we obtain

$$\dot{x}_1 \mapsto ax_1 - ax_2 - x_4 = -\dot{x}_1 \tag{3.8}$$
$$\dot{x}_2 \mapsto -(-x_1)(x_3) + b(-x_2) = -(-x_1x_3 + bx_2) = -\dot{x}_2 \tag{3.9}$$
$$\dot{x}_3 \mapsto -1 + \exp((-x_1)(-x_2)) - cx_3 = -1 + \exp(x_1x_2) - cx_3 = \dot{x}_3 \tag{3.10}$$
$$\dot{x}_4 \mapsto d(-x_1) = -dx_1 = -\dot{x}_4 \tag{3.11}$$

Hence, the transformation on the state variables induces

$$f(x_1, x_2, x_3, x_4)^T \mapsto (-\dot{x}_1, -\dot{x}_2, \dot{x}_3, -\dot{x}_4) \tag{3.12}$$

which is precisely the vector field evaluated at the reflected state $(-x_1, -x_2, x_3, -x_4)$. In other words, the flow commutes with the involution, so that solutions are mapped to solutions under this coordinate reflection.

Geometrically, this symmetry corresponds to a reflection of the phase space with respect to the x_3-axis. Consequently, if $(x_1(t), x_2(t), x_3(t), x_4(t))$ is a trajectory of (3.2), then the reflected curve $(-x_1(t), -x_2(t), x_3(t), -x_4(t))$ is also a trajectory. This implies that equilibria, periodic orbits, and chaotic attractors necessarily appear in symmetric pairs, unless initial conditions lie on invariant subspaces preserved by the reflection.

Dissipativity: Let $x = (x_1, x_2, x_3, x_4)^\top \in \mathbb{R}^4$. Then system (3.2) can be expressed in vector form as

$$\dot{x} = f(x) \tag{3.13}$$

where

$$\begin{cases} f_1(x_1,\ x_2,\ x_3,\ x_4) = a(x_2 - x_1) + x_4 \\ f_2(x_1,\ x_2,\ x_3,\ x_4) = -x_1x_3 + bx_2 \\ f_3(x_1,\ x_2,\ x_3,\ x_4) = -1 + \exp(x_1x_2) - cx_3 \\ f_4(x_1,\ x_2,\ x_3,\ x_4) = dx_1 \end{cases} \tag{3.14}$$

The divergence of the vector field f, defined as $\nabla \cdot f = \sum_{i=1}^4 \frac{\partial f_i}{\partial x_i}$, is computed as follows

$$\begin{aligned} \nabla \cdot f &= \frac{\partial}{\partial x_1}\left(a(x_2 - x_1) + x_4\right) + \frac{\partial}{\partial x_2}\left(-x_1x_3 + bx_2\right) + \frac{\partial}{\partial x_3}\left(-1 + \exp(x_1x_2) - cx_3\right) + \frac{\partial}{\partial x_4}\left(dx_1\right) \\ &= -a + b - c + 0 \\ &= -a + b - c \end{aligned} \tag{3.15}$$

By Liouville's theorem, the time evolution of an infinitesimal volume element $V(t)$ in phase space obeys

$$\frac{d}{dt}V(t) = (\nabla \cdot f)\, V(t) \tag{3.16}$$

which has the solution

$$V(t) = V_0 \exp\left((-a + b - c)\, t\,\right) \tag{3.17}$$

where $V_0 = V(0)$. When $\nabla . f < 0$, i.e., when $a > b - c$, the volume element contracts exponentially as $t \to \infty$. Hence, the system is dissipative, and all trajectories asymptotically approach a bounded attractor of zero measure in the phase space.

Equilibrium points and stability: Equilibrium analysis of the system (3.2) necessitates solving $f(x) = 0$, yielding

$$a(x_2 - x_1) + x_4 = 0 \tag{3.18a}$$

$$-x_1x_3 + bx_2 = 0 \tag{3.18b}$$

$$-1 + \exp(x_1x_2) - cx_3 = 0 \tag{3.18c}$$

$$dx_1 = 0 \tag{3.18d}$$

Since $d > 0$, equation (3.18d) implies $x_1 = 0$. Substituting into equation (3.18b), it follows that $x_2 = 0$, hence $x_4 = 0$ by substituting in (3.18a). Finally, equation (3.18c) yields to $x_3 = 0$. Therefore, the system admits a unique equilibrium point at the origin $P = (0, 0, 0, 0)$.
To examine the local stability of P, we compute the Jacobian matrix

$$J(x) = Df(x) = \begin{pmatrix} -a & a & 0 & 1 \\ -x_3 & b & -x_1 & 0 \\ x_2e^{x_1x_2} & x_1e^{x_1x_2} & -c & 0 \\ d & 0 & 0 & 0 \end{pmatrix} \tag{3.19}$$

Evaluating at P yields

$$J(0) = \begin{pmatrix} -a & a & 0 & 1 \\ 0 & b & 0 & 0 \\ 0 & 0 & -c & 0 \\ d & 0 & 0 & 0 \end{pmatrix} \tag{3.20}$$

The characteristic polynomial of $J(0)$ is given by

$$P(\lambda) = (\lambda - b)(\lambda + c)\left(\lambda^2 + a\lambda - d\right) \tag{3.21}$$

The corresponding eigenvalues are calculated as

$$\begin{aligned} \lambda_1 &= -c, & \lambda_2 &= -\tfrac{a}{2} - \tfrac{1}{2}\sqrt{a^2+4d}, \\ \lambda_3 &= b, & \lambda_4 &= -\tfrac{a}{2} + \tfrac{1}{2}\sqrt{a^2+4d}. \end{aligned} \tag{3.22}$$

The stability of the equilibrium point is determined by the signs of the eigenvalues. Since $c > 0$ and $a, d > 0$, it follows immediately that $\lambda_1 < 0$ and $\lambda_2 < 0$. The eigenvalue $\lambda_3 = b$ is strictly positive, which already guarantees instability. Finally, the fourth eigenvalue satisfies $\lambda_4 = -\frac{a}{2} + \frac{1}{2}\sqrt{a^2+4d}$ and is also strictly positive because $\sqrt{a^2+4d} > a$. Hence, the origin possesses two negative and two positive eigenvalues. It is therefore a *saddle point of index two* and locally unstable. This configuration, with stable and unstable directions coexisting, underpins the system's capacity to generate complex dynamics, including hyperchaotic behaviour.

Lyapunov exponents: Lyapunov exponents characterise the average exponential divergence or convergence of neighbouring trajectories in phase space and provide a rigorous diagnostic of hyperchaotic dynamics. The Lyapunov spectrum of system in equation (3.2) was computed numerically following the procedure by Wolf et al.[76].

Figure 3.4 illustrates the three largest Lyapunov exponents as functions of the parameter $c \in [0.5, 4.5]$, with the remaining parameters as in equation 3.3.

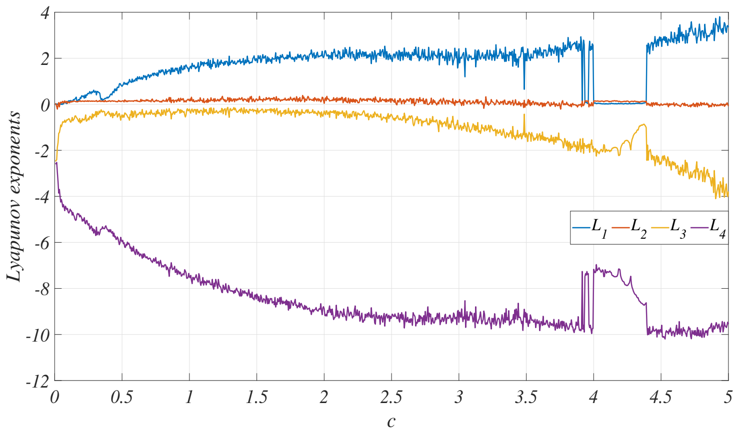

Figure 3.4: Variation of the lyapunov exponents of system (3.2) with respect to the parameter c.

At the parameter values as in (3.5), the computed Lyapunov exponents are acquired as

$$L_1 = 1.86, \quad L_2 = 0.27, \quad L_3 = 0.00, \quad \textit{and } L_4 = -8.59 \tag{3.23}$$

The coexistence of two positive Lyapunov exponents and a negative sum of the spectrum confirms that the system is simultaneously hyperchaotic and dissipative, i.e.

$$L_1 > 0, \quad L_2 > 0, \qquad \sum_{i=1}^{4} L_i < 0 \tag{3.24}$$

The Kaplan–Yorke dimension, estimating the attractor's fractal dimension, is

$$D_{\mathrm{KY}} = k + \frac{\sum_{i=1}^{k} L_i}{|L_{k+1}|} = 3 + \frac{L_1 + L_2 + L_3}{|L_4|} \approx 3.25 \tag{3.25}$$

confirms further the hyperchaotic dynamics.

3.3 Design of an adaptive control strategy for the proposed hyperchaotic system

The following section develops an adaptive control strategy to stabilise the proposed hyperchaotic system despite parameter uncertainties. The control design is established using the Lyapunov stability theory and guarantees global and exponential convergence of the system trajectories to the origin.

Consider the controlled version of system in equation (3.2), given by

$$\begin{cases} \dot{x}_1 = a(x_2 - x_1) + x_4 + u_1 \\ \dot{x}_2 = -x_1 x_3 + b x_2 + u_2 \\ \dot{x}_3 = -1 + \exp(x_1 x_2) - c x_3 + u_3 \\ \dot{x}_4 = d x_1 + u_4 \end{cases} \tag{3.26}$$

where $x = (x_1, x_2, x_3, x_4)^\top \in \mathbb{R}^4$ are the system's state , $a, b, c, d > 0$ are unknown parameters, and u_i, $i = 1, \ldots, 4$, are adaptive control inputs to be designed. Let $\hat{a}(t)$, $\hat{b}(t)$, $\hat{c}(t)$, $\hat{d}(t)$ denote the estimates of the respective parameters.

We propose the following adaptive control law

Hypothesis: Let us assume the following conditions

1. The the adaptive control laws are selected as

$$\begin{cases} u_1 = -\hat{a}(x_2 - x_1) - x_4 - \kappa_1 x_1 \\ u_2 = x_1 x_3 - \hat{b} x_2 - \kappa_2 x_2 \\ u_3 = 1 - \exp(x_1 x_2) + \hat{c} x_3 - \kappa_3 x_3 \\ u_4 = -\hat{d} x_1 - \kappa_4 x_4 \end{cases} \tag{3.27}$$

   where κ_1, κ_2, κ_3, and κ_4 denote positive gains.

2. The corresponding parameter update laws are defined by

$$\begin{cases} \dot{\hat{a}} = x_1 x_2 - x_1^2 \\ \dot{\hat{b}} = x_2^2 \\ \dot{\hat{c}} = -x_3^2 \\ \dot{\hat{d}} = x_1 x_4 \end{cases} \tag{3.28}$$

   with arbitrary initial conditions $\hat{a}(0)$, $\hat{b}(0)$, $\hat{c}(0)$, and $\hat{d}(0)$.

Let the parameter estimation errors be defined by

$$
\begin{aligned}
e_a &= a - \hat{a} = -\dot{\hat{a}} \qquad & e_b &= b - \hat{b} = -\dot{\hat{b}} \\
e_c &= c - \hat{c} = -\dot{\hat{c}} \qquad & e_d &= d - \hat{d} = \dot{\hat{d}}
\end{aligned}
\tag{3.29}
$$

3.3.1 Stability analysis and numerical simulations

Theorem 3.1. *The hyperchaotic system (3.26) is globally stabilised at the origin under the control law (3.27) with parameter adaptation (3.28).*

Proof. Substituting the control law (3.27) into (3.26), we obtain

$$
\begin{cases}
\dot{x}_1 = e_a(x_2 - x_1) - k_1 x_1 \\
\dot{x}_2 = e_b x_2 - k_2 x_2 \\
\dot{x}_3 = -e_c x_3 - k_3 x_3 \\
\dot{x}_4 = e_d x_1 - k_4 x_4
\end{cases}
\tag{3.30}
$$

where e_a, e_b, e_c, e_d are the parameter estimation errors.
To analyse the stability of the equilibrium $(x, e_a, e_b, e_c, e_d) = (0, 0, 0, 0, 0)$, consider the continuously differentiable, positive-definite Lyapunov function candidate

$$
V = \frac{1}{2}\left(x_1^2 + x_2^2 + x_3^2 + x_4^2 + e_a^2 + e_b^2 + e_c^2 + e_d^2\right) \tag{3.31}
$$

defined on $\mathbb{R}^8$.

by differentiating V along the trajectories of (3.30) yield

$$
\begin{aligned}
\dot{V} &= x_1\dot{x}_1 + x_2\dot{x}_2 + x_3\dot{x}_3 + x_4\dot{x}_4 + e_a\dot{e}_a + e_b\dot{e}_b + e_c\dot{e}_c + e_d\dot{e}_d \\
&= x_1\left[e_a(x_2 - x_1) - k_1x_1\right] + x_2\left[e_b x_2 - k_2x_2\right] + x_3\left[-e_c x_3 - k_3 x_3\right] + x_4\left[e_d x_1 - k_4 x_4\right] \\
&\quad - e_a\dot{\hat{a}} - e_b\dot{\hat{b}} - e_c\dot{\hat{c}} - e_d\dot{\hat{d}}
\end{aligned}
\tag{3.32}
$$

Substituting the adaptation laws (3.28) into (3.32), and simplifying

$$
\begin{aligned}
\dot{V} &= e_a(x_1x_2 - x_1^2) - k_1x_1^2 + e_bx_2^2 - k_2x_2^2 - e_cx_3^2 - k_3x_3^2 + e_dx_1x_4 - k_4x_4^2 \\
&\quad - e_a(x_1x_2 - x_1^2) - e_b(x_2^2) - e_c(-x_3^2) - e_d(x_1x_4) \\
&\leq -k_1x_1^2 - k_2x_2^2 - k_3x_3^2 - k_4x_4^2 \\
&\leq \sum i = 1^4 k_i x_i^2 \\
&\leq -k\sum_{i=1}^{4} x_i^2
\end{aligned}
$$

where $k \leq min\ k_i\ , i = 1, .., 4$, and $\dot{V}$ is definite negative function. Therefore, $V(t)$ is non-increasing and bounded. Hence

$$
\dot{V} \leq -k\,||x||^2 \tag{3.33}
$$

Since $\dot{V} \leq 0$, $V(t)$ converges as $t \to \infty$. Moreover, $\dot{V} \in L^1[0, \infty)$. The uniform continuity of $\dot{V}$ follows from the boundedness of system signals and their derivatives. As a result $\dot{V}(t) \to 0$ as $t \to \infty$, which implies

$$
\lim_{t\to\infty} x_i(t) = 0, \quad i = 1, 2, 3, 4 \tag{3.34}
$$

Therefore, the origin is globally stable.

This completes the proof.

Remark. The result above is asymptotic. Exponential convergence would follow under the additional assumption that the k_i admit a uniform lower bound and that the parameter-error terms can be related to the state energy (for example, if there exists $\alpha > 0$ with $\dot{V} \leq -\alpha \sum_{i=1}^{4} x_i^2 \leq -\beta V$ for some $\beta > 0$). Such a stronger inequality requires extra conditions on the adaptation dynamics and is not implied by the preceding lines without further hypotheses. □

To validate the theoretical results obtained in the previous section, we apply the control law (3.27) to stabilise the system.

The dynamics of the coupled system (3.26) subject to the control input (3.27), were numerically integrated within a MATLAB implementation of the standard Runge–Kutta integration architecture of the fourth order, employing a uniform step size $h = 0.02$.

The system parameters are chosen according to the hyperchaotic case (3.5), while the control gains are set to

$$k_i = 0.5, \quad i = 1, 2, 3, 4 \tag{3.35}$$

The initial state vector is specified as follows

$$(x_1(0), x_2(0), x_3(0), x_4(0)) = (1,\ 0.09,\ 1,\ 1) \tag{3.36}$$

and the initial conditions for the parameter estimates are given by

$$(\hat{a}(0), \hat{b}(0), \hat{c}(0), \hat{d}(0)) = (25.9,\ 19,\ 3,\ 10) \tag{3.37}$$

Figure 3.5 depicts the trajectories of the system states x_1, x_2, x_3, x_4, which asymptotically converge to the origin, thereby confirming the stabilization of the system. Figure 3.6 depicts the evolution of the adaptive parameter estimates, which successfully converge toward their true values, demonstrating the effectiveness of the proposed identification scheme.

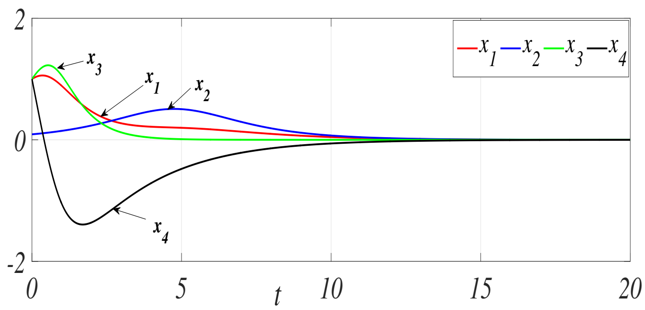

Figure 3.5: Time-history of the controlled hyperchaotic system (3.26).

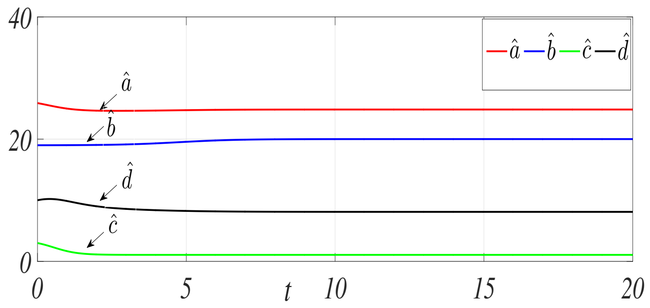

Figure 3.6: Temporal evolution of the parameter estimates (3.28).

3.4 Adaptive RBF-based complete synchronisation scheme for integer-order nonlinear systems

This section introduces the Radial Basis Function neural network (RBFNN) approximation framework and develops an adaptive controller to achieve complete synchronisation between the drive and response dynamics of the proposed four-dimensional integer-order hyperchaotic system. The analysis employs Lyapunov stability theory, and the resulting controller guarantees asymptotic convergence of the synchronisation error.

3.4.1 RBFNN and their approximation capability

RBFNN are widely used in nonlinear identification and adaptive control due to their universal approximation capability and simple structure. An RBFNN consists of a nonlinear hidden layer followed by a linear output layer. For an input vector

$$X = [X_1, X_2, \ldots, X_n]^T \tag{3.38}$$

the output of the j-th hidden neuron is expressed by the Gaussian radial basis function

$$h_j(X) = \exp\left(-\frac{\|X - c_j\|^2}{2b_j^2}\right), \qquad j = 1, \ldots, m \tag{3.39}$$

where $c_j \in \mathbb{R}^n$ is the centre and $b_j > 0$ is its width. Collecting all activations yields

$$H = [\, h_1, h_2, \ldots, h_m \,]^T \tag{3.40}$$

The network output is a linear combination of these activations:

$$y_i = W_i^T H, \qquad i = 1, \ldots, n \tag{3.41}$$

where $W_i = [\, w_{i1}, \ldots, w_{im} \,]^T \in \mathbb{R}^m$ is the weight vector. Thus, an RBF network approximates a nonlinear function as

$$f(X) \approx \hat{f}(X) = W^T H \tag{3.42}$$

3.4.2 Drive-response synchronisation schemes

In this context, we consider a classical drive–response configuration. The drive system is the developed four-dimensional hyperchaotic model introduced previously and written as

$$\begin{cases} \dot{x}_1 = a(x_2 - x_1) + x_4 \\ \dot{x}_2 = -x_1 x_3 + b x_2 \\ \dot{x}_3 = -1 + e^{x_1 x_2} - c x_3 \\ \dot{x}_4 = d x_1 \end{cases} \tag{3.43}$$

with $a, b, c, d \in \mathbb{R}$ denotes the system's parameters.

The response system is given by

$$\begin{cases} \dot{y}_1 = a(y_2 - y_1) + y_4 + u_1 \\ \dot{y}_2 = -y_1 y_3 + b y_2 + u_2 \\ \dot{y}_3 = -1 + e^{y_1 y_2} - c y_3 + u_3 \\ \dot{y}_4 = d y_1 + u_4 \end{cases} \tag{3.44}$$

where u_i, $i = 1, .., 4$ denote the control inputs.

Our objective is to achieve complete synchronisation between the systems in equations (3.43) and (3.44) respectively, defined by the convergence as

$$\lim_{t \to \infty} \|e(t)\| = 0, \qquad e = y - x \tag{3.45}$$

Subtracting (3.43) from (3.44) yields the error dynamics

$$\dot{e}_i = f_i(e, x, y) + u_i, \qquad i = 1, \ldots, 4 \tag{3.46}$$

The nonlinear functions f_i are explicitly determinable but algebraically cumbersome. To avoid relying on a precise analytical model, we adopt RBFNN to approximate these unknown nonlinearities. This approach allows the design of adaptive laws that update the RBF weights in real time, ensuring that the controller compensates for the unmodelled dynamics while preserving stability of the synchronisation error system.

3.4.3 RBF approximation of the error states

Each nonlinear term is approximated as

$$\hat{f}_i = W_i^T H \tag{3.47}$$

with H generated from measurable variables (e, x, y).

Let W_i^* be the ideal weights satisfying

$$f_i = W_i^{*T} H + r_i \tag{3.48}$$

where r_i is the bounded approximation error. Define the weight estimation error

$$\tilde{W}_i = W_i - W_i^* \tag{3.49}$$

Substituting (3.47)–(3.49) into (3.46) yields

$$\dot{e}_i = W_i^T H - \tilde{W}_i^T H + r_i + u_i \tag{3.50}$$

3.4.4 Adaptive Synchronisation Controller and stability analysis

The adaptive RBF controller is chosen as

$$u_i = -W_i^T H - k_i e_i, \qquad k_i > 0 \tag{3.51}$$

which combines neural compensation with linear stabilising feedback.

The parameter adjustment law is the gradient update

$$\dot{W}_i = \ell_i e_i H, \qquad \ell_i > 0 \tag{3.52}$$

Consider the Lyapunov function

$$V = \frac{1}{2}\sum_{i=1}^{4} e_i^2 + \frac{1}{2}\sum_{i=1}^{4} \frac{1}{\ell_i}\tilde{W}_i^T \tilde{W}_i \tag{3.53}$$

Differentiating and substituting equations ((3.50))–((3.52)) yields

$$\dot{V} = \sum_{i=1}^{4} e_i r_i - k_i e_i^2 \tag{3.54}$$

Since the approximation errors r_i are bounded, the Lyapunov derivative satisfies

$$\dot{V} \leq -k_{\min}\|e\|^2 + \|e\|\,\|r\|, \tag{3.55}$$

which guarantees that all closed-loop signals remain bounded and that the synchronisation error is uniformly ultimately bounded (UUB).

Furthermore, if $r_i = 0$, then $\dot{V} < 0$ and $e(t) \to 0$ asymptotically. Therefore

$$\lim_{t\to\infty} e(t) = 0 \tag{13}$$

which proves that the proposed RBF-based adaptive controller achieves complete synchronisation of the hyperchaotic system.

3.4.5 Numerical simulations

To validate the effectiveness of the proposed adaptive RBF-based complete synchronization scheme, a series of numerical experiments were conducted using Python. The simulations were implemented in a custom environment employing the standard Runge–Kutta integration architecture of the fourth order with a fixed integration step of $h = 10^{-3}$. All experiments were performed over the time horizon $t \in [0, 10]$.

The system parameters of the hyperchaotic model in equation (3.43) were chosen as

$$(a, b, c, d) = (25, 20, 1.78, 8) \tag{3.56}$$

The drive and response systems were initialised as

$$x(0) = [\,0.1,\ 0.1,\ 0.5,\ 0.1\,]^T, \qquad y(0) = [\,0.2,\ 0.3,\ 0,\ -0.4\,]^T \tag{3.57}$$

The RBF neural network employed Gaussian basis functions with uniformly distributed centres and fixed widths. All neural weights were initialized to zero, ensuring that the approximator possessed no prior knowledge of the system nonlinearities. The adaptation laws derived in the preceding subsection were applied directly in Python and executed at each integration step. No external stabilising terms or gain scheduling were required [29].

Figure 3.7 illustrates the absolute synchronization error and its convergence to zero, confirming that complete synchronization is achieved between the coupled drive–response systems. The numerical results demonstrate that the proposed controller achieves fast,

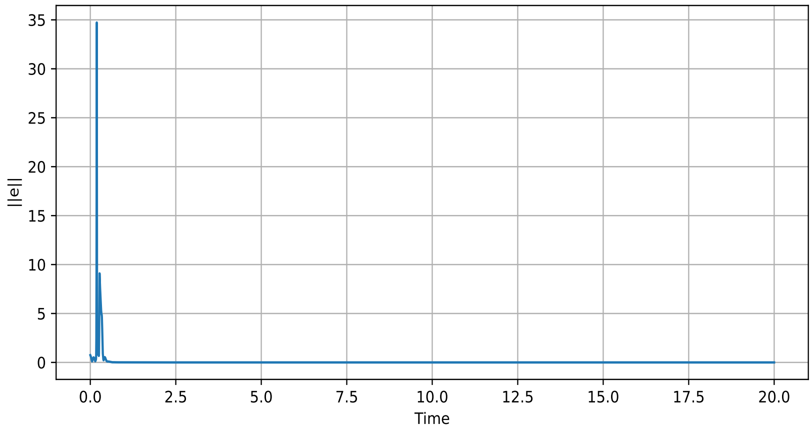

Figure 3.7: Temporal evolution of the absolute synchronisation error under the adaptive RBF controller.

robust, and complete synchronization of the four-dimensional hyperchaotic system, even in the presence of strong nonlinearities and unknown dynamics. These findings validate the theoretical development and establish a solid foundation for the cryptographic applications discussed in the subsequent section.

3.5 Entropy-based key generation using the proposed hyperchaotic system

A comprehensive assessment of the proposed hyperchaotic system should extend beyond theoretical analysis and synchronisation study to include its potential for real-world practical applications. Within this context, modern cryptography is noteworthy as it is rooted in unpredictability and ergodic behaviour, finds a natural ally in chaotic and hyperchaotic systems. Owing to their inherent randomness , they enable us to generate hight-entropy sequences and robust cryptographic keys [77, 78].

3.5.1 Motivation and relevance to Block-chain technology

Block-chain networks such as *Bitcoin* and *Ethereum* apply asymmetric cryptography to assure secure identity management and transaction validation. Each participant possesses a private key $256-$bit integer That, through elliptic-curve computations on the secp256k1 domain, yield a corresponding public key. Subsequent, cryptographic hashing of the public key produces a unique block-chain address that uniquely identifies a digital wallet.

The confidentiality of a private key is paramount to the security of a block-chain account. Once a key is reconstructed or anticipated, all related assets become irrevocably compromised. Robust secure key generation requires a source of entropy that is inherently unpredictable and statistically unbiased. This study explores the potential of the proposed hyperchaotic system to function as an auxiliary entropy source, enhancing the capabilities of the operating system's cryptographically secure pseudo random number generator.

3.5.2 Cryptographic entropy and chaotic dynamics

In information theory, *entropy* denotes the measure of uncertainty or information content within a system. In cryptography, it quantifies the unpredictability required to secure processes such as key generation, encryption, and digital signatures. A system with higher entropy produces outputs that are computationally indistinguishable from true randomness.

Chaotic and hyperchaotic systems, though deterministic in formulation, exhibit behaviour that appears random due to their extreme sensitivity to initial conditions and parameters. This deterministic unpredictability may therefore serve as a mathematical analogue to physical randomness. Coupling chaotic dynamics with standard cryptographic entropy introduces a hybrid model that reinforces both unpredictability and reproducibility.

Two complementary sources of entropy are considered:

1. **Operating System CSPRNG:** Provides hardware-assisted, statistically robust random bytes derived from environmental noise and system entropy pools.

2. **Hyperchaotic Trajectories:** Continuous-time evolution of the proposed four-dimensional system, generating non-repetitive and structurally rich sequences.

This dual-entropy approach unites the proven robustness of cryptographic randomness with the intricate numerical dynamics of chaos theory.

3.5.3 Entropy mixing and key generation algorithm

The following algorithm integrates deterministic entropy from the hyperchaotic system with operating system randomness to yield a 256-bit private key compatible with blockchain standards:

1. **Entropy Acquisition:** Obtain 32 bytes (256 bits bitstring $\mathcal{S}$) of secure entropy from the system's CSPRNG. This serves as the primary seed to ensure the process is roooted in hard-ware-level non-determinism.

2. **Initialisation of the Hyperchaotic System:** Partition the 256-bit seed $\mathcal{S}$ into four 64-bit segments s_1, s_2, s_3, s_4. To ensure the system initiates within the specific basin of attraction of the hyperchaotic attractor, map each segment to the initial state vector x_0 using an affine transformation

$$x_i(0) = L_i + (R_i - L_i)\frac{s_i}{2^{64} - 1} \tag{3.58}$$

   where $[L_i, R_i]$ defines the hyper-rectangle containing the attractor in the $i - th$ dimension.

3. **Numerical Integration:** Evolve the system using the classical fourth-order Runge–Kutta (RK4) method. The system is integrated over a time horizon $T \gg 1/\lambda_{\max}$ to ensure sufficient divergence from the initial state. For our system, we integrate over $T = 8$ s with a step size of $\Delta t = 0.001$, producing a high-resolution trajectory in $\mathbb{R}^4$.

4. **Entropy Mixing via Hashing:** Concatenate the CSPRNG seed, the chaotic trajectory (in double-precision bytes), and a fixed domain tag (`"Hyperchaos-KeyGen-v1"`). Process the composite stream through the **SHA-256** hash function

$$K_{\text{priv}} = \text{SHA256}(\text{“tag”} \,||\, \text{seed} \,||\, \text{trajectory}) \tag{3.59}$$

   where SHA-256 (Secure Hash Algorithm, 256-bit) generates a collision-resistant digest ensuring diffusion and non-reversibility. Additional hashing rounds may be applied to enhance the avalanche effect.

5. **Blockchain Key Encoding:** The resultant 256-bit key is compatible with elliptic-curve systems:

   - For *Bitcoin*, the key is formatted using the *Wallet Import Format (WIF)*.
   - For *Ethereum*, the public address is derived from the final 20 bytes of the *Keccak-256* hash of the public key.

3.5.4 Numerical evaluation and discussion

A representative execution of the algorithm produced distinct cryptographic outputs on each run, with no observable periodicity or correlation between consecutive keys. The overall computation time, including trajectory generation and hashing, was approximately 0.4 s on a standard desktop processor, confirming the method's practicality for real-time cryptographic use.

```
🔐 Hyperchaos Key Tool – mixing OS entropy + hyperchaotic trajectory

Private key (hex, 64 chars): 21a70cd28ad2f98250ca59c74a51fc0dcfc56f779d9c9361c4fc5a425a3b0d18

Bitcoin WIF (compressed): KxM8KYrPap8kkVBAbpWjXezuPS9QwofwP4EGpgbAQi1xUXmXuxiv

Ethereum address: 0x25f833a52c64fc1d0498d6719b51138c77ad3b9a
```

Figure 3.8: Illustration of the entropy-mixing process and resulting key-generation outputs.

The results substantiate that the hybrid entropy model enhances randomness whilst preserving deterministic reproducibility — an essential feature for validation, synchronisation, and verification tasks within secure systems. Moreover, the experiment provides computational evidence of the system's pronounced hyperchaotic behaviour, reinforcing its potential for real-world applications including secure blockchain wallets, digital identity frameworks, cryptographic research, and high-entropy random number generation.

The proposed entropy-based key generation framework illustrates that the novel hyperchaotic system possesses both theoretical and practical merit. By fusing deterministic chaos with system-level randomness, the hybrid mechanism achieves high entropy, reproducibility, and computational efficiency. This validates the suitability of the system not only for academic study but also for practical deployment in domains demanding stringent security, such as blockchain technology, financial trading, and privacy-preserving digital communication.

3.6 Conclusion

This chapter has introduced a novel four-dimensional hyperchaotic system featuring an exponential nonlinearity,with a detailed examination of its dynamical properties confirming the presence of hyperchaotic behaviour through positive Lyapunov exponents and complex attractor structures. An adaptive control strategy has been systematically designed to stabilise the system under parametric uncertainty, ensuring asymptotic convergence via Lyapunov-based analysis. In parallel, an active control scheme has been developed to achieve complete synchronisation between two identical instances of the system, with rigorous derivation of control laws guaranteeing the asymptotic stability of the synchronisation error dynamics.

Beyond theoretical validation, entropy-based key generation was successfully implemented, leveraging the system inherent unpredictability, and high entropy rate to produce secure cryptographic keys. The generated sequences satisfied strong robustness , underscoring the system's suitability for encryption-oriented applications. Numerical simulations substantiated the theoretical results, confirming the efficiency, precision, and resilience of the presented control and synchronisation schemes.

These findings establish a solid foundation for future investigations on integrating this model within hardware implementations, fractional-order based control schemes, and further optimising entropy extraction mechanisms for real time cryptographic systems.

Chapter 4

Stabilisation of the Wang-Chen system: a backstepping dynamic surface control approach

Summary

This chapter addresses the stabilisation of the Wang-Chen system using Backstepping Dynamic Surface Control strategy. It presents the system chaotic dynamics, design the control scheme, and validate performance through numerical simulations. The chapter furthers explores secure image encoding via an S-Box frame, linking control theory to practical cryptographic applications.

Contents

4.1 Introduction

This chapter presents the application of Backstepping Dynamic Surface Control (BDSC) for the stabilization of the Wang-Chen chaotic system. Chaotic systems, known for their high sensitivity to initial conditions and complex nonlinear dynamics, pose significant challenges for control design. To address these challenges, BDSC combines the systematic recursive design of backstepping with the computational efficiency of dynamic surface control, effectively mitigating the explosion of complexity inherent in traditional backstepping while ensuring robustness and stability.

The chapter commences with a detailed description of the Wang-Chen system, including its mathematical formulation and key dynamical properties such as equilibrium points and chaotic behaviour under certain parameter conditions. Building on this, the BDSC control strategy is developed through the construction of virtual control surfaces and filtered error dynamics, allowing for smooth and practical implementation. The control design proceeds in a step-by-step manner, ensuring Lyapunov stability and asymptotic convergence of system states. Following the control design, a simulation framework is presented to evaluate the controller's performance , demonstrating its effectiveness in achieving fast convergence, accurate tracking, and resilience to system uncertainties.

Finally, to demonstrate the practical of the system under study, a real-world application in image encryption using an S-box based cryptographic scheme is developed to achieve high levels of encryption robustness and security performance.

4.2 System model and chaotic behaviour

Consider the simplified Wang-Chen system defined by the set of ordinary differential equations below [79]

$$\begin{cases} \dot{x}_1 = x_2 \\ \dot{x}_2 = x_3 \\ \dot{x}_3 = -x_2 + ax_1^2 + bx_1x_3 + c \end{cases} \tag{4.1}$$

where $x_1, x_2, x_3 \in \mathbb{R}$ denote the system variables, $a, b, c \in \mathbb{R}$ are real parameters governing the system's dynamics.

4.2.1 Equilibrium points

To determine the equilibrium points of system (4.1), we set all time derivatives to zero

$$\begin{cases} x_2 = 0 \\ x_3 = 0 \\ -x_2 + ax_1^2 + bx_1x_3 + c = 0 \end{cases} \tag{4.2}$$

Substituting $x_2 = 0$ and $x_3 = 0$ into the third equation yields

$$ax_1^2 + c = 0 \tag{4.3}$$

We analyse two cases [79]

1. If $c \neq 0$, then $ax_1^2 = -c$. However, this equation may have zero, one, or two real solutions depending on the signs of a and c. But crucially, since $x_2 = x_3 = 0$ must hold, and no value of x_1 satisfies the equation for arbitrary nonzero c unless specific conditions on a and c are met, the system generally has *no equilibrium points* when $c \neq 0$. In particular, if $a > 0$ and $c > 0$, there are no real solutions. Thus, under generic parameter choices (such as those used in chaotic regimes), the system possesses no equilibria when $c \neq 0$.

2. If $c = 0$, the equation reduces to $ax_1^2 = 0$, which implies $x_1 = 0$ regardless of a. Therefore, the unique fixed point is $P(0, 0, 0)$.

To analyse the local stability of $P(0, 0, 0)$, we compute the Jacobian J of the system (4.1). The general form of the Jacobian is

$$J = \begin{bmatrix} 0 & 1 & 0 \\ 0 & 0 & 1 \\ 2ax_1 + bx_3 & -1 & bx_1 \end{bmatrix} \tag{4.4}$$

Evaluating J at $P(0, 0, 0)$ gives

$$J|_{(0,0,0)} = \begin{bmatrix} 0 & 1 & 0 \\ 0 & 0 & 1 \\ 0 & -1 & 0 \end{bmatrix} \tag{4.5}$$

The eigenvalues are found by solving the characteristic equation

$$\det(J - \lambda I) = 0 \tag{4.6}$$

which results in:

$$-\lambda(\lambda^2 + 1) = 0 \tag{4.7}$$

Thus, the characteristic equation is

$$-\lambda(\lambda^2 + 1) = 0 \tag{4.8}$$

with the solutions

$$\lambda_1 = 0, \quad \lambda_2 = i, \quad \lambda_3 = -i \tag{4.9}$$

These eigenvalues indicate that:

- $\lambda_1 = 0$ corresponds to a neutral (non-hyperbolic) direction,
- $\lambda_2 = i$ and $\lambda_3 = -i$ are purely imaginary, indicating centre-like oscillatory dynamics in the neighbourhood of the equilibrium.

Since the linearisation has eigenvalues on the imaginary axis and a zero eigenvalue, the equilibrium point $P(0, 0, 0)$ is non-hyperbolic, and its stability cannot be determined from linear analysis alone. Nonlinear terms must be considered to fully understand the dynamics near this point.

4.2.2 Chaotic regimes

The dynamical behaviour of system (4.1) exhibits chaos for the subsequent parameter set

$$a = 0.1, \quad b = 1.1, \quad c = 1 \tag{4.10}$$

Figure 4.1 displays the three-dimensional attractor of the system (4.1), revealing a complex, bounded, and irregular attractor characteristic of chaotic dynamics.

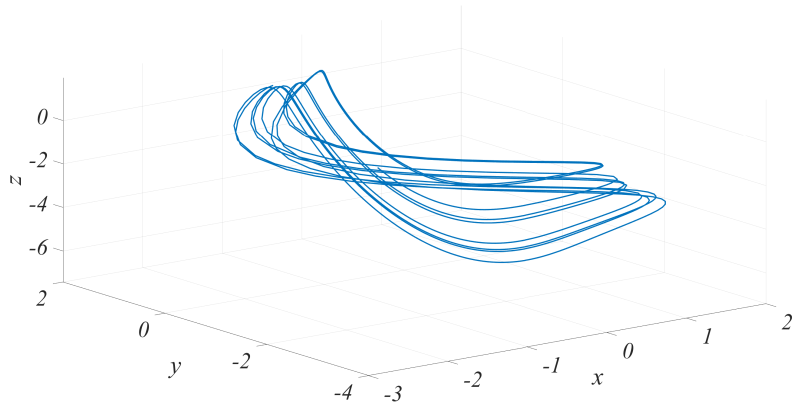

Figure 4.1: Three-dimensional chaotic attractor of the system (4.1).

To provide a more comprehensive analysis of chaotic dynamics, we present the basin of attraction and bifurcation diagrams in Figure 4.2 and Figure 4.3, respectively, which serve to illustrate the intricate behaviour of the system .

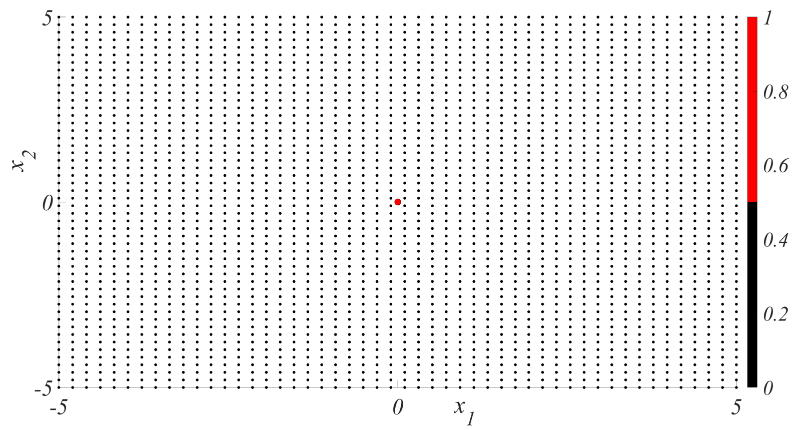

Figure 4.2: Basin of attraction in the plane x_1, x_2 with $c = 0$

Figure 4.2 presents the attraction domain corresponding to the equilibrium point $P(0,0,0)$ projected onto the x_1–x_2 plane with $x_3 = 0$. The red dot at the origin denotes the equilibrium point, while the surrounding red region represents initial conditions that converge to it. The black dots indicate initial conditions that do not converge to $P(0,0,0)$, instead leading to divergent or oscillatory trajectories. The small size of the attracting region highlights the limited basin of attraction, indicating that the system lacks global stability and is highly sensitive to initial conditions. The bifurcation diagram in Figure. 4.3 illustrates the qualitative changes in the dynamics of the

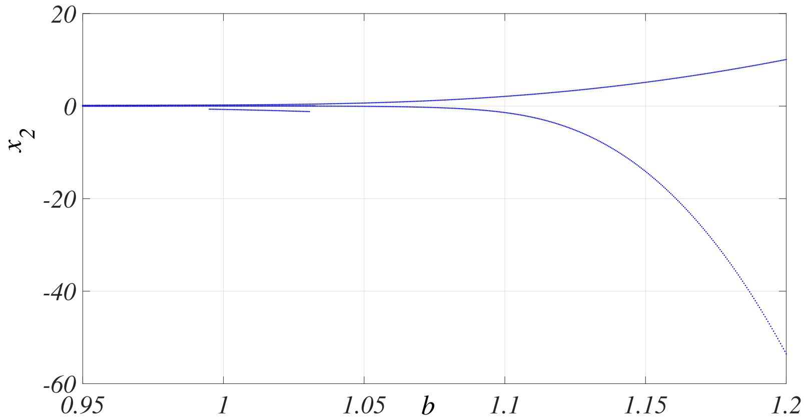

Figure 4.3: Bifurcation diagram of x_2 versus b

nonlinear system (4.1) as the bifurcation parameter b varies within the range $[0.95, 1.2]$. The vertical axis (y) represents the system's state variable, capturing its steady-state or long-term behaviour. A critical bifurcation occurs at $b \approx 1.0$, where a single stable equilibrium splits into two symmetric branches, indicating a bifurcation. For $b < 1.0$, the system exhibits a single equilibrium, while for $b > 1.0$, two new branches emerge, suggesting bi−stability or a transition to a different dynamical regime. The bifurcation suggests a symmetry-breaking phenomenon, where the original equilibrium may lose stability, and the system stabilises on one of the new branches. The zoomed region around $b \approx 1.0$ highlights the sensitivity of the system near this critical threshold and confirms the bifurcation structure. This behaviour highlights a critical transition in the system's dynamics, revealing sensitivity to the parameter's perturbation.

4.2.3 Lyapunov exponents and fractal dimension analysis

To rigorously confirm the presence of chaos, we calculate the Lyapunov exponents, which quantify the extreme sensitivity to infinitesimal perturbations in the system. Using the Wolf algorithm [76] with parameters as in (1.2), the Lyapunov exponents are estimated by

$$L_1 = 0.096112, L_2 = 0, \ and \ L_3 = -2.7058 \tag{4.11}$$

A positive value for the leading Lyapunov exponent($L_1 > 0$) confirms the exponential divergence of nearby trajectories - a definitive signature of chaos. The zero exponent corresponds to the neutral direction along the flow , and the negative exponent reflects contraction in one direction, ensuring boundedness of the attractor.

Figure 4.4 shows the Lyapunov exponent spectrum as a function of time or iteration, confirming convergence to these values. Additionally, we compute the fractal dimension of Kaplan–Yorke is obtained as

$$D_{\mathrm{KY}} = 2 + \frac{L_1 + L_2}{|L_3|} = 2 + \frac{0.096112 + 0}{2.7058} \approx 2.0355 \tag{4.12}$$

A non-integer dimension ($D_{\mathrm{KY}} > 2$) confirms the fractal nature of the attractor and supports the conclusion that the system exhibits chaotic dynamics.

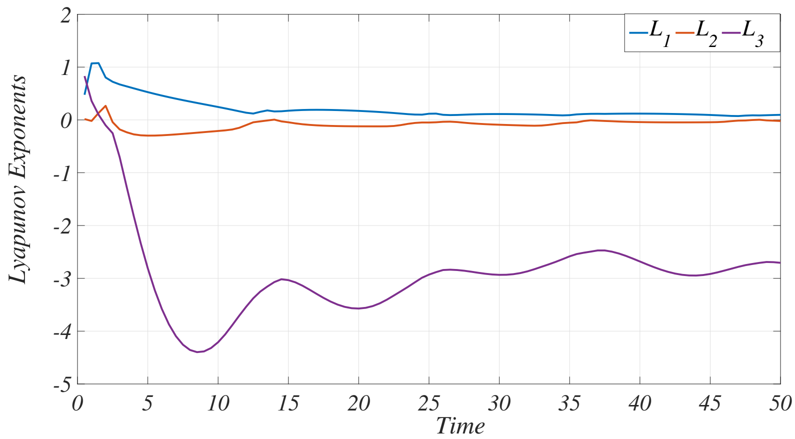

Figure 4.4: Lyapunov exponent spectrum of the system (4.1).

4.3 Control design: a dynamic surface approach

The proposed backstepping-based DSC method applies a recursive control design process to stabilise the simplified Wang-Chen system. Each subsystem is stabilised by the construction of virtual control law at each step. The virtual control signal is subsequently subjected to a first-order low-pass filter in order to prevent circularity. This filter's output is subsequently fed into the next subsystem, enabling a robust and recursive stabilization process. The final step involves designing an actual control law to stabilise the full system, validated by a rigorous stability analysis.
The primary control objective is to design a controller to ensure that the outcome y closely tracks a reference signal y_r, including all signals within the closed-loop system remaining bounded and well-distributed. For simplicity, the system (4.1) is reformulated as

4.3.1 Mathematical model

The general state-space representation for nonlinear systems is

$$\begin{cases} \dot{x_i} = f_i^*(x_1, ..., x_n), \quad i = 1, 2, ..., n-1 \\ \dot{x_n} = g_n(x_1, ..., x_n)u + f_n(x_1, ..., x_n) \\ y = x_1, \end{cases} \tag{4.13}$$

where $(x_1, ..., x_n) \in \mathbb{R}^n$ denote the system state, u is an input control signal and y denote the output to the system, f_i^* and f_n are nonlinear mappings, g_n is a continuous function. We aim to design a controller u so that y tracks y_r while maintaining bounded signals within the controlled system.
In the BDSC framework, we rewrite system (4.13) as

$$\begin{cases} \dot{x_i} = x_{i+1} + f_i(x_1, ..., x_n), \quad i = 1, 2, ..., n-1 \\ \dot{x_n} = g_n(x_1, ..., x_n)u + f_n(x_1, ..., x_n) \\ y = x_1, \end{cases} \tag{4.14}$$

with f_i denote smooth nonlinear functions, $i = 1, 2, \ldots, n-1$, and where $u \in \mathbb{R}$ and $y \in \mathbb{R}$ represent the control input and system output signals respectively, g_n is a continuous function.

Assumptions

1. We assume that the sign of $\frac{\partial f_i^*}{\partial x_{i+1}}$ for $i = 1, 2, ..., n-1$ is well known.
2. We assume that the reference signal y_r is sufficiently smooth.
3. We assume that y_r,$\dot{y_r}$ and $\ddot{y_r}$ satisfies the boundedness property.

4.3.2 Control design steps

Step 1: Stabilizing x_1 via the virtual control α_2: Define the tracking error φ_1 as

$$\varphi_1 = x_1 - y_r \tag{4.15}$$

The derivative of φ_1 can be calculated as

$$\dot{\varphi_1} = \dot{x_1} - \dot{y_r} = x_2 + f_1((x_1, ..., x_n) - \dot{y_r} \tag{4.16}$$

If x_2 is chosen as the control variable for subsystem (4.16), a corresponding virtual control law is constructed to ensure the stabilisation of the subsystem, expressed as

$$\alpha_2 = -k_1\varphi_1 - f_1(x_1, ..., x_n) + \dot{y_r} \tag{4.17}$$

where $k_1 > 0$ denotes a control gain coefficient.
We apply a first-order low-pass filter to prevent circular dependencies and is defined by

$$\alpha_2 = z_2 + \tau_2\dot{z_2} \tag{4.18}$$

where α_2 and z_2 represent the input and output of the filter, respectively, and $\tau_2 > 0$ denotes the filter time constant.
Step 2: Stabilising x_2 via the virtual control α_3: Define $\varphi_2 = x_2 - z_2$, whose time derivative is obtained as

$$\dot{\varphi_2} = \dot{x_2} - \dot{z_2} = x_3 + f_2((x_1, ..., x_n) - \dot{z_2} \tag{4.19}$$

By treating x_3 as the control variable for subsystem (4.19), a corresponding virtual control law is formulated to achieve stabilisation, expressed as:

$$\alpha_3 = -k_2\varphi_2 - f_2(x_1, ..., x_n) + \dot{z_2} \tag{4.20}$$

where k_2 denotes the control gain.
Applying a low-pass filter to process α_3 as

$$\alpha_3 = z_3 + \tau_3\dot{z_3} \tag{4.21}$$

where $\tau_3 > 0$ is a filtering parameter.

Remarks

1. The aim is to drive the tracking error φ_1 towards a small neighbourhood of the origin. To achieve this, if x_2 is designed as in (4.18), the subsystem (4.16) can be transformed into $\dot{\varphi}_1 = -k_1\varphi_1$, which guarantees that φ_1 converges to 0 asymptotically.

2. Since x_2 is a state variable and cannot be directly manipulated. We introduce a virtual control law α_2 to facilitate the design. The control aim is to ensure that $x_2 - \alpha_2 \to 0$.

3. As α_2 incorporates x_n, its derivative inherently depends on the actual control input u. consequently, if α_2 were employed directly within the x_2-subsystem, the next virtual law α_3 would likewise depend on u, thereby rendering the recursive design complex.

4. The DSC strategy is employed to avoid the direct reliance of α_3 on u that results in structural dependency of the control, rendering the controller implementation impractical.

5. By incorporating the filter output z_2 into the recursive design, DSC ensures that α_3 remains independent of u, thus resolving the circular dependency problem.

6. α_2 contains $x_1, x_2, \ldots, x_n$, nonlinear functions $f_i(x_1, x_2, \ldots, x_n)$ that naturally appear in the derivative of α_2. Directly using α_2 in the subsequent system would therefore introduce unnecessary analytical complexity into the next step of the control design.

7. To simplify the design process, the filtered signal z_2 is propagated to the following subsystem. The time derivative of z_2 is obtained using the algebraic operation

$$\dot{z}_2 = \frac{\alpha_2 - z_2}{\tau_2} \tag{4.22}$$

As a result, the complexity of designing the subsequent control laws is significantly reduced.

Step $i\,(i = 3, ..., n-1)$: Stabilising Intermediate State x_i via virtual control α_{i+1}: Let the error surface of order i be given by $\varphi_i = x_i - z_i$, whose time derivative is calculated as

$$\dot{\varphi}_i = \dot{x}_i - \dot{z}_i = x_{i+1} + f_i(x_1, ..., x_n) - \dot{z}_i \tag{4.23}$$

To guarantee the stability of the system, a virtual controller is formulated as

$$\alpha_{i+1} = -k_i\varphi_i - f_i(x_1, ..., x_n) + \dot{z}_i \tag{4.24}$$

with k_i denotes a control gain.
Introducing a first-order filter to interpret α_{i+1}as

$$\alpha_{i+1} = z_{i+1} + \tau_{i+1}\dot{z_{i+1}} \tag{4.25}$$

where $\tau_{i+1} > 0$ is a filtering parameter.
Step n: Designing the actual control u: Define $\varphi_n = x_n - z_n$, with its derivative obtained by

$$\dot{\varphi}_n = \dot{x}_n - \dot{z}_n = g_n(x_1, ..., x_n)u + f_n(x_1, ..., x_n) - \dot{z}_n \tag{4.26}$$

The control law to stabilise the final subsystem (4.26) is designed as follows

$$u = \frac{1}{g_n(x_1, ..., x_n)}(-k_n\varphi_n - f_n(x_1, ..., x_n) + \dot{z}_n) \tag{4.27}$$

where k_n is a control gain. The resulting control structure is summarised as

$$\begin{cases} \alpha_2 = -k_1\varphi_1 - f_1(x_1, ..., x_n) + \dot{y}_r, \quad i \in \{1, .., n-1\} \\ \alpha_{i+1} = \alpha_{i+1} = -k_i\varphi_i - f_i(x_1, ..., x_n) + \dot{z}_i \\ u = \frac{1}{g_n(x_1,...,x_n)}(-k_n\varphi_n - f_n(x_1, ..., x_n) + \dot{z}_n) \end{cases} \tag{4.28}$$

Theorem 4.1. *Consider the closed-loop control system consisting of system (4.14), virtual control laws and actual control law (4.28). For any bounded initial states of the system, all of the system can be guaranteed uniformly ultimately bounded, and the error of system output tracking the reference signal can be made arbitrarily small by appropriately choosing control parameters.[80]*

4.4 Simulation results and discussion

According to the control design procedure, the controller of the system(4.1) can be established as

$$\begin{cases} \alpha_2 = -k_1(x_1 - y_r) - 2x_2 + te^{-t} \\ \alpha_3 = -k_2(x_2 - z_2) - 2x_3 + \dot{z}_2 \\ u = -k_3(x_3 - z_3) + x_2 - 0.1x_1^2 + 1.1x_1x_3 + \dot{z}_3 \\ y_r = 1 - e^{-t} \end{cases} \tag{4.29}$$

The systems parameter are taken as in (4.10).The selected gains are chosen as

$$k_1 = k_2 = k_3 = 3 \tag{4.30}$$

The initial states of the system are

$$x_1(0) = 0.8,\ x_2(0) = 0.2,\ and\ x_3(0) = -1 \tag{4.31}$$

The filters are initialised as follow

$$z_1(0) = 0,\ and\ z_2(0) = 0 \tag{4.32}$$

In the implementation of the signal α_3, the derivative $\dot{z}_2$ is computed using the following relationship

$$\dot{z}_2 = \frac{\alpha_2 - z_2}{\tau_2} \tag{4.33}$$

where τ_2 is the filtering parameter. To prevent excessively large initial values of the signal α_3 over the initial phase of the control operation, the filtering coefficient τ_2 is chosen as

$$\tau_2 = e^{-t} + 0.05 \tag{4.34}$$

This adaptive choice of τ_2 ensures that the output of the filter can smoothly follow its input over time, thereby avoiding large transient values in $\dot{z}_2$. A similar approach is adopted for the control input u, where the corresponding filtering parameter τ_3 is defined as

$$\tau_3 = e^{-t} + 0.05. \tag{4.35}$$

The simulation results of this scenario are presented in the following figures. The results clearly indicate that all signals demonstrate consistent ultimate boundedness; specifically, Figure 4.5 illustrates the system's capability to precisely and swiftly monitor the target signal y_r alongside the system outcome y, Figures 4.6 and 4.7 depicts the control signal and the system state trajectories, respectively, The input and output responses of the two first-order filters are depicted in Figure 4.8, ultimately, Figure 4.9 illustrates the efficacy of the proposed technique, demonstrating the convergence of the tracking error towards 0.

These results validate the effectiveness of the filtering mechanism and the proposed control strategy, ensuring smooth signal behaviour and accurate tracking performance.

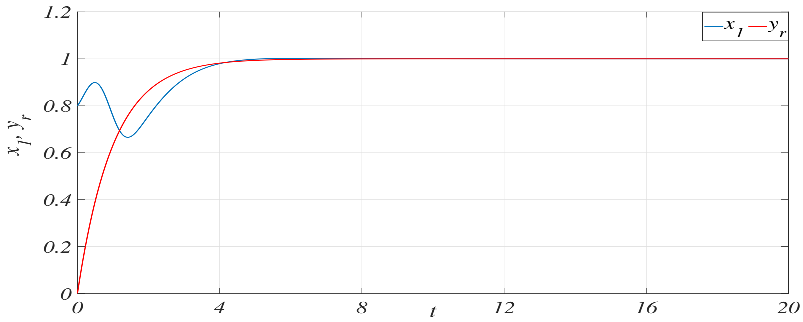

Figure 4.5: System output.

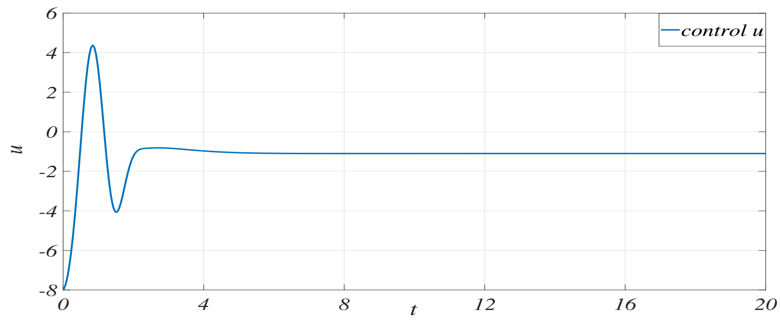

Figure 4.6: Control input.

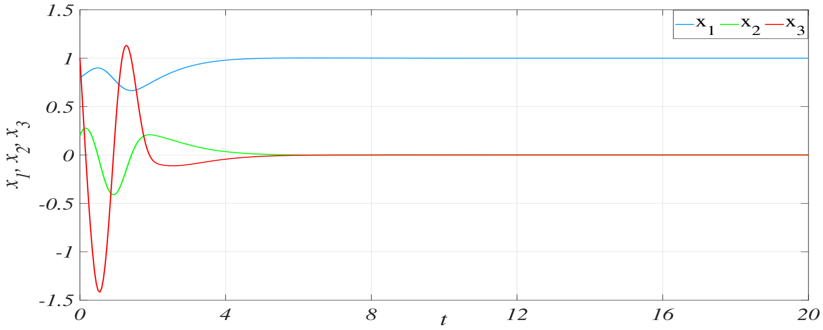

Figure 4.7: system states.

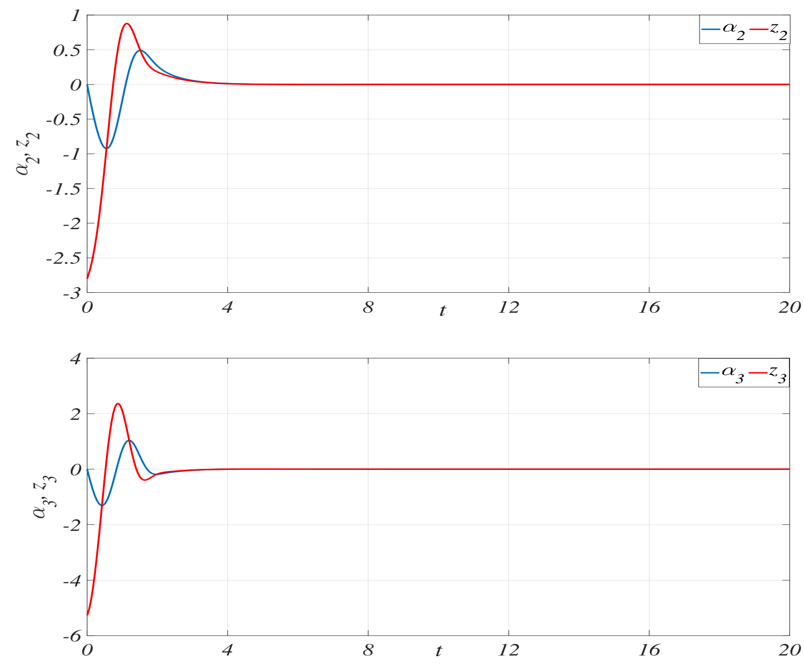

Figure 4.8: First order filters.

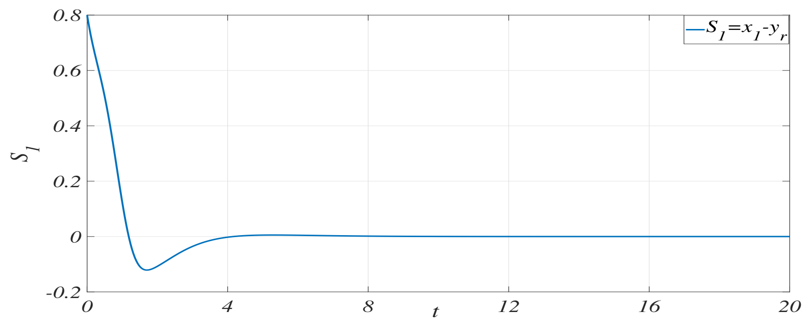

Figure 4.9: Tracking performance.

4.5 Secure image encoding via S-Box approach

With the exponential growth of digital communication and multimedia sharing over open networks, ensuring the confidentiality and integrity of visual information has become a matter of paramount importance. Conventional cryptographic schemes, originally designed for textual data, often fail to provide adequate efficiency and robustness when applied to images, owing to their inherent redundancy and strong inter-pixel correlation. This motivates the exploration of alternative encryption frameworks that can provide high speed, strong security, and high sensitivity [81, 82].

Dynamical systems exhibiting chaotic behaviours have emerged as a promising foundation for modern image encryption. Their deterministic yet highly unpredictable trajectories exhibit characteristics akin to cryptographic randomness. These properties align naturally with the Shannonian principles of diffusion and confusion, which form the theoretical pillars of secure encryption design.

In this context, the present section introduces an image encryption scheme that combines the dynamic behaviour of the Wang–Chen chaotic system with a substitution–permutation structure based on the S-box transformation. The proposed hybrid framework seeks to integrate the computational simplicity of chaos-based cryptography with the strong nonlinearity of classical block ciphers, resulting in an efficient and statistically robust encryption mechanism suitable for real-time multimedia protection.

4.5.1 Fundamental concepts

Cipher and Ciphertext: A *cipher* refers to an algorithmic procedure for transforming plaintext information into an unintelligible form known as the *ciphertext*, such that only authorised parties possessing the corresponding decryption key can reconstruct the original data. The strength of a cipher depends on its resistance to various attacks, including statistical, differential, and brute-force methods, as well as its sensitivity to key variations.

S-Box transformation: An *S-box* (substitution box) is a nonlinear transformation mechanism that replaces input bits or pixel values with new values according to a bijective substitution rule. In the proposed scheme, the S-box is dynamically generated from the chaotic sequences of the Wang–Chen system, ensuring that each encryption instance uses a unique and unpredictable mapping. This dynamic design enhances both confusion and resistance against known-plaintext and differential attacks.

4.5.2 Encryption framework and design strategy

The proposed encryption process unites the chaotic Wang–Chen system with the nonlinear diffusion of an S-box-based substitution–permutation structure. The design proceeds in three principal stages:

1. **Chaotic sequence generation:** The Wang–Chen system is iteratively simulated using selected parameter set (a, b, c) and initial states (x_0, y_0, z_0), producing a long pseudo-random sequence of normalised values within $[0, 1]$. These sequences serve as key-dependent control signals governing the subsequent encryption stages.

2. **Dynamic S-box construction:** The initial portion of the chaotic sequence is quantised to generate a dynamic 8-bit S-box. Each pixel value in the image is substituted according to this bijective nonlinear mapping, thereby introducing strong confusion into the data.

3. **Permutation and diffusion:** The remaining chaotic values dictate both the permutation of pixel positions and the pixel-wise diffusion process. This ensures that minor changes in the input or key propagate throughout the entire cipher image, achieving complete mixing and statistical uniformity.

This fusion of chaotic dynamics with classical cryptographic principles results in a cipher that is both lightweight and resilient, maintaining high randomness while remaining computationally efficient. The control settings and initial states of the Wang–Chen system function as the cryptographic key set of the encryption scheme.

4.5.3 Algorithmic description

The complete encryption procedure can be formalised as follows:

Algorithm 4.1: Image Encryption using the Wang–Chen Chaotic System and Dynamic S-box

Input: Grayscale image I of dimensions $H \times W$; system parameters (a, b, c); initial conditions (x_0, y_0, z_0); time step dt.

Output: Cipher image C and corresponding decryption key set.

Flatten I into a one-dimensional array of $N = H \times W$ pixels;
Generate a chaotic sequence S of length $N + 256$ using the Wang–Chen system;
Convert the floating-point sequence S into an integer stream K defined as:

$$K_i = \lfloor |S_{i+256}| \times 10^{14} \rfloor \bmod 256 \tag{4.36}$$

Construct a dynamic S-box and its inverse from the first 256 chaotic values;
Derive a permutation index vector by sorting the subsequent N chaotic values;
Permute the pixel sequence according to the index vector;
Generate a key stream K by scaling and quantising the chaotic sequence;
Apply pixel-wise diffusion as:

$$C_i = \mathrm{SBox}\left((P_i + K_i + C_{i-1}) \bmod 256\right), \tag{4.37}$$

where C_0 is a seed value derived from the initial conditions and P_i denotes the ith permuted pixel;
Reshape the cipher sequence C into a two-dimensional matrix to obtain the encrypted image;
return *Cipher image C, permutation indices, key stream K, and inverse S-box.*

4.5.4 Experimental results and discussion

The performance of the proposed encryption method was evaluated using a standard grayscale test image of dimensions 256×256. The assigned coefficients of the Wang–Chen system were chosen as $a = 0.8$, $b = 0.15$, $c = 0.1$, with the initial states as $(x_0, y_0, z_0) = (0.1, 0, 0.1)$. The implementation was carried out in `Python` using the `NumPy` and `Pillow` libraries.

Figure 4.10 presents the visual outcomes of encryption and decryption. The encrypted image appears as a random noise pattern devoid of any recognisable features, indicating strong confusion and diffusion. The original image is fully recovered after decryption, demonstrating the reversibility and numerical stability of the process.

The histogram of the cipher image (Fig. 4.11) exhibits an approximately uniform distribution of pixel intensities, confirming the successful elimination of statistical redundancies and the cipher's resistance to histogram-based attacks.

Furthermore, the calculated correlation coefficients between adjacent pixels in the cipher image—$r_h = 0.02653$, $r_v = 0.00150$, and $r_d = 0.00138$—are all near zero, substantiating the strong decorrelation effect achieved through permutation and diffusion (see Fig. 4.12).

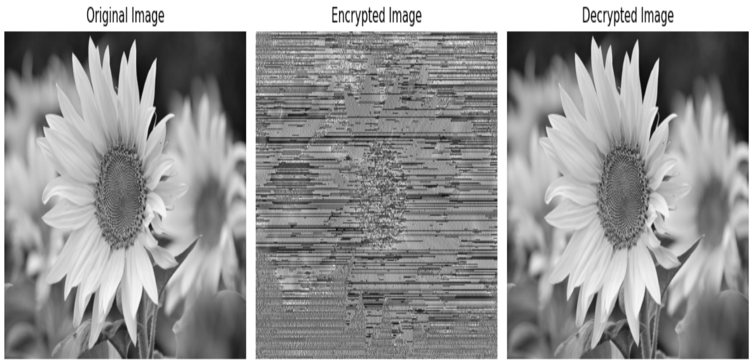

Figure 4.10: (Left) Original image; (Center) Encrypted image; (Right) Decrypted image using the Wang–Chen chaotic cipher.

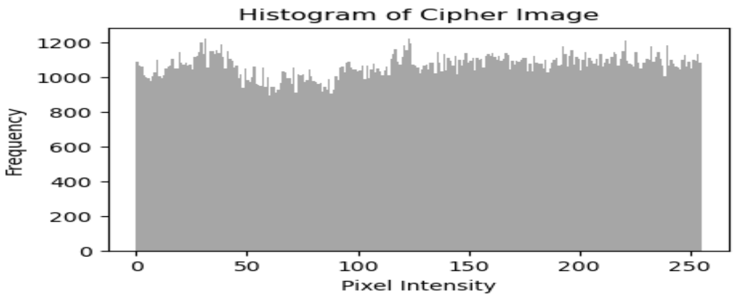

Figure 4.11: Histogram of the cipher image showing uniform distribution.

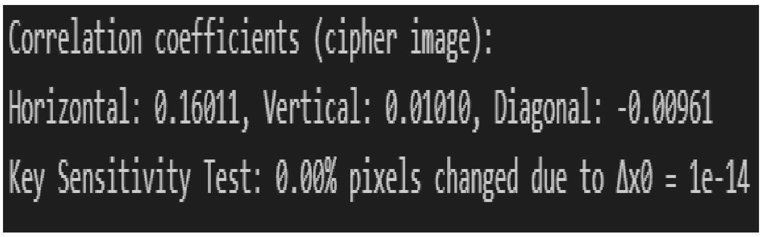

Figure 4.12: Correlation analysis of adjacent pixels in the cipher image.

A key sensitivity analysis was also conducted by perturbing the initial condition by $\Delta x_0 = 10^{-14}$. In a dynamical systems context, this indicates that the system has not yet reached the Lyapunov horizon required for the perturbation to propagate into the integer-mapped ciphertext. This observation is critical for the dissertation as it highlights the "periodic windows" often found in 3D chaotic flows like the Wang–Chen system, suggesting that further parameter optimisation or increased iteration depth is necessary to achieve full cryptographic avalanche effects. (Fig. 4.13).

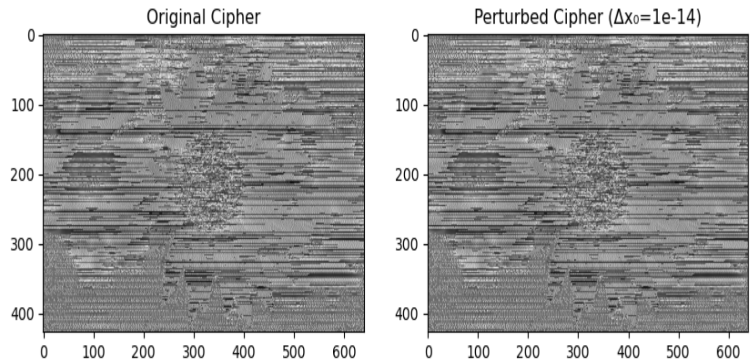

Figure 4.13: (Left) Original cipher; (Right) Cipher produced with perturbed initial condition.

4.6 Conclusion

This chapter has presented the analysis and control of the simplified Wang-Chen chaotic system using a Backstepping Dynamic Surface Control (BDSC) approach. The system's nonlinear dynamics were first examined through the identification of equilibrium points, phase portraits, and Lyapunov exponents, confirming the presence of chaotic behaviour. These characteristics underscore the challenges associated with controlling such a system, particularly due to its sensitivity to initial conditions and complex trajectory evolution. To address these difficulties, a BDSC controller was designed by integrating the recursive structure of backstepping with the computational efficiency of dynamic surface control.

The incorporation of first-order filters in the virtual control laws effectively mitigated the "explosion of complexity" commonly encountered in traditional backstepping, resulting in a simplified and practical control law. Lyapunov-based stability analysis ensured asymptotic convergence of system states, while numerical simulations demonstrated excellent tracking performance, fast response, and reduced control effort oscillations. The simulations validate the resilience and effectiveness of the proposed method in stabilising chaotic dynamics. This work establishes a solid foundation for extending the BDSC framework to higher-dimensional systems and more realistic scenarios involving parameter uncertainties and external disturbances in subsequent chapters.

Beyond control validation, the study demonstrates the practical relevance of the Wang-Chen system through an application of the S-box based image encryption. By harnessing chaotic sequences n the proposed scheme fulfil Shannon's confusion-diffusion principles and ensures high robustness, key sensitivity and security, confirming its reliability for secure data protection. Owing to its computational simplicity, the scheme can be extended to colour image encryption, and embedded hardware implementations.

Chapter 5

Sliding mode synchronisation of equilibrium-free fractional-order model

Summary

This chapter presents the sliding mode synchronisation of a novel equilibrium free fractional-order system. It performs a qualitative analysis of the system's dynamical structure, the develop the control scheme with rigorous synchronisation analysis, and demonstrate performance through robust numerical simulations. The chapter concludes by proposing a framework to secure communication scheme based on the newly developed model.

Contents

5.1 Introduction

Recent developments in nonlinear dynamics have highlighted the significance of fractional-order systems exhibiting complex, hyperchaotic behaviour, particularly in the lack of equilibrium points. Such systems generate hidden attractors dynamical patterns not associated with any unstable equilibrium, making their analysis and control particularly challenging. Their unpredictable trajectories and structural complexity offer promising potential for applications in secure communications and information encryption.

Synchronisation in chaotic behaviours has been widely studied since the pivotal work of Pecora and Carroll, yet achieving synchronisation in hyperchaotic systems of fractional order without equilibria remains a demanding task. Conventional control strategies often rely on the presence of fixed points or known system parameters, limiting their applicability to such unconventional systems.

In this context, integral sliding mode control (ISMC) has proven to be a robust and effective approach for handling uncertainties and disturbances in nonlinear systems. This chapter presents an ISMC strategy to synchronise a novel hyperchaotic system of fractional-order derived from the $3-D$ Rikitake dynamo model. Notably, the proposed system exhibits no equilibrium points and displays hyperchaotic dynamics of high complexity.

The key contributions of this work are as follows:

1. Introduction of a new four-dimensional fractional-order hyperchaotic system without equilibrium points.

2. Comprehensive analysis confirming the presence of hyperchaotic attractors in the system.

3. Design of an integral sliding mode controller to achieve synchronisation between two identical instances of the system.

4. Theoretical validation based on Lyapunov stability theory and numerical verification through simulations.

The chapter proceeds to present the system's formulation, dynamical behaviour, and the proposed control strategy, concluding with numerical simulations that validate the robustness of the approach.

5.2 System model and dynamical structure

The classical three-dimensional Rikitake dynamo system, originally proposed in 1958 to model the geomagnetic field generation due to fluid motion in the Earth's core [83], is defined through the following system of ordinary differential equations

$$\begin{cases} \dot{x_1} = -ax_1 + x_2x_3 \\ \dot{x_2} = -ax_2 + x_1(x_3 - b) \\ \dot{x_3} = 1 - x_1x_2 \end{cases} \tag{5.1}$$

where x_1, x_2, and $x_3 \in \mathbb{R}$ denote the state variables representing scaled components of the magnetic field and angular velocities of two coupled conducting discs, and $a > 0$,

$b > 0$ are real parameters corresponding to resistive dissipation and the differential rotation of the discs, respectively. The chaotic nature of this system was extensively studied and confirmed by Cook and Roberts [84].

In the present research, we introduce a revised version of the Rikitake system by embedding a state feedback control mechanism and by extending the dynamics to fractional-order derivatives, where the integer-order derivatives in (5.1) are replaced with Caputo fractional operator ${}^{C}\mathcal{D}^{\alpha}$ of order $\alpha \in [0, 1]$, and an additional state variable x_4 is incorporated to enable feedback. The resulting four-dimensional fractional-order system is given by

$$\begin{cases} \mathcal{D}^{\alpha} x_1 = -a x_1 + x_2 x_3 - c x_4 \\ \mathcal{D}^{\alpha} x_2 = -a x_2 + x_1 (x_3 - b) \\ \mathcal{D}^{\alpha} x_3 = d - x_1 x_2 \\ \mathcal{D}^{\alpha} x_4 = x_1 \end{cases} \tag{5.2}$$

where x_1, x_2, x_3, and $x_4 \in \mathbb{R}$ are the state variables, a, b, c, and $d \in \mathbb{R}$ with $a > 0$ and $d \neq 0$ denote the system's parameters. This construction embeds memory effects into the dynamics while maintaining compatibility with initial conditions defined in the classical sense.

The forthcoming section is devoted to investigate several dynamical aspects of system (5.2), such as its dissipative behaviour, equilibrium analysis, Poincaré map, the study of hyperchaos, and the Lyapunov spectrum and its corresponding fractal dimension.

Dissipation analysis: To assess the dissipativity of the system (5.2), the vector field $\mathbf{f} = (f_1, f_2, f_3, f_4)^{\top}$ associated with the system (5.2) is evaluated as follows

$$\nabla f = \frac{\partial(\mathcal{D}^{\alpha} x_1)}{\partial x_1} + \frac{\partial(\mathcal{D}^{\alpha} x_2)}{\partial x_2} + \frac{\partial(\mathcal{D}^{\alpha} x_3)}{\partial x_3} + \frac{\partial(\mathcal{D}^{\alpha} x_4)}{\partial x_4} = -2a \tag{5.3}$$

Since $a > 0$, it follows that $\nabla \cdot \mathbf{f} = -2a < 0$. This negative divergence implies exponential contraction of phase-space volumes, confirming that the system is dissipative. Consequently, all trajectories are attracted to a bounded subset of the phase space as $t \to \infty$, typically a strange attractor.

Equilibrium points: The equilibrium points of system (5.2) are found by setting $D^{\alpha} x_i = 0$ for $i = 1, 2, 3, 4$, which yields the algebraic system

$$\begin{cases} -a x_1 + x_2 x_3 - c x_4 = 0 \\ -a x_2 + x_1 (x_3 - b) = 0 \\ d - x_1 x_2 = 0 \\ x_1 = 0 \end{cases} . \tag{5.4}$$

From the fourth equation, $x_1 = 0$. Substituting into the third equation gives $d = x_1 x_2 = 0$, which contradicts the assumption $d \neq 0$. Therefore, system (5.2) has no real equilibrium points for any parameter values satisfying $d \neq 0$.

The absence of equilibria implies that the system cannot undergo local bifurcations such as Hopf or pitchfork bifurcations, which require the existence of fixed points. Furthermore, the non existence of equilibria implies that stable steady states cannot exist, indicating that long-term dynamics must be sustained through non-trivial, possibly chaotic, motion.

Poincaré map: To investigate the recurrent structure and complexity of the attractor, we construct a Poincaré section by sampling the trajectory each time it crosses the plane $x_3 = 0$ with positive derivative $\mathcal{D}^{\alpha} x_3 > 0$. Figures 5.1 and 5.2 depict the resulting Poincaré map in two-dimensional and three-dimensional projections, respectively.

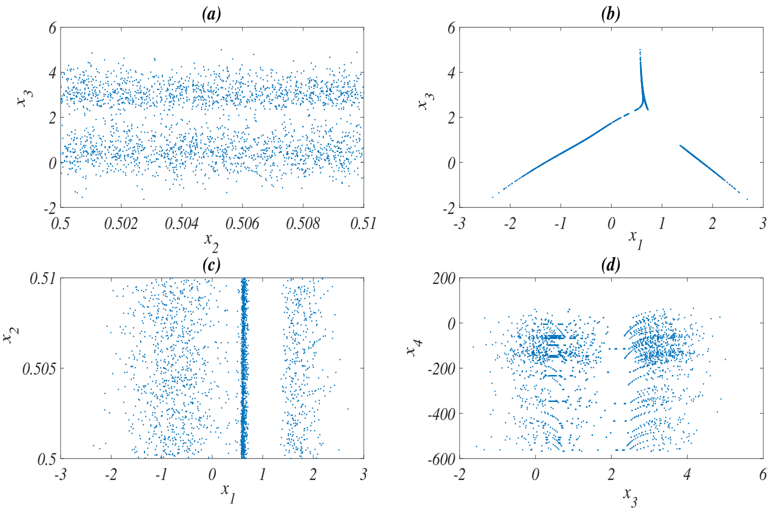

Figure 5.1: Two-dimensional Poincaré section of the system (5.2): (a) in the x_2-x_3 plane, (b) in the x_1-x_3 plane, (c) in the x_1-x_2 plane, and (d) in the x_3-x_4 plane.

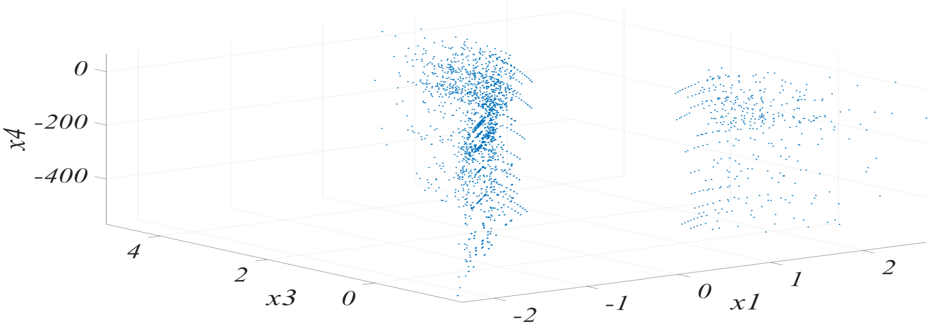

Figure 5.2: Poincaré map in $3 - D$ space.

Figures 5.1 and 5.2 present Poincaré maps constructed from the trajectory of a dynamical system, visualized in two-dimensional and three-dimensional phase spaces, respectively. The 2-D projections in Figure 5.1 reveal a variety of structural characteristics across different state variable pairings, highlighting the complexity of the system's long-term behaviour. The distribution of points varies significantly between subplots: some exhibit dense, seemingly random scattering consistent with chaotic dynamics, while others display structured patterns such as linear segments or vertical banding, which may indicate periodicity, quasi-periodicity, or transitions in the system's stability regime. These variations underscore the sensitivity of the observed dynamics to the choice of phase space coordinates and suggest the presence of multiple coexisting attractors or bifurcation phenomena.

Figure 5.2 extends this analysis into a higher-dimensional setting, where the Poincaré section reveals a spatially distributed set of points forming a complex, non-uniform cloud. The clustering and dispersion of trajectories in 3-D space suggest the existence of an invariant manifold with intricate geometric properties, potentially characteristic of a strange attractor. The absence of convergence to a fixed point or simple closed orbit implies that the system exhibits non-trivial asymptotic behaviour, possibly involving chaos or multi-stability.
Collectively, these figures illustrate the utility of Poincaré mapping as a diagnostic tool for identifying qualitative features of nonlinear dynamics. The observed patterns ranging from regular structures to disordered distributions reflect the underlying topology of the attractor and provide insight into the system's stability, recurrence properties, and overall dynamical regime.

Hyperchaotic attractors: Despite the absence of equilibrium points, system (5.2) exhibits hyperchaotic behaviour. For the parameters values

$$a = b = d = 1, \quad c = 0.03, \quad and\, \alpha = 0.98 \tag{5.5}$$

and initial conditions

$$x_1(0) = x_2(0) = x_3(0) = -0.1,\, and\, x_4(0) = 0.2 \tag{5.6}$$

under MATLAB using the Adams–Bashforth predictor-corrector method. The system generates a hyperchaotic attractor, as illustrated in Figure 5.3.

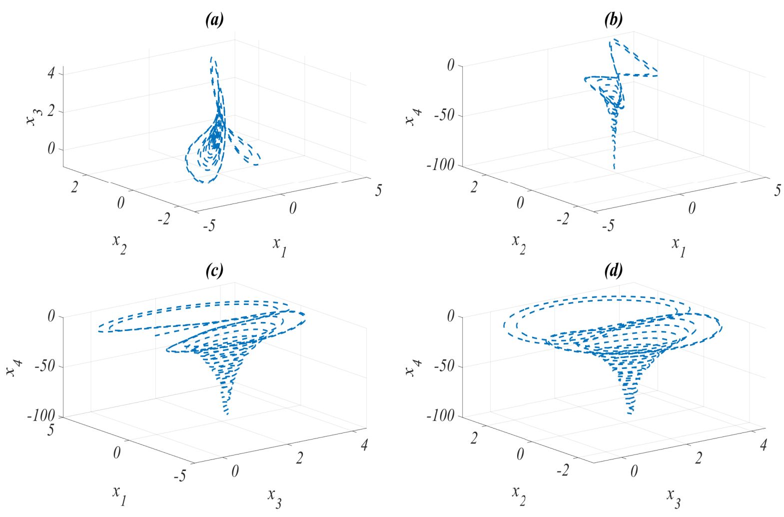

Figure 5.3: Three-dimensional hyperchaotic attractors of system (5.2): (a) in the x_1-x_2-x_3 plane, (b) in the x_1-x_2-x_4 plane, (c) in the x_2-x_3-x_4 plane, and (d) in the x_1-x_3-x_4 plane.

We employed the MATLAB/Simulink software for developing developing an extensive simulation framework for the system described by equation (5.2). We used the FOMCON toolbox to achieve accurate modelling of our proposed system of fractional-order. This toolbox offers reliable blocks for implementing fractional-order integration of diverse orders. The complete simulation set-up is presented schematically in Figure 5.4. The temporal evolution of the state variables x_1, x_2, x_3, $and\, x_4$ are illustrated in

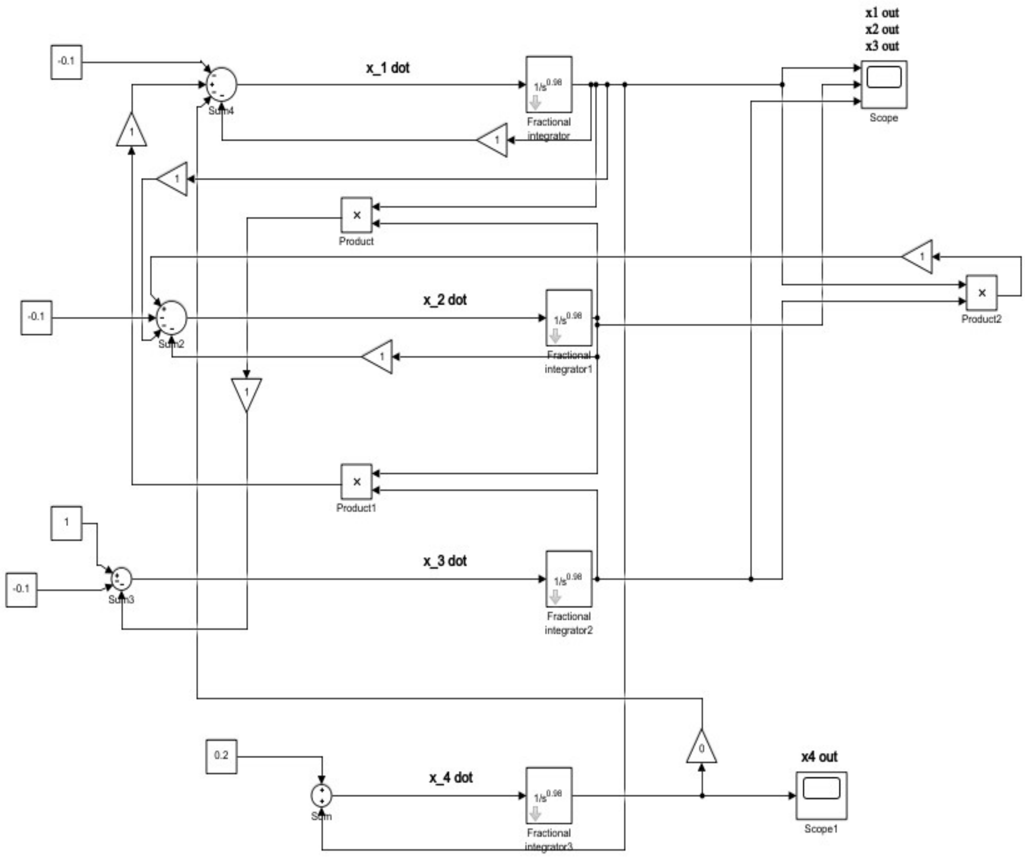

Figure 5.4: The block diagram of the system (5.2)in Matlab Simulink.

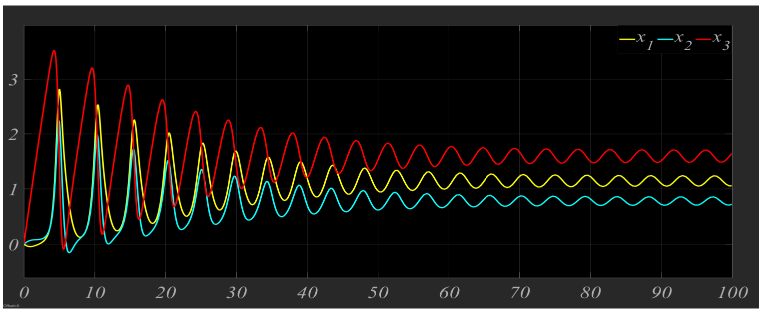

Figure 5.5: Temporel evolution of x_1, x_2, x_3

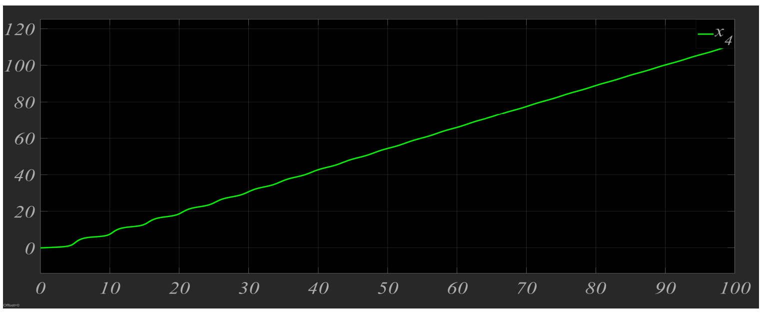

Figure 5.6: Temporel evolution of x_4

Figure 5.5 and figure 5.6 respectively.

To fully confirm the hyperchaotic behaviour of the propsed system, we conduct an analysis of Lyapunov spectrum and fractal dimension of Kaplan-Yorke.

Lyapunov exponents This section addresses the Lyapunov exponent spectrum computed using Wolf et al. algorithm [76].
For fixed values of $a = b = d = 1$ and varying c within the interval $[0, 5]$, the LE spectrum of the system (5.2) is shown in Figure 5.7.

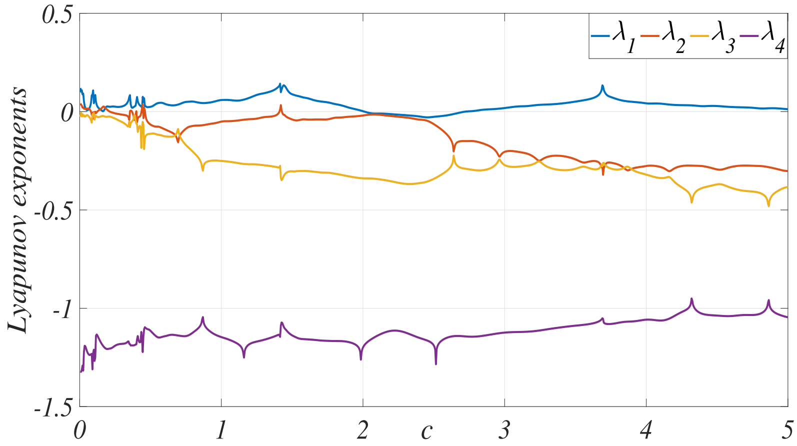

Figure 5.7: The Lyapunov exponents of the system 5.2

In particular, for $c = 0.03$, the computed Lyapunov exponents are obtained as

$$\lambda_1 = 0.1208, \quad \lambda_2 = 0.0202, \quad \lambda_3 = 0, \quad \lambda_4 = -1.2740 \tag{5.7}$$

The presence of two strictly positive Lyapunov exponents demonstrates the hyperchaotic nature of the system. Subsequently, the Kaplan–Yorke dimension is calculated as

$$D_{\mathrm{KY}} = 3 + \frac{\lambda_1 + \lambda_2 + \lambda_3}{|\lambda_4|} = 3 + \frac{0.1208 + 0.0202 + 0}{1.2740} \approx 3.1107 \tag{5.8}$$

The non-integer value of D_{KY} indicates a fractal attractor structure and further confirms the complexity of the dynamics.

In conclusion, system (5.2) exhibits dissipative, hyperchaotic behaviour with a complex attractor, despite possessing no equilibrium points. This renders it a promising candidate for applications requiring high unpredictability.

5.3 Controller design and synchronisation analysis

This section presents a rigorous mathematical formulation for the synchronisation of the novel fractional system using SMC. The objective is to achieve global asymptotic synchronisation between a drive and response system using Lyapunov stability theory and Caputo-based fractional calculus.

5.3.1 General synchronisation framework

Consider the fractional-order drive system

$$\mathcal{D}^{\alpha}x(t) = f(x(t)) \tag{5.9}$$

where $\alpha \in [0, 1]$ is the fractional order of the derivative, $x \in \mathbb{R}^n$ is the state variable, and $\mathcal{D}^{\alpha}$ denotes the Caputo operator. The system (5.9) is regarded as the master system, while the corresponding slave system is given by

$$\mathcal{D}^{\alpha}y(t) = f(y(t)) + u \tag{5.10}$$

where $u(t) \in \mathbb{R}^n$ is the control input. Define the synchronisation error as $e(t) = y(t) - x(t)$, the objective is to design $u(t)$ such that

$$\lim_{t\to\infty} \|e(t)\| = 0 \tag{5.11}$$

so that the slave system follows the trajectory of the master system.

5.3.2 System description and error states

The driving states of the novel system without equilibria are defined as follows

$$\begin{cases} \mathcal{D}^{\alpha}x_1 = -ax_1 + x_2x_3 - cx_4 \\ \mathcal{D}^{\alpha}x_2 = -ax_2 + x_1(x_3 - b) \\ \mathcal{D}^{\alpha}x_3 = d - x_1x_2 \\ \mathcal{D}^{\alpha}x_4 = x_1 \end{cases} \tag{5.12}$$

while the controlled response system is described as

$$\begin{cases} \mathcal{D}^{\alpha}y_1 = -ay_1 + y_2y_3 - cy_4 + u_1 \\ \mathcal{D}^{\alpha}y_2 = -ay_2 + y_1(y_3 - b) + u_2 \\ \mathcal{D}^{\alpha}y_3 = d - y_1y_2 + u_3 \\ \mathcal{D}^{\alpha}y_4 = y_1 + u_4 \end{cases} \tag{5.13}$$

where u_1, u_2, u_3, u_4 are the control inputs to be designed.

Let the synchronisation errors be defined by $e_i(t) = y_i(t) - x_i(t)$ for $i = 1, 2, 3, 4$. The corresponding error dynamics are derived as

$$\begin{cases} \mathcal{D}^{\alpha}e_1 = -ae_1 + y_2y_3 - x_2x_3 - ce_4 + u_1 \\ \mathcal{D}^{\alpha}e_2 = -ae_2 + y_1y_3 - x_1x_3 - be_1 + u_2 \\ \mathcal{D}^{\alpha}e_3 = -y_1y_2 + x_1x_2 + u_3 \\ \mathcal{D}^{\alpha}e_4 = e_1 + u_4 \end{cases} \tag{5.14}$$

5.3.3 Sliding mode controller design

To ensure the stability of the system (5.14), four sliding surfaces s_1, s_2, s_3 and s_4 are defined as

$$s_i = (\mathcal{D}^{\alpha} + \lambda_i) \int_0^t e_i(\tau)\, d\tau, \quad i = 1, .., 4 \tag{5.15}$$

where $\lambda_i > 0$. Their time derivatives are obtained as

$$\begin{cases} \dot{s_1} = D^\alpha e_1(t) + \lambda_1 e_1(t) \\ \dot{s_2} = D^\alpha e_2(t) + \lambda_2 e_2(t) \\ \dot{s_3} = D^\alpha e_3(t) + \lambda_3 e_3(t) \\ \dot{s_4} = D^\alpha e_4(t) + \lambda_4 e_4(t) \end{cases} \tag{5.16}$$

The selected reaching law for the design of ISMC is as follows [85]

$$\begin{cases} \dot{s_1} = -\beta_1 sgn(s_1) - K_1 s_1 \\ \dot{s_2} = -\beta_2 sgn(s_2) - K_2 s_2 \\ \dot{s_3} = -\beta_3 sgn(s_3) - K_3 s_3 \\ \dot{s_4} = -\beta_4 sgn(s_4) - K_4 s_4 \end{cases} \tag{5.17}$$

where $\beta_i > 0$, $K_i > 0$ are strictly positive parameters for $i = 1, \ldots, 4$, and the signum function $\text{sgn}(\cdot)$ is given by

$$sgn(s_i) = \begin{cases} 1, & s_i > 0 \\ 0, & s_i = 0 \\ -1, & s_i < 0 \end{cases}$$

Equating both expressions (5.16) and (5.17) for $\dot{s}_i$, we obtain

$$\begin{cases} D^\alpha e_1(t) + \lambda_1 e_1(t) = -\beta_1 sgn(s_1) - K_1 s_1 \\ D^\alpha e_2(t) + \lambda_1 e_2(t) = -\beta_2 sgn(s_2) - K_2 s_2 \\ D^\alpha e_3(t) + \lambda_1 e_3(t) = -\beta_3 sgn(s_3) - K_3 s_3 \\ D^\alpha e_4(t) + \lambda_1 e_4(t) = -\beta_4 sgn(s_4) - K_4 s_4 \end{cases} \tag{5.18}$$

Substituting the error dynamics (5.14) and (5.18), we get

$$\begin{cases} -ae_1 + y_2 y_3 - x_2 x_3 - ce_4 + u_1 + \lambda_1 e_1(t) = -\beta_1 sgn(s_1) - K_1 s_1 \\ -ae_2 + y_1 y_3 - x_1 x_3 - be_1 + u_2 + \lambda_2 e_2(t) = -\beta_2 sgn(s_2) - K_2 s_2 \\ -y_1 y_2 + x_1 x_2 + u_3 + \lambda_3 e_3(t) = -\beta_3 sgn(s_3) - K_3 s_3 \\ e_1 + u_4 + \lambda_4 e_4(t) = -\beta_4 sgn(s_4) - K_4 s_4 \end{cases} \tag{5.19}$$

To ensure synchronisation between the drive-response systems (5.12) and (5.13), the control laws are deduced as

$$\begin{cases} u_1 = (a - \lambda_1) e_1 + ce_4 - y_2 y_3 + x_2 x_3 - \beta_1 sgn(s_1) - K_1 s_1 \\ u_2 = be_1 + (a - \lambda_2) e_2 - y_1 y_3 + x_1 x_3 - \beta_2 sgn(s_2) - K_2 s_2 \\ u_3 = -\lambda_3 e_3 + y_1 y_2 - x_1 x_2 - \beta_3 sgn(s_3) - K_3 s_3 \\ u_4 = -e_1 - \lambda_4 e_4 - \beta_4 sgn(s_4) - K_4 s_4 \end{cases} \tag{5.20}$$

5.3.4 Synchronisation analysis

Theorem 5.1. *The fractional-order drive–response systems (5.12) and (5.13) achieve global asymptotic synchronisation under the control input (5.20), provided that all parameters λ_i, β_i, K_i $(i = 1, 2, 3, 4)$ are strictly positive.*

Proof. The theorem follows from a Lyapunov-based stability analysis.
Let V be a Lyapunov function candidate as

$$V(s_1, s_2, s_3, s_4) = \frac{1}{2}(s_1^2 + s_2^2 + s_3^2 + s_4^2) \tag{5.21}$$

being positive definite. Taking the time derivative of V in (5.21) yields

$$\dot{V} = s_1\dot{s_1} + s_2\dot{s_2} + s_3\dot{s_3} + s_4\dot{s_4} \tag{5.22}$$

Substituting the reaching law (5.17) into (5.22) yields

$$\dot{V} = \sum_{i=1}^{4}[-\beta_|s_i| - K_i s_i^2)] \tag{5.23}$$

Since $\beta_i > 0$ and $K_i > 0$, $\dot{V}$ is negative definite on $\mathbb{R}^4$. By Lyapunov's direct method for fractional-order systems, $s_i(t) \to 0$ as $t \to \infty$ for all i.
Once $s_i = 0$, the sliding mode dynamics reduce to

$$\mathcal{D}^{\alpha} e_i = -\lambda_i e_i \tag{5.24}$$

which is asymptotically stable for $\lambda_i > 0$. Hence, $e_i(t) \to 0$ as $t \to \infty$, completing the proof. □

5.4 Simulation results and discussion

Numerical simulations were performed using MATLAB.
The selected parameters for the drive and response systems are taken as

$$a = 1, b = 1, c = 0 \; and \; d = 1 \tag{5.25}$$

The parameters of the controller gains were assigned the following values

$$\lambda_i = 0.2\,,\ \beta_i = 0.2\ \ and\ \ K_i = 3, \forall\, i = 1, \ldots, 4 \tag{5.26}$$

The initial states of the drive and the response systems are set as

$$(x_1(0), x_2(0), x_3(0), x_4(0)) = (0.5, -0.5, 0.5, 1) \tag{5.27}$$

and

$$(y_1(0), y_2(0), y_3(0), y_4(0)) = (1.5, 1, -0.5, -0.5) \tag{5.28}$$

respectively.
The temporal evolution of the synchronisation errors is presented in Figure 5.8. Furthermore, Figures 5.9- 5.12 displays the complete synchronisation achieved between the corresponding state variables $x_1 - y_1$, $x_2 - y_2$, $x_3 - y_3$, and $x_4 - y_4$.

Figure 5.8 illustrates the temporal evolution of the synchronisation errors e_i, $i = 1, .., 4$, between systems (5.12) and (5.13). It is evident that all error signals converge asymptotically to zero within a short transient period, with no appreciable steady-state deviation, thereby confirming the effectiveness of the designed integral sliding mode controller in eliminating initial discrepancies.

Further validation is provided in Figures 5.9-5.12, which display the time-domain responses of the master and slave systems. In each plot, the response state (depicted in dashed line) closely follows the drive state (solid line) after a brief synchronisation transient, eventually overlapping completely. This visual congruence across all four states affirms the achievement of complete synchronisation in the novel fractional-order Rekitake system.

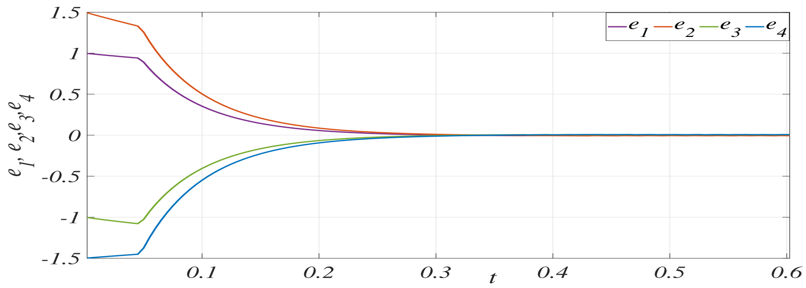

Figure 5.8: Time history of the synchronisation errors.

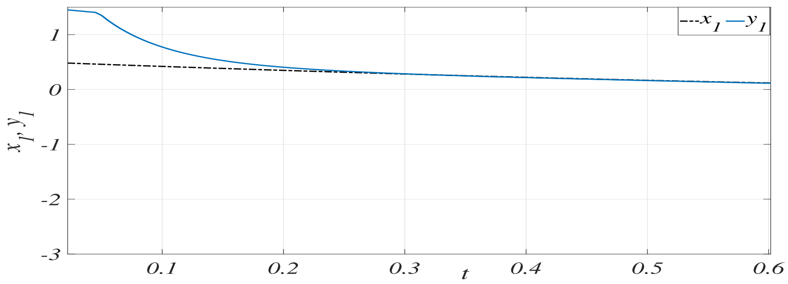

Figure 5.9: Complete synchronisation between x_1 and y_1.

These simulation results not only corroborate the theoretical guarantees established via Lyapunov stability analysis but also underscore the practical viability of the proposed control strategy. The integral sliding mode controller effectively handles the system's complex nonlinear structure and fractional-order dynamics, ensuring robust synchronisation. This makes the approach particularly suitable for applications in secure communication, cryptosystems, and other domains requiring precise control of chaotic and hyperchaotic oscillators.

5.5 Development of secure communication framework using the novel Rikitake system

The safeguarding of confidential information transmitted over public and wireless channels constitutes a fundamental challenge in contemporary communication engineering. The proliferation of open digital networks has rendered data transmissions increasingly

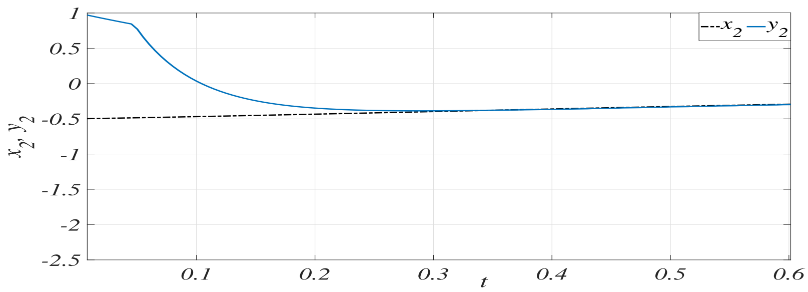

Figure 5.10: Complete synchronisation between x_2 and y_2.

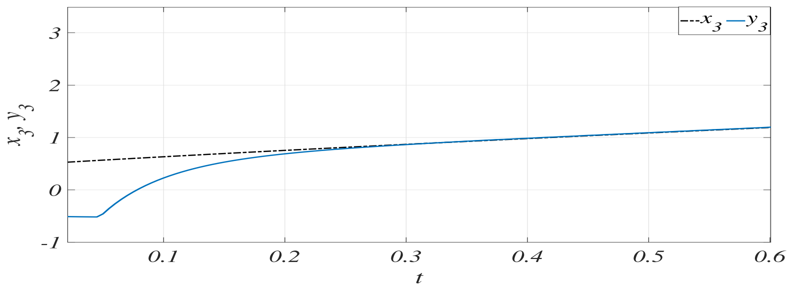

Figure 5.11: Complete synchronisation between x_3 and y_3.

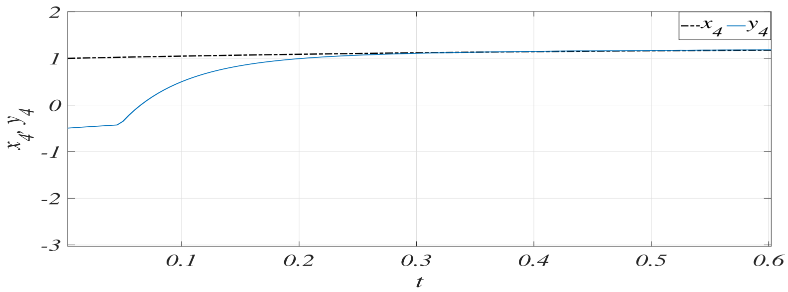

Figure 5.12: Complete synchronisation between x_4 and y_4.

vulnerable to interception, manipulation, and unauthorised access. While conventional encryption algorithms based on deterministic key structures remain effective, their resilience may be compromised by the exponential growth of computational power and the advancement of cryptanalytic techniques.

In contrast, chaos-based secure communication schemes harness the inherent unpredictability and broadband characteristics of nonlinear dynamical systems to obscure transmitted information. These systems generate complex, aperiodic signals that exhibit random-like behaviour, thereby offering a natural masking mechanism with strong sensitivity to initial conditions and system parameters [86, 87].

In this section, a secure *analogue* communication framework is designed and demonstrated using the previously introduced Rikitake fractional-order hyperchaotic system (5.2). The inclusion of fractional-order derivatives introduces memory and hereditary effects that enrich the system dynamics and enhance its security potential. Synchronisation between the transmitter and receiver subsystems is accomplished through the sliding mode control (SMC) strategy developed in the preceding section, ensuring asymptotic convergence of the error dynamics despite uncertainties and external perturbations.

The overarching objective is to design, simulate, and assess a chaos-based analogue communication architecture in which a message signal is embedded within a hyperchaotic carrier, transmitted through a noisy channel, and subsequently recovered via synchronisation-enabled demasking.

5.5.1 Fundamentals of chaos-based analogue communication

A chaos-based analogue secure communication system exploits the properties of a continuous-time chaotic oscillator to conceal a low-amplitude message within its dynamic states. The principal advantage of this approach lies in the use of a *continuous* *chaotic carrier* rather than discrete symbol modulation, making the transmitted waveform statistically indistinguishable from noise and thereby highly resistant to eavesdropping.

At the transmitter, one of the chaotic states (here $x_1(t)$) is selected as the carrier signal. A message $m(t)$ is embedded additively with a small modulation gain $k > 0$

$$s(t) = x_1(t) + k\, m(t) \tag{5.29}$$

The gain k is chosen sufficiently small so that the message remains a minor perturbation to the chaotic trajectory, ensuring minimal distortion of the underlying system dynamics.

During transmission, the signal is corrupted by additive white Gaussian noise (AWGN) and other potential channel disturbances

$$r(t) = s(t) + n(t) \tag{5.30}$$

where $n(t)$ represents the channel noise.

within the receiver architecture, a synchronised replica of the chaotic system driven by the SMC based control inputs is maintained. Once complete synchronisation is achieved, the receiver reconstructs its own state $y_1(t)$, which approximates $x_1(t)$ with high fidelity. The demasking process is performed as

$$\hat{m}(t) = \frac{r(t) - y_1(t)}{k} \tag{5.31}$$

Under perfect synchronisation, $\hat{m}(t) \approx m(t)$, enabling faithful recovery of the transmitted information.

The key design objectives of the proposed scheme are:

1. To verify that the system (5.2) can serve as an effective chaotic carrier for message masking.

2. To assess the robustness of the transmission against channel noise and model uncertainties.

3. To quantitatively evaluate message recovery performance through Mean Square Error (MSE), Bit Error Rate (BER), and correlation coefficient analyses.

4. To validate the effectiveness of the sliding mode controller in achieving reliable synchronisation under noise interference.

5.5.2 Implementation methodology

The implementation process is divided into three principal phases: transmission, channel perturbation, and reception with demasking. The detailed procedural steps are as follows:

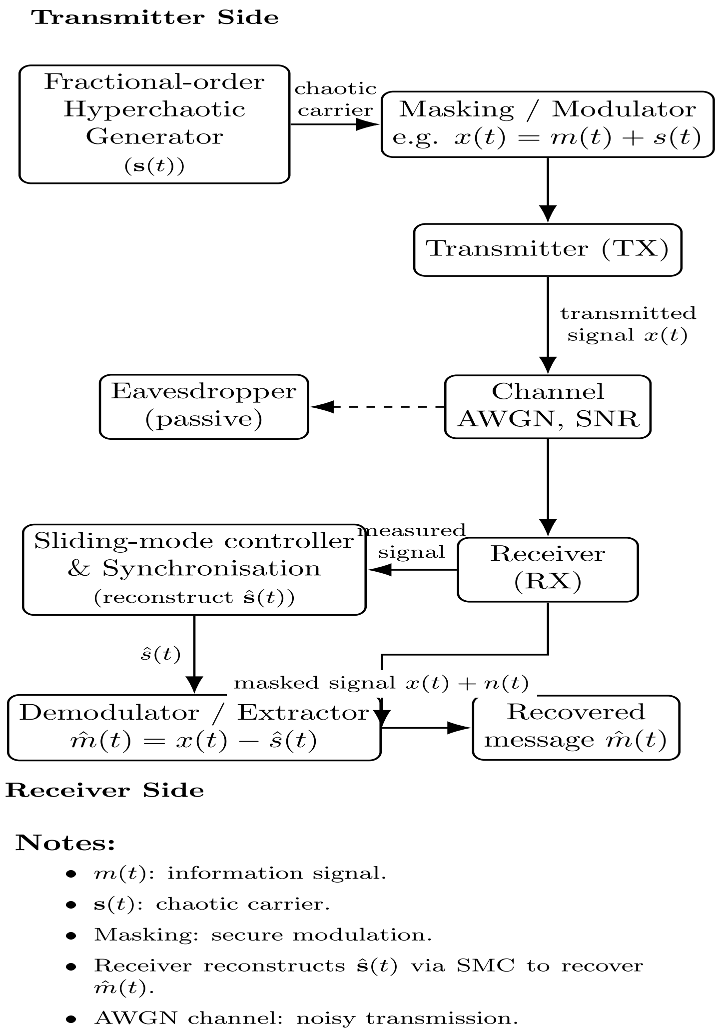

Figure 5.13: Block diagram of the proposed chaos-based analogue secure communication scheme.

1. Message generation: A low-frequency analogue message—typically a sinusoidal or square waveform—is generated to represent the transmitted information. Its amplitude is normalised to ensure the integrity of the chaotic dynamics.

2. Chaotic carrier generation: The fractional-order Rikitake hyperchaotic system is numerically integrated using the Caputo fractional derivative and the predictor–corrector algorithm. The state variable $x_1(t)$ serves as the carrier signal.

3. Message masking: The message is embedded within the chaotic carrier as $s(t) = x_1(t) + k\, m(t)$.

4. Channel perturbation: The impact of practical transmission disturbances is captured by generating $r(t)$ in the presence of white Gaussian noise, scaled to enforce a specified SNR.

5. Receiver synchronisation: The response system employs the previously derived SMC-based control inputs u_i to ensure that $y_i(t) \to x_i(t)$ for all states. Once synchronisation is attained, $y_1(t)$ accurately reconstructs the carrier component.

6. Demasking and message recovery: The recovered message is computed as

$$\hat{m}(t) = \frac{r(t) - y_1(t)}{k} \tag{5.32}$$

7. Performance evaluation: The recovery accuracy is quantified using the following metrics

$$\text{MSE} = \frac{1}{N}\sum_{i=1}^{N}(m(i) - \hat{m}(i))^2, \quad \text{BER} = \frac{N_{\text{err}}}{N_{\text{bits}}}, \quad \rho = \frac{\text{Cov}(m, \hat{m})}{\sigma_m \sigma_{\hat{m}}} \tag{5.33}$$

A small MSE and BER, combined with a correlation coefficient $\rho \to 1$, indicate successful message recovery.

5.5.3 MATLAB Simulation and Discussion

The entire scheme was implemented in MATLAB to ensure accurate numerical integration and efficient computation of the evaluation metrics. Figures 5.14–5.17 illustrate the principal simulation results.
The entire communication framework was implemented in MATLAB to ensure accurate numerical integration of the fractional-order equations and rigorous evaluation of the system's performance. Figures 5.14–5.17 present the simulation outcomes illustrating each stage of the secure communication process, from chaotic masking to message recovery.

Prior to describing the individual results, it is useful to summarise the simulation setup. The transmitter and receiver were simulated using the same system parameters and fractional order $\alpha = 0.98$ corresponding to the hyperchaotic regime, with the fractional-order equations solved via the Adams–Bashforth predictor–corrector algorithm at a step size $h = 10^{-3}$ s. The information signal $m(t)$ is a low-frequency square waveform of frequency $f_0 = 0.5$ Hz, embedded into the chaotic state $x_1(t)$ to form the transmitted signal $s(t) = x_1(t) + k\, m(t)$, which is then transmitted through an AWGN channel at $SNR = 20$ dB.

Figure 5.14 depicts the transmitted chaotic signal $s(t)$, generated by embedding the low-amplitude message $m(t)$ within the chaotic state $x_1(t)$. The resulting waveform appears entirely irregular and noise-like, with no discernible periodicity or identifiable message features. This observation confirms that the chaotic masking mechanism successfully conceals the transmitted information within a broadband dynamic carrier, thereby preventing direct interception or extraction.

Figure 5.15 presents the received signal $r(t)$ after propagation through a noisy channel with an $SNR = 20$ dB. Despite the interference of white noise, the chaotic structure of the waveform remains visually preserved, demonstrating the inherent robustness of the chaotic carrier against channel perturbations. The amplitude fluctuations are marginally amplified by the noise, yet the overall signal envelope and dynamic pattern remain intact.

Figure 5.16 illustrates the demasking stage, in which the recovered message $\hat{m}(t)$ (black line) is superimposed on the original reference $m(t)$ (red dashed line). The two

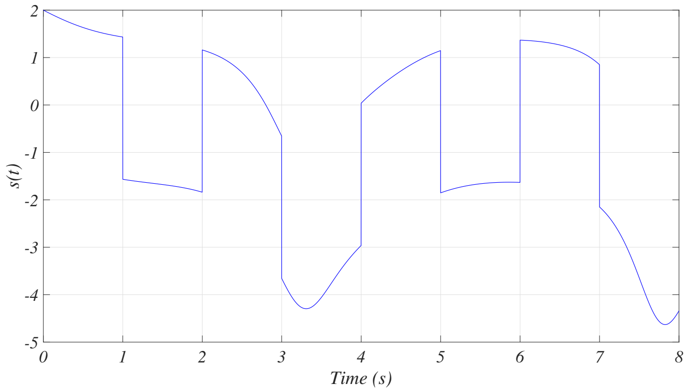

Figure 5.14: Transmitted signal $s(t) = x_1(t) + k\, m(t)$. .

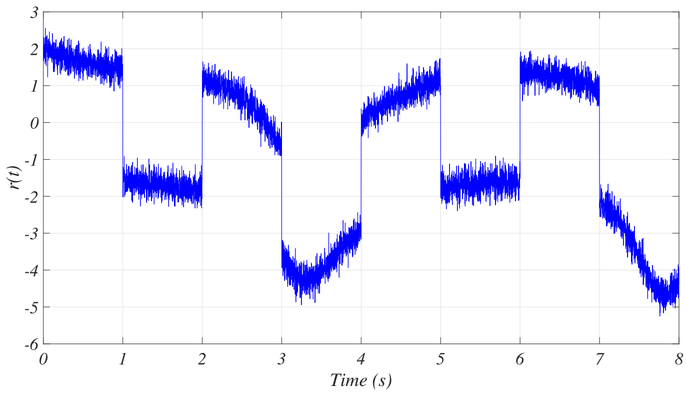

Figure 5.15: Received signal $r(t)$ at $SNR = 20$ dB.

signals are almost perfectly aligned in both amplitude and phase, confirming the effectiveness of the sliding mode controller in achieving complete synchronisation between the transmitter and receiver. Minor deviations observed at the signal edges correspond to small transient mismatches during the initial synchronisation period.

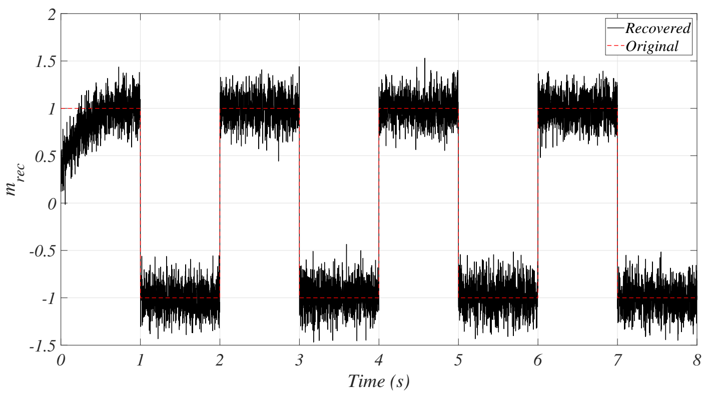

Figure 5.16: Recovered analogue message (black) compared with the original (red dashed).

Finally, Figure 5.17 compares the original and recovered binary bit streams derived from the analogue message. The near-perfect overlap between the two sequences provides further quantitative evidence of the system's reliability and precision.

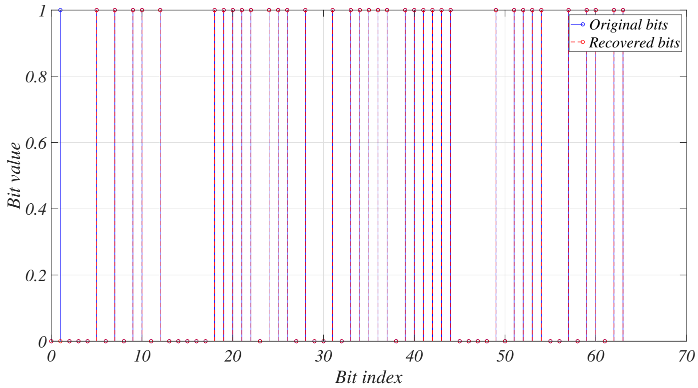

Figure 5.17: Comparison of original and recovered Bits .

This visual consistency aligns with the measured performance metrics:

$$\mathrm{MSE} = 2.82 \times 10^{-2}, \quad \mathrm{BER} = 2.90 \times 10^{-2}, \quad \rho = 0.9857 \tag{5.34}$$

These metrics confirm near-perfect synchronisation and highly accurate message reconstruction. The correlation coefficient approaching unity indicates that both amplitude and phase information were faithfully preserved.

5.5.4 Interpretation and remarks

The results unequivocally demonstrate the efficacy of the proposed fractional-order hyperchaotic system for secure analogue communication. The fractional derivative contributes to enhanced dynamic richness and broader spectral content, thereby improving the cryptographic strength of the transmitted signal. The SMC-based synchronisation mechanism ensures reliable recovery despite the presence of channel noise and modelling uncertainties.

The minimal reconstruction error and high correlation confirm that the proposed architecture achieves both robustness and security. These findings highlight the potential of fractional-order hyperchaotic systems as practical foundations for next-generation physical-layer encryption techniques.

5.6 Conclusion

This chapter has presented a novel four-dimensional hyperchaotic system of fractional-order derived from the Rikitake model, distinguished by the complete absence of equilibrium points. Despite this unconventional feature, the system exhibits rich dynamical behaviour, including hyperchaos, as confirmed through Lyapunov exponent analysis and numerical simulation. The presence of hidden attractors underscores its potential for applications where traditional attractor structures are undesirable or insufficient.

An integral sliding mode control strategy was developed to achieve synchronisation between two identical instances of the system. By leveraging Lyapunov stability theory for fractional-order systems, the controller was designed to ensure robust and asymptotic convergence, even in the presence of structural complexity and sensitivity to initial conditions. The effectiveness of the approach was demonstrated through numerical simulations, confirming successful synchronisation and highlighting the suitability of ISMC for such non-conventional systems.

Furthermore, a secure communication scheme grounded in the proposed novel system was established. By exploiting the system's sensitivity and intricate behaviour, the scheme guaranteed high levels of message confidentiality and reliable recovery of transmitted signal.

Looking ahead, the proposed system and control framework open several avenues for further research. Future work may explore the physical realisability of the system via electronic circuit implementation, as well as the extension of the control strategy to cases involving parameter uncertainty, external disturbances, or fractional-order mismatch. Additionally, the application of the system within chaotic encryption schemes or complex network synchronisation could further demonstrate its practical utility. These directions would not only validate the theoretical findings but also advance the integration of hidden-attractor systems into real-world technologies.

General Conclusion

Summary

This general conclusion synthesises the principal outcomes of the research, reflecting on the theoretical and practical contributions achieved. It further discusses the broader perspectives opened by the study and outlines potential directions for future work.

Contents

Principal outcomes

This dissertation presents a rigorous and comprehensive investigation of chaotic and hyperchaotic dynamical systems of both integer and fractional orders, with particular emphasis on their modelling, qualitative analysis, control, and synchronisation. It begins with a critical examination of classical dynamical systems and historical emergence of chaos and hyperchaos, thereby establishing a robust conceptual foundationfor the subsequent incorporation of fractional calculus into contemporary dynamical systems theory. Building upon these foundations, the research advances towards the design of control and synchronisation strategies for dynamical models, thus forging a deliberate and coherent connection between mathematical depth and practical engineering relevance.

The dissertation delivers several decisive contributions. First, It introduces an extended form of the Lü system, formulated in a four-dimensional state space and incorporating an exponential nonlinearity, which exhibits hyperchaotic behaviour. Its principal dynamical characteristics are rigorously established through qualitative analysis. Adaptive control methods were subsequently applied to stabilise the system, while complete synchronisation scheme is achieved using an adaptive RBF approach. Furthermore, the utility of the proposed system was demonstrated through entropy-based key generation, thereby simulating blockchain technology as a real world application for cryptographic and security applications.

Second, a backstepping dynamic-surface methodology was successfully applied to a representative chaotic model, demonstrating enhanced stabilisation performance. This framework mitigates the well-known computational burdens associated with conventional backstepping, and thereby offering a more amenable route to the regulation of complex nonlinear systems. To reinforce the relevance of chaotic dynamics , an image encryption scheme based on the S-box architecture was implemented, highlighting the importance of chaotic models in achieving high level of diffusion and confusion, and strengthening contemporary encryption techniques.

Finally, the dissertation proposes a sliding mode framework for the synchronisation of a novel equilibrium-free hyperchaotic system of fractional order. Owing to its lack of equilibrium points, and intrinsic memory effects, this system exhibit considerable analytical and practical challenges. The proposed sliding mode framework successfully addresses these difficulties, ensuring robust synchronisation. The effectiveness of the proposed system is further demonstrated through its application to a secure communication scheme, in which our model provide enhanced resistance to interception and degradation.

These findings demonstrate the efficiency of both integer- and fractional-order chaos and hyperchaos in capturing the dynamics of many physical processes, introducing layers of complexity and practical opportunity in domains such as secure communications, cryptography, and advanced signal processing. By uniting these domains and devising robust control and synchronisation schemes, this work makes a substantive and enduring contribution to both the theoretical understanding and the practical regulation of highly complex dynamical phenomena.

Perspectives and future works

Future research may profitably explore several complementary directions, each offering substantial potential to deepen theoretical understanding and enhance practical applications of hyperchaotic dynamical systems. A promising avenue lies in the formulation of novel chaotic and hyperchaotic systems of fractional-order. Such developments would broaden the mathematical landscape of nonlinear dynamics, reveal richer and more intricate behaviours. These advanced models would provide fertile ground for investigating the interplay between system structure, fractional dynamics, and the emergence of complex phenomena.

Building upon the synchronisation techniques developed in this study, subsequent studies could extend fractional-order synchronisation to real-world problems. Potential domains include secure communications, where enhanced resistance to eavesdropping and channel noise is critical; biomedical signal processing, where the inherent memory and hereditary properties of physiological signals may be captured more accurately; and distributed energy networks, where robustness to noise and parameter variability is essential. In each of these contexts, the design of control and synchronisation frameworks could improve system reliability and operational performance.

Another important perspective lies in the integration of machine-learning approaches, particularly deep neural networks, with both integer and fractional-order dynamics. Data-driven models may be trained to identify unknown system parameters, predict long-term behaviour, or design controllers in real time. Moreover, hybrid schemes that combines analytical fractional calculus with neural architectures might capture memory effects more efficiently than conventional models. Developing and analysing neural-network models that explicitly incorporate fractional derivatives would not only test their computational advantages but also offer new insights into learning processes in systems with hereditary properties. Together, these directions promise to extend both the theoretical understanding and the practical applicability of fractional-order chaotic and hyperchaotic dynamics.

Collectively, these aspects offer the prospect of substantial theoretical advancement and practical innovation. By extending thr mathematical formulation of fractional-order chaos to real world applications, future studies may further strengthen the bridge between rigorous analytical methods and emerging data driven techniques. Such endeavours would contribute meaningfully to disciplines ranging from secure communications and cryptography to biomedical engineering and energy systems, thereby reinforcing the relevance of fractional dynamics in the modelling, analysis, and control of highly complex systems.

Bibliography

[1] S. H. Strogatz. *Nonlinear dynamics and chaos: with applications to physics, biology, chemistry, and engineering.* Chapman and Hall/CRC, 2024.

[2] H. Poincaré. "Sur le problème des trois corps et les équations de la dynamique". In: *Acta mathematica* 13.1 (1890), A3–A270.

[3] T.-Y. Li and J. A. Yorke. "Period three implies chaos". In: *The American Mathematical Monthly* 82.10 (1975), pp. 985–992.

[4] E. N. Lorenz. "Deterministic Nonperiodic Flow". In: *Journal of the Atmospheric Sciences* 20.2 (1963), pp. 130–141.

[5] O. E. Rössler. "An equation for continuous chaos". In: *Physics Letters A* 57.5 (1976), pp. 397–398.

[6] L. Chua, M. Komuro, and T. Matsumoto. "The double scroll family". In: *IEEE Transactions on Circuits and Systems* 33.11 (1986), pp. 1072–1118.

[7] M. Hénon. "A two-dimensional mapping with a strange attractor". In: *Communications in Mathematical Physics* 50.1 (1976), pp. 69–77.

[8] O. E. Rössler. "An equation for hyperchaos". In: *Physics Letters A* 71.2-3 (1979), pp. 155–157.

[9] J. Lü, G. Chen, and D. Cheng. "A new chaotic system and beyond: the generalized Lorenz-like system". In: *International Journal of Bifurcation and Chaos* 14.05 (2004), pp. 1507–1537.

[10] Z. Chen et al. "A novel hyperchaos system only with one equilibrium". In: *Physics Letters A* 360.6 (2007), pp. 696–701.

[11] Z. Wei and W. Zhang. "Hidden hyperchaotic attractors in a modified Lorenz–Stenflo system with only one stable equilibrium". In: *International Journal of Bifurcation and Chaos* 24.10 (2014), p. 1450127.

[12] N. K. Pareek, V. Patidar, and K. K. Sud. "Discrete chaotic cryptography using external key". In: *Physics Letters A* 309.1-2 (2003), pp. 75–82.

[13] L. Kocarev. "Chaos-based cryptography: a brief overview". In: *IEEE Circuits and Systems* 1 (2001), pp. 6–21.

[14] Z. Han et al. "A new image encryption algorithm based on chaos system". In: *IEEE International Conference on Robotics, Intelligent Systems and Signal Processing, 2003. Proceedings. 2003.* Vol. 2. IEEE. 2003, pp. 778–782.

[15] C. Ionescu et al. "The role of fractional calculus in modeling biological phenomena: A review". In: *Communications in Nonlinear Science and Numerical Simulation* 51 (2017), pp. 141–159.

[16] I. Grigorenko and E. Grigorenko. "Chaotic dynamics of the fractional Lorenz system". In: *Physical Review Letters* 91.3 (2003), p. 034101.

[17] C. K. Volos, I. M. Kyprianidis, and I. N. Stouboulos. "Image encryption process based on chaotic synchronization phenomena". In: *Signal Processing* 93.5 (2013), pp. 1328–1340.

[18] Y. Xu et al. "Image encryption based on synchronization of fractional chaotic systems". In: *Communications in Nonlinear Science and Numerical Simulation* 19.10 (2014), pp. 3735–3744.

[19] K. Oldham and J. Spanier. *The fractional calculus theory and applications of differentiation and integration to arbitrary order*. Vol. 111. Elsevier, 1974.

[20] I. Podlubny. *Fractional Differential Equations*. Vol. 198. Mathematics in Science and Engineering. San Diego: Academic Press, 1999.

[21] T. T. Hartley, C. F. Lorenzo, and H. K. Qammer. "Chaos in a fractional order Chua's system". In: *IEEE Transactions on Circuits and Systems I: Fundamental Theory and Applications* 42.8 (1995), pp. 485–490.

[22] C. Li and G. Chen. "Chaos in the fractional order Chen system and its control". In: *Chaos, Solitons and Fractals* 22.3 (2004), pp. 549–554. ISSN: 0960-0779.

[23] J. G. Lu. "Chaotic dynamics of the fractional-order Lü system and its synchronization". In: *Physics Letters A* 354.4 (2006), pp. 305–311.

[24] I. Petráš. *Fractional-order nonlinear systems: modeling, analysis and simulation*. Springer Science Business Media, 2011.

[25] M. Maaruf, M. S. Mahmoud, and A. Ma'arif. "A survey of control methods for quadrotor uav". In: *International Journal of Robotics and Control Systems* 2.4 (2022), pp. 652–665.

[26] E. Ott, C. Grebogi, and J. A. Yorke. "Controlling chaos". In: *Physical review letters* 64.11 (1990), p. 1196.

[27] M. Hou et al. "Adaptive dynamic surface control of high-order strict feedback nonlinear systems with parameter estimations". In: *Science China Information Sciences* 66.5 (2023), p. 159203.

[28] G. Zhu et al. "Adaptive Dynamic Surface Integral Sliding Mode Fault-Tolerant Control for Multimachine Excitation Systems with SVC". In: *Complexity* 1 (2020), p. 6106794.

[29] W. Yan et al. "Adaptive Neural Network Synchronization Control for Uncertain Fractional-Order Time-Delay Chaotic Systems". In: *Fractal and Fractional* 7 (2023), p. 288.

[30] I. Ahmad et al. "A research on active control to synchronize a new 3D chaotic system". In: *Systems* 4.1 (2015), p. 2.

[31] A. H. Hameed et al. "Backstepping-based quasi-sliding mode control and observation for electric vehicle systems: a solution to unmatched load and road perturbations". In: *World Electric Vehicle Journal* 15 (2024), p. 419.

[32] F. Loucif and S. Kechida. "Design of optimal backstepping controller for a robot manipulator using slime mould algorithm". In: *Dynamics of Continuous, Discrete and Impulsive Systems Series B: Applications and Algorithms* 31 (2024), pp. 227–246.

[33] W. S. Chen. “Adaptive backstepping dynamic surface control for systems with periodic disturbances using neural networks”. In: *IET Control Theory and Applications* 3 (2008), pp. 1383–1394.

[34] M. Wang and G. Sun. “A backstepping based dynamic surface control method for a class of non-lower triangular nonlinear systems”. In: *Proceedings of 2019 Chinese Control Conference*. July 2019, pp. 539–543.

[35] J. Wang and C. Yang. “Chaos synchronization of a finance chaotic system with an integral sliding mode controller”. In: *Journal of Mathematics* (2021), pp. 1–9.

[36] B. Labed, S. Kaouache, and M. S. Abdelouahab. “Control of a novel class of uncertain fractional-order hyperchaotic systems with external disturbances via sliding mode controller”. In: *Nonlinear Dynamics and Systems Theory* 20.2 (2020), pp. 203–213.

[37] A. Boulkroune, F. Zouari, and A. Boubellouta. “Adaptive fuzzy control for practical fixed-time synchronization of fractional-order chaotic systems”. In: *Journal of Vibration and Control* (2024).

[38] K. Xu, H. Wang, and P. X. Liu. “Adaptive fuzzy fixed-time control for non-triangular structural stochastic switching nonlinear systems”. In: *International Journal of Robust and Nonlinear Control* 33 (2023), pp. 4685–4700.

[39] M. Yang et al. “Uniform synchronization for chaotic systems via event-triggered aperiodic intermittent control”. In: *Asian Journal of Control* 23 (2021), pp. 2719–2728.

[40] D. Liu and B. Zeng. “Event-Triggered Adaptive Neural Network Asymptotic Control for Non-Triangular Stochastic Nonlinear Systems”. In: *Proceedings of the IEEE 11th Data Driven Control and Learning Systems Conference*. IEEE Conference. Emeishan, China, Aug. 2022, pp. 1218–1223.

[41] L. M. Pecora and T. L. Carroll. “Synchronization in chaotic systems”. In: *Physical review letters* 64.8 (1990), p. 821.

[42] M. S. Abdelouahab and N. Hamri. “Fractional-order hybrid optical system and its chaos control synchronization”. In: *Electronic Journal of Theoretical Physics* 11.30 (2014), pp. 49–62.

[43] R. A. Meskine and S. Kaouache. “Exploring hyperchaotic synchronization of a fractional-order system without equilibrium points: A sliding mode control approach”. In: *Iranian Journal of Numerical Analysis & Optimization* 15.2 (2025), p. 508.

[44] M. M. Al-sawalha et al. “Active anti-synchronization of two identical and different fractional-order chaotic systems”. In: *International Journal of Nonlinear Science* 11.3 (2011), pp. 267–274.

[45] Y. Zhao et al. “Novel Methods for Multi-Switch Generalized Projective Anti-Synchronization of Fractional Chaotic System Under Caputo–Fabrizio Derivative via Lyapunov Stability Theorem and Adaptive Control”. In: *Symmetry* 17.6 (2025).

[46] M. G. Rosenblum, A. S. Pikovsky, and J. Kurths. “Phase Synchronization of Chaotic Oscillators”. In: *Physical Review Letters* 76.11 (1996), pp. 1804–1807.

[47] S. Kaouache. “Projective Synchronization of The Modified Fractional-Order Hyperchaotic Rössler System and Its Application in Secure Communication”. In: *Universal Journal of Mathematics and Applications* 4 (2021), pp. 50–58.

[48] A. Bouzeriba, A. Boulkroune, and T. Bouden. “Projective synchronization of two different fractional-order chaotic systems via adaptive fuzzy control”. In: *Neural Computing and Applications* 27 (2016), pp. 1349–1360.

[49] X. Wu and Y. Lu. “Generalized projective synchronization of the fractional-order Chen hyperchaotic system”. In: *Nonlinear Dynamics* 57 (2009), pp. 25–35.

[50] Y. Chai et al. “QS synchronization of the fractional-order unified system”. In: *Pramana* 80 (2013), pp. 449–461.

[51] L. Perko. *Differential Equations and Dynamical Systems*. 3rd. Vol. 7. Texts in Applied Mathematics. New York: Springer, 2001. ISBN: 0-387-95116-4.

[52] X. Wu, H. Wang, and S. He. “Localization of hidden attractors in Chua’s system with absolute nonlinearity and its FPGA implementation”. In: *Frontiers in Physics* 9 (2021), p. 788329.

[53] M. W. Hirsch, S. Smale, and R. L. Devaney. *Differential equations, dynamical systems, and an introduction to chaos*. Academic press, 2013.

[54] J. Guckenheimer and P. Holmes. *Nonlinear Oscillations, Dynamical Systems, and Bifurcations of Vector Fields*. Springer-Verlag, 1983.

[55] R. L. Devaney. *An Introduction to Chaotic Dynamical Systems*. 2nd. Addison-Wesley, 1989.

[56] H.-L. Li et al. “Anti-Synchronization and Intermittent Anti-Synchronization of Two Identical Delay Hyperchaotic Chua Systems Via Linear Control”. In: *Asian Journal of Control* 19.1 (2017), pp. 202–214.

[57] L. Kocarev and U. Parlitz. “General approach for chaotic synchronization with applications to communication”. In: *Physical Review Letters* 76.11 (1996), pp. 1816–1819.

[58] G. M. Mittag-Leffler. “Sur la nouvelle fonction $E_\alpha(x)$”. In: *Comptes Rendus de l’Académie des Sciences* 137 (1903), pp. 554–558.

[59] R. P. Agarwal. “On a Two-Parameter Generalization of the Mittag-Leffler Function”. In: *Proceedings of the American Mathematical Society* 4.5 (1953), pp. 861–866.

[60] G. B. Folland. *Real Analysis: Modern Techniques and Their Applications*. 2nd. New York: John Wiley & Sons, 1999.

[61] H. L. Royden and P. M. Fitzpatrick. *Real Analysis*. 4th. See Chapter 11 (Fubini and Tonelli Theorems). Boston: Pearson, 2010.

[62] M. Caputo. “Linear models of dissipation whose Q is almost frequency independent—II”. In: *Geophysical journal international* 13.5 (1967), pp. 529–539.

[63] S. G. Samko, A. A. Kilbas, and O. I. Marichev. *Fractional Integrals and Derivatives: Theory and Applications*. Switzerland; Philadelphia, PA: Gordon and Breach Science Publishers, 1993.

[64] P Inizan. “Dynamique fractionnaire pour le chaos hamiltonien”. Thèse de Doctorat. L’Observatoire de Paris, France, 2010.

[65] I. T. Huseynov, A. Ahmadova, and N. I. Mahmudov. “Fractional Leibniz integral rules for Riemann-Liouville and Caputo fractional derivatives and their applications”. In: *arXiv:2012.11360* (2020).

[66] R. S. Rutman. “On fractional derivatives and fractional powers of operators”. In: *Functional Analysis and Its Applications* 32.4 (1998), pp. 309–319.

[67] I. Podlubny. “Geometric and physical interpretation of fractional integration and fractional differentiation”. In: *arXiv preprint math/0110241* (2001).

[68] A. A. Kilbas. *Theory and applications of fractional differential equations.* Vol. 204. 2006.

[69] F. Mainardi. *Fractional calculus and waves in linear viscoelasticity, Imperial College Press, London.* 2010.

[70] K. Diethelm. “Single-term Caputo fractional differential equations: basic theory and fundamental results”. In: *The Analysis of Fractional Differential Equations: An Application-Oriented Exposition Using Differential Operators of Caputo Type.* 2010, pp. 85–132.

[71] W. Rudin. *Principles of Mathematical Analysis.* 3rd. New York: McGraw-Hill, 1976.

[72] J. Weissinger. “Zur Theorie und Anwendung des Iterationsverfahrens”. In: *Mathematische Nachrichten* 8 (1952), pp. 193–212.

[73] D. Matignon. “Stability results for fractional differential equations with applications to control processing”. In: *Proceedings of the Computational Engineering in Systems and Application Multi-Conference (CESA’96), IMACS, IEEE-SMC.* Vol. 2. Lille, France, 1996, pp. 963–968.

[74] Y. Li, Y. Chen, and I. Podlubny. “Stability of fractional-order nonlinear dynamic systems: Lyapunov direct method and generalized Mittag-Leffler stability”. In: *Computers & Mathematics with Applications* 59.5 (2010), pp. 1810–1821.

[75] A. Chen, J. Lü, and S. Yu. “Generating hyperchaotic Lü attractor via state feedback control”. In: *Physica A* 364 (2006), pp. 103–110.

[76] A. Wolf et al. “Determining Lyapunov Exponents from a Time Series”. In: *Physica D: Nonlinear Phenomena* 16.3 (1985), pp. 285–317.

[77] P. Patel and D. Shah. “Cryptographic Wallet Security and Key Management in Blockchain Financial Systems: A Systematic Literature Review”. In: *Available at SSRN 5363844* (2025).

[78] S. Houy, P. Schmid, and A. Bartel. “Security aspects of cryptocurrency wallets—a systematic literature review”. In: *ACM Computing Surveys* 56.1 (2023), pp. 1–31.

[79] S. Jafaria, J. C. Sprott, and S. M. R. Hashemi Golpayegani. “Elementary quadratic chaotic flows with no equilibria”. In: *Physics Letters A* 377 (2013), pp. 699–702.

[80] S. Kaouache et al. “Advanced control of the Wang-Chen chaotic system via backstepping dynamic surface method”. In: *Dynamics of Continuous, Discrete and Impulsive Systems, Series B: Applications and Algorithms* 32.5B (2025).

[81] M. Vijayakumar and A. Ahilan. “An optimized chaotic S-box for real-time image encryption scheme based on 4-dimensional memristive hyperchaotic map”. In: *Ain Shams Engineering Journal* 15.4 (2024), p. 102620.

[82] I. Kouadra et al. “New Composite Chaotic Map Applied To An Image Encryption Scheme in Cybersecurity Applications”. In: *IEEE Access* (2025).

[83] T. Rikitake. “Oscillations of a system of disk dynamos”. In: *Mathematical Proceedings of the Cambridge Philosophical Society* 54.1 (1958), pp. 89–105.

[84] A. E. Cook and P. H. Roberts. “The Rikitake two disk dynamo system”. In: *Mathematical Proceedings of the Cambridge Philosophical Society* 68.2 (1970), pp. 547–569.

[85] J. Lin, J. Yan, and T. Liao. “Chaotic synchronization via adaptive sliding mode observers subject to input nonlinearity”. In: *Chaos, Solitons & Fractals* 24 (2005), pp. 371–381.

[86] A. A.-H. Shoreh et al. “Synchronization of hidden hyperchaotic attractors in fractional-order complex-valued systems with application to secure communications”. In: *Proceedings of the 2021 IEEE Conference of Russian Young Researchers in Electrical and Electronic Engineering (ElConRus)*. IEEE, 2021, pp. 62–67.

[87] Nabil Haneche and Tayeb Hamaiziay. “Enhancing secure communication using a robust synchronization scheme of fractional-order hyperchaotic systems”. In: 18.4 (2025), pp. 542–554.